SEA CHANGE. PHYTOPLANKTON CHANGE TOO? THERMAL ADAPTATION OF THE MARINE DIATOM *THALASSIOSIRA PSEUDONANA* IN RESPONSE TO TEMPERATURE: AN EVOLUTIONARY SCENARIO

By

Daniel Roy O'Donnell

A DISSERTATION

Submitted to
Michigan State University
in partial fulfillment of the requirements
for the degree of

Integrative Biology—Doctor of Philosophy
Ecology, Evolutionary Biology and Behavior—Dual Major

2018

ABSTRACT

SEA CHANGE. PHYTOPLANKTON CHANGE TOO? THERMAL ADAPTATION OF THE MARINE DIATOM *THALASSIOSIRA PSEUDONANA*: AN EVOLUTIONARY SCENARIO

By

Daniel Roy O'Donnell

Rapid evolution in response to environmental change will likely be a driving force determining the distribution of species across the biosphere in coming decades. This is especially true of microorganisms, many of which may evolve in step with warming, including phytoplankton, the diverse photosynthetic microbes forming the foundation of most aquatic food webs. I tested the capacity of a globally important, model marine diatom *Thalassiosira pseudonana*, for rapid evolution in response to temperature. Selection at 16 and 31°C for 350 generations led to significant divergence in several temperature response traits, demonstrating local adaptation and the existence of tradeoffs associated with adaptation to different temperatures. In contrast, competitive ability for nitrogen (commonly limiting in marine systems), measured after 450 generations of temperature selection, did not diverge in a systematic way between temperatures. After 500 generations of temperature selection, *T. pseudonana* populations had diverged in their thermal reaction norms for fatty acid composition and in their carbon, nitrogen, phosphorus and chlorophyll *a* contents. Divergence in C:N:P stoichiometry was not apparent. 31°C-selected populations showed morphological evidence of selection for more efficient nutrient uptake at high temperatures. This study shows how rapid thermal adaptation affects important growth, nutrient uptake and utilization, and cellular physiology and morphology traits in a key marine phytoplankton species, and may thus play a role in long-term physiological, ecological and biogeographic responses to climate change.

This dissertation is dedicated to Uncle Joe
and Aunt Martha.

As a young boy, I once pointed to the
inside of a trout I was gutting and asked
my dad, “Hey, what’s that thing?”

“Beats me”, he said. “Ask your Uncle Joe
and Aunt Martha. They’re scientists.”

The rest is history.

ACKNOWLEDGEMENTS

Dr. Elena Litchman has been the perfect boss, adviser, teacher and friend. I have always come out of meetings with Elena feeling better than when I went in. Dr. Chris Klausmeier is among a rarified subset of my elders who have permanently rewired my brain. He is a uniquely gifted thinker and educator. Drs. Jen Lau and Gary Mittelbach exemplify the uncommon character of academics who take pride in caring about and nurturing those who look up to them. In the unlikely event I someday achieve at their level, I hope I can be as nice as they are.

I hope that someday I can be as good at my job as Pam Woodruff and Ally Hutchens are at theirs. I wanted for nothing in the Litchman lab. Stacey Vander Wulp, Linda Danhof, and Dr. Zhi-yan "Rock" Du also went out of their way to help me, even though I'm not even in their labs. Dr. Kay Gross has had my back in more ways than even I will ever know. Andy Fogiel, Tyler Brownell, Jennifer Smith, Jennae Roseboom, and countless other KBS staff worked tirelessly to pick up after me and make sure I had everything I needed, even when I made that task as burdensome as humanly possible for them. Dr. Colin Kremer taught me more about statistics on a given day than I learned in all of my stats courses combined.

My proudest and happiest moments in research were all thanks to my mentees, Carolyn Hamman, Evan Johnson, Connie High, Farhana Haq, Claire Harper, Olivia Porth, Sophie Beery and Ayley Shortridge. I hope I have left as lasting a mark on their lives as they have left on mine.

No person survives a PhD without the support of their friends and loved ones. My wife, Abhijna, has stood by me for worse, for poorer, and in sickness. When I suffered, she suffered with me. When I lost my mind, she helped me find it again. There are many others to thank. They know who they are. Except Felix. He probably doesn't get it.

TABLE OF CONTENTS

LIST OF TABLES

LIST OF FIGURES

KEY TO SYMBOLS

T_{opt}	Thermal optimum for per-capita population growth
CT_{max}	Upper critical temperature for per-capita population growth
CT_{min}	Lower critical temperature for per-capita population growth
μ_{max}	Maximum per-capita growth rate
μ_{opt}	Per-capita population growth rate at T_{opt}
C	Carbon
N	Nitrogen
P	Phosphorus
Chl *a*	Chlorophyll *a*
NO_3	Nitrate
a_{NO3}	Nitrate growth affinity
CI	Confidence Interval
df	degrees of freedom
MS	Mean squares
RSE	Residual squared errors
n	Sample size
SE	Standard error
FA	Fatty acid
SFA	Saturated fatty acid
UFA	Unsaturated fatty acid
MUFA	Monounsaturated fatty acid

PUFA	Polyunsaturated fatty acid
DMSO	Dimethyl sulfoxide
bv	biovolume
MCL	Mean chain length (C atoms per FA molecule)
WUnSat	Degree of unsaturation (double bonds per FA molecule)
dAIC	Difference in Akaike's Information Criterion
LRT	Likelihood ratio test
Tukey HSD	Tukey's Honestly Significant Difference
SA_{tot}	Total surface area
SA_{valve}	Valve surface area
SA_{girdle}	Girdle surface area
V	Volume

INTRODUCTION

Temperature is a universal control on biological rates, including the physiological processes involved in the acquisition of resources and their conversion into biomass, and ultimately the vital rates of individuals and populations. Given the omnipresent control temperature exerts on biological systems, the current, unprecedented rate of change in global temperature regimes inevitably affects the biosphere at every level of organization, from ecosystems down to genes. The ecological effects of rising global temperatures on ecosystem function, community structure and composition, and population dynamics and range limits are already apparent (reviewed in Walther *et al.* 2002), and are likely to continue into the foreseeable future (Cramer *et al.* 2001; Sarmiento *et al.* 2004; Colwell *et al.* 2008; Thomas *et al.* 2012). However, the abilities of populations to adapt evolutionarily to a rapidly changing climate are only beginning to be understood (Parmesan 2006; Skelly *et al.* 2007; Listmann *et al.* 2016). The aim of this dissertation is to determine whether and how an ecologically indispensable group of organisms, the phytoplankton, may respond evolutionarily to global climate change. I examined this question through the lens of experimental evolution to determine the capacity of a common, ubiquitous marine diatom to undergo rapid evolution—that is, to evolve at a rate greater than or comparable to the current rate of change of global sea surface temperatures.

Understanding the evolutionary capacity of phytoplankton is crucial to predicting the effects of global climate change on marine ecology, global biogeochemistry, and even human health (Kang 2011) and food security (Litzow *et al.* 2006; Barange *et al.* 2014). Phytoplankton are responsible for ~50% of global net primary production, and are fundamental drivers of global carbon, nitrogen, phosphorus, and other biogeochemical cycles (Redfield 1958; Field *et al.* 1998;

Falkowski *et al.* 1998). They are the foundation of most marine and freshwater food webs, and may be the single most important source of omega-3 fatty acids consumed by humans (Arts *et al.* 2001; Kang 2011). They are also indicator species, responding quickly and dramatically to environmental change (Nehring 1998; Hampton *et al.* 2008; Boyce *et al.* 2010). Given their vast population sizes and rapid rates of reproduction, a comprehensive understanding of the responses of phytoplankton to global climate change requires an integrative approach in which their physiology, their ecology, and their evolution are studied in concert.

I subjected the ubiquitous model marine diatom *Thalassiosira pseudonana* to temperatures at the low and high extremes of its thermal tolerance range for 500 generations and quantified evolutionary divergence in a number of key physiological traits. I first examined the effects of directional temperature selection on *T. pseudonana*'s thermal reaction norm for per-capita population growth rate. I then tested the effects of temperature selection on the thermal reaction norms of a set of organismal traits—fatty acid content and composition, carbon-nitrogen-phosphorus stoichiometry, chlorophyll *a* content, photosynthetic carbon assimilation efficiency, and cell morphology—that are known to depend on temperature (Eppley 1972; James *et al.* 1989; Yvon-Durocher *et al.* 2017), and that are of great ecological importance.

This dissertation contributes to a nascent but growing body of knowledge about rapid thermal adaptation in phytoplankton and about thermal adaptation in general. It expands on the known modes of variation of the thermal reaction norm (Izem & Kingsolver 2005), and offers a glimpse of some mechanisms that may underlie adaptation to temperature. Importantly, this work also illuminates a number of unanswered questions about the genetic basis of thermal adaptation, the relevance of the results to other species, and the ecological outlook for species that are able to evolve in step with rising global temperatures and for the communities they inhabit.

REFERENCES

REFERENCES

Arts MT, Ackman RG, Holub BJ. 2001. "Essential fatty acids" in aquatic ecosystems: a crucial link between diet and human health and evolution. *Canadian Journal of Fisheries and Aquatic Sciences* **58**:122-137.

Barange M, Marino G, Blanchard JL, Scholtens J, Harle J, *et al.* 2014. Impacts of climate change on marine ecosystem production in societies dependent on fisheries. *Nature Climate Change* **4**:211-216.

Boyce DG, Lewis MR, Worm B. 2010. Global phytoplankton decline over the past century. *Nature* **466**:591-596.

Colwell RK, Brehm G, Cardelús CL, Gilman AC, Longino JT. 2008. Global warming, elevational range shifts, and lowland biotic attrition in the wet tropics. *Science* **322**:258-261.

Cramer W, Bondeau A, Woodward FI, Prentice IC, Betts RA, *et al.* 2001. Global response of terrestrial ecosystem structure and function to CO_2 and climate change: results from six dynamic global vegetation models. *Global Change Biology* **7**:357-373.

Eppley RW. 1972. Temperature and phytoplankton growth in the sea. *Fisheries Bulletin* **70**:1063-1085.

Falkowski PG, Barber RT, Smetacek V. 1998. Biogeochemical controls and feedbacks on ocean primary production. *Science* **281**:200-201.

Field CB, Behrenfeld MJ, Randerson JT, Falkowski PG. Primary production of the biosphere: integrating terrestrial and oceanic components. *Science* **281**:237-240.

Hampton SE, Izmest'eva LR, Moore MV, Katz SL, Dennis B, *et al.* 2008. Sixty years of environmental change in the world's largest freshwater lake – Lake Baikal, Siberia. *Global Change Biology* **14**:1947-1958.

Izem R, Kingsolver JG. 2005. Variation in continuous reaction norms: quantifying directions of biological interest. *The American Naturalist* **166**:277-289.

James CM, Al-Hinty S, Salman AE. 1989. Growth and ω3 fatty acid and amino acid composition of microalgae under difference temperature regimes. *Aquaculture* **77**:337-351.

Kang JX. Omega-3: a link between global change and human health. *Biotechnology Advances* **29**:388-390.

Listmann L, LeRoch M, Schlüter L, Thomas MK, Reusch TBH. 2016. Swift thermal reaction norm evolution in a key marine phytoplankton species. *Evolutionary Applications* **9**:1156-1164.

Litzow MA, Bailey KM, Prahl FG, Heintz R. 2006. Climate regime shifts and reorganization of fish communities: the essential fatty acid limitation hypothesis. *Marine Ecology Progress Series* **315**:1-11.

Nehring S. 1998. Establishment of thermophilic phytoplankton species in the North Sea: biological indicators of climatic changes? *ICES Journal of Marine Science* **55**:818-823.

Parmesan C. 2006. Ecological and evolutionary responses to recent climate change. *Annual Review of Ecology, Evolution and Systematics* **37**:637-669.

Redfield AC. 1958. The biological control of chemical factors in the environment. *American Scientist* **46**:205-221.

Sarmiento JL, Slater R, Barber L, Bopp L, Doney SC, *et al.* 2004. Response of ocean ecosystems to climate warming. *Global Biogeochemical Cycles* **18**:GB3003.

Skelly DK, Liana NJ, Possingham HP, Freidburg LK, Farrugia TJ, *et al.* 2007. Evolutionary responses to climate change. *Conservation Biology* **21**:1353-1355.

Thomas MK, Kremer CT, Klausmeier CA, Litchman E. 2012. A global pattern of thermal adaptation in marine phytoplankton. *Science* **338**:1085-1088.

Walther G-R, Post E, Convey P, Menzel A, Parmesan C, *et al.* 2002. Ecological responses to recent climate change. *Nature* **416**:389-395.

Yvon-Durocher G, Dossena M, Trimmer M, Woodward G, Allen AP. 2015. Temperature and biogeography of algal stoichiometry. *Global Ecology and Biogeography* **24**:562-570.

CHAPTER 1: Rapid thermal adaptation in a marine diatom reveals constraints and tradeoffs

Introduction

The dependence of physiological processes on temperature is perhaps the most important factor determining the fitness of organisms across latitudinal and altitudinal gradients, and thus their distributions and abundances on Earth. Due to climate warming, many studies have focused on the temperature dependence of physiological traits (e.g., photosynthesis, respiration, per-capita population growth) near the upper bounds of organisms' thermal tolerance ranges (Rowan, 2004; Bradford, 2013; Listmann et al., 2016) and the ecological consequences of temperatures rising beyond those ranges (Rowan, 2004; Bradford, 2013; Listmann et al., 2016; Thomas et al., 2012). Studies have increasingly focused on the potential for rapid evolution of traits in response to temperature change, and how such evolution may mitigate the ecological impacts of climate warming (Hoffmann & Sgrò, 2011; Schlüter et al., 2014; Listmann et al., 2016).

Evolution on ecological timescales may be commonplace (Schoener, 2011) and can 'rescue' populations from potentially catastrophic environmental change (Gomulkiewicz & Holt, 1995; Bell, 2013; Schiffers et al., 2013). In particular, the enormous population sizes and fast reproduction of microorganisms, on the order of hours to days, offer many opportunities for rapid evolution in response to environmental change. Phytoplankton are a diverse and often overlooked microbial group of global importance: they are the foundation of most marine and freshwater food webs and are major drivers of global biogeochemical cycles, carrying out ~50 % of global carbon fixation (Field et al., 1998) and linking nitrogen and phosphorus cycles (Redfield, 1958). Rising temperatures may negatively impact phytoplankton productivity, biomass and species diversity (Boyce et al., 2010; Thomas et al., 2012). However, rapid

adaptation to warming may mitigate some ecological impacts of climate change (Litchman et al., 2012; Listmann et al., 2016). For example, evolutionary change in the thermal optimum for per-capita population growth (T_{opt}) and the maximum temperature at which positive growth is possible (CT_{max}) in response to ocean warming may reduce heat-induced mortality, allowing some species to persist at low latitudes where they might otherwise go regionally extinct (Thomas et al., 2012).

A number of recent evolution experiments have investigated how marine phytoplankton may evolve to cope with environmental change (Reusch & Boyd, 2013), though most have focused only on increased atmospheric pCO_2 and/or ocean acidification (Crawfurd et al., 2011; Lohbeck et al., 2012; Jin et al., 2013). Thermal adaptation has been studied experimentally in only a couple of phytoplankton species, only one of which, a coccolithophorid, was a marine species of global importance (Schlüter et al., 2014; Padfield et al., 2015; Listmann et al., 2016). It is therefore difficult to predict if other ecologically important groups, such as diatoms that contribute up to 25% of all global carbon fixation (Nelson et al., 1995), would respond similarly. Moreover, while we may expect T_{opt} and CT_{max} to increase after evolving at high temperatures (Listmann et al., 2016; Schaum et al., 2017), knowledge of how other important traits may change in response to elevated temperatures is limited, though some significant work has been done on rapid temperature-dependent evolution of metabolic traits in freshwater chlorophytes (Padfield et al., 2015; Schaum et al., 2017). Schlüter et al., (2014) found that after one year of experimental adaptation to elevated temperature (26.3 °C), the marine coccolithophore *Emiliania huxleyi* evolved a higher population growth rate, smaller cell diameter and lower particulate organic and inorganic carbon content compared to cold (15 °C)-adapted populations. Hinners *et al.* (2017) found that 100-year-old resurrected strains of the marine dinoflagellate *Apocalathium*

malmogiense did not differ in cell size or in its thermal reaction norm for growth compared to current strains, but that it did form resting cysts at a higher rate.

Large-scale evolutionary change in nutrient utilization traits in response to changing climate could significantly impact biogeochemical cycling (Field *et al.*, 1998). A number of studies have examined the interactive effects of temperature and nutrient on per-capita population growth rates in phytoplankton (Tilman et al., 1981; Thomas et al., 2017), and some have tested the effects of temperature on elemental (C, N, P) stoichiometry. Martiny et al., (2016) studied temperature effects on growth and elemental stoichiometry in several *Prochlorococcus* species, but did not find consistent trends across closely related species, suggesting that effects of thermal adaptation on nutrient utilization traits are idiosyncratic and not necessarily consistent; Thrane et al., (2017) conducted a large, factorial experiment to elucidate the effect of temperature on optimal N:P supply ratio in the freshwater chlorophyte *Chlamydomonas reinhardtii*; and Yvon-Durocher et al., (2017) studied temperature effects on seston stoichiometry in a mesocosm community, emphasizing long-term evolutionary effects on cellular stoichiometry, also in *C. reinhardtii*. However, this study is novel in that it directly tests whether a key measure of competitive ability for nitrate, nitrate growth affinity, evolves in distinct temperature environments in the model marine diatom *Thalassiosira pseudonana*.

Biological rates in ectotherms vary continuously across temperature and are, thus, often referred to as "function-valued traits" (Kingsolver et al., 2001). Our understanding of how diverse function-valued traits may evolve in different organisms is limited. Tradeoffs (e.g., generalist-specialist or resource-allocation tradeoffs) may be important in determining how the shapes of trait functions, including the thermal reaction norm, evolve (Angilletta et al., 2003). The trait values derived from thermal reaction norms and many other function-valued traits are

non-independent across temperature gradients (Angilletta et al., 2003); thus, selection at one temperature may alter rates (e.g., population growth rate) at every other temperature along the thermal reaction norm. The underlying mechanisms of thermal adaptation and its associated tradeoffs may lie in any of myriad of metabolic and physiological pathways within the organism. For example, allocation of resources to constitutive adaptations to cold environments may preclude those resources from being used to synthesize heat shock proteins when the environment unexpectedly warms; nitrate uptake machinery optimized for warm environments may not function well in cold environments; membrane lipids may be comprised of many highly unsaturated fatty acids in a cold-adapted organism, but such fatty acids lead to excessive membrane fluidity in a warm environment (Jiang & Gao, 2004); or, in any of these cases, plasticity in traits (i.e., in a generalist) may lower the maximum achievable functionality of each trait at every temperature (a generalist-specialist tradeoff).

While recent studies showed that T_{opt} and CT_{max} increase after evolving at higher temperatures (Listmann et al., 2016), we do not know how the whole thermal reaction norm may evolve in phytoplankton; for example, adaptation to high temperatures may lead to a decrease in fitness at low temperatures, as previously observed in bacteria (Bennett & Lenski, 1993) and bacteriophages (Knies et al., 2006). Selection may change the slope and curvature (first and second derivatives) of the thermal reaction norm as well (Kutcherov, 2016), especially if some cardinal temperatures are more evolutionarily labile than others (Araújo et al., 2013). For example, by comparing the peak sharpness at T_{opt} and the width (°C) of the upper tail of the thermal reaction norm in cold- versus warm-selected populations, we may make inferences regarding the evolutionary lability of the maximum growth rate at T_{opt} (μ_{opt}), and of T_{opt} itself, relative to that of CT_{max}; the upward concavity below T_{opt} and the location of the inflection point

on the thermal reaction norm contribute greatly to the magnitude of tradeoffs between growth at temperatures below T_{opt} versus above, which can be indicative of generalist-specialist and/or resource allocation tradeoffs (Gilchrist, 1995; Angilletta et al., 2003).

The thermal reaction norm for population growth depends on the temperature dependences of enzyme activities (Ratkowsky et al., 2005; Corkrey et al., 2014), and few processes or pathways within the cell should be immune to the effects of directional temperature selection (Nedwell, 1999; Padfield et al., 2015; Baker et al., 2016; Schaum et al., 2017). Depending on the genes affected, changes in growth rate may be accompanied by changes in traits not directly associated with the thermal reaction norm. For example, stoichiometry may respond to thermal adaptation due to changes in relative resource requirements of phytoplankton cells, which in turn may affect species' competitive abilities (e.g. for N and P) and ultimately global biogeochemical cycles (Redfield, 1958; Litchman et al., 2007; Baker et al., 2016). An increase in maximum growth rate at the selection temperature may lead to a decrease in affinity for a given nutrient due to a tradeoff between allocation of cellular resources to reproduction versus nutrient uptake (Grover, 1991; Klausmeier et al., 2004). If the nutrient in question is never limiting, selection may favor a high maximum growth rate over affinity, and the tradeoff may ultimately result in a weakening of competitive ability for that nutrient in the selection environment. Moreover, adaptation to high temperature may require higher investment in repair machinery, such as heat shock proteins, potentially increasing the demand for nitrogen and other nutrients.

Here, we performed a 350-generation selection experiment on a model marine diatom, *Thalassiosira pseudonana*, to determine whether and how its thermal performance curves evolve and diverge under selection at two different temperatures, above and below the growth optimum,

and whether other key traits, such as nitrate utilization traits, evolve as well. Post-selection, we conducted temperature and nutrient-dependent growth assays to assess evolutionary divergence in temperature and nutrient traits resulting from thermal adaptation.

Materials and Methods

Temperature selection experiment

We obtained a monoculture of *Thalassiosira pseudonana* CCMP1335 (Hustedt) Hasle et Heimdal from the Provasoli-Guillard National Center for Culture of Marine Phytoplankton (CCMP), Maine, USA, and isolated a single cell by plating on agarose ESAW marine culture medium (Harrison et al., 1980). Nitrogen (as $NaNO_3$), phosphorus (as $NaH_2PO_4 \cdot H_2O$) and silicon (as $NaSiO_3 \cdot 9H_2O$) concentrations were 549 μmol l^{-1}, 22.4 μmol l^{-1}, and 106 μmol l^{-1}, respectively. We cultured the resulting colony in a flask of ESAW medium until it reached a high density. "Generation zero" was on April 14, 2014, when we propagated ten replicate populations from the progenitor culture ("selection lines" hereafter) into 20 ml ESAW medium in 50 ml Cellstar polystyrene tissue culture flasks with breathable caps (Greiner Bio-One GmbH, Frickenhausen, Germany), which we gently agitated daily to keep cells in suspension. We assigned five replicates to the 16°C treatment and the other five to 31°C. These two temperatures were below and above the previously-recorded thermal optimum (T_{opt}) of *T. pseudonana* (between 24 and 26°C) (Boyd et al., 2013) under similar culture conditions. We chose these selection temperatures so that the maximum growth rates (μ_{max}) at the two temperatures were roughly equal (~0.8 d^{-1} at the start of the experiment). The low temperature treatment was close to the ancestral maintenance temperature of 14°C (see technical specifications on CCMP1335 culture maintenance at https://ncma.bigelow.org/catalogsearch/result/?q=1335) and 16°C was

thus used for the main comparison of the evolution in response to different temperatures. Such a comparison allows isolation of the selection effect of temperature itself from the effect of the cultivation regime, as both temperature treatments experience the same maintenance for the duration of the experiment. In contrast, the common comparison in many experimental evolution studies of the treatment and the ancestral strain that did not experience the same selection regime may confound the effect of the focal selection force and the culturing conditions.

Selection lines were maintained in temperature-controlled growth chambers at 110 μmol photons m^{-2} s^{-1} under a 14:10 light:dark cycle (note that this is 10 µmol photons m^{-2} s^{-1} higher than the light level in Boyd et al., (2013), but still in the saturating range). All lines were maintained in ESAW medium for ~50 generations at a dilution rate of 0.5 d^{-1} (diluted daily), after which (August 12, 2014) all cultures were transferred to L1 medium (Guillard & Hargraves, 1993) due to poor culture health in ESAW. L1 was made using 43.465 g l^{-1} artificial sea salt (Tropic Marin, Wartenberg, Germany), which yields a specific gravity of 1.025, similar to natural seawater, with $NaNO_3$, $NaH_2PO_4 \cdot H_2O$, and $NaSiO_3 \cdot 9H_2O$ concentrations of 882 μmol l^{-1}, 36.3 μmol l^{-1}, and 107 μmol l^{-1}, respectively. Upon switching culture media, we also altered the dilution regime, such that 10^6 cells (usually ~0.5-1.0 ml) were transferred to fresh medium every 4 d (with occasional deviations of ±1 d). The selection lines required an additional ~50 generations to adjust to the new dilution regime before consistent growth rates and culture health were achieved. These changes led to a substantial reduction in the variability of growth rates over time. Cell densities of all replicate cultures were determined at each transfer for the remainder of the experiment using a CASY particle counter (Schärfe System GmbH, Reutlingen, Germany), and average population growth rates for each propagation period determined by taking $\log(N_t/N_0)/t$, where N is the population density and t is time in days.

Temperature-dependent growth assays

To evaluate evolutionary change in thermal reaction norms after ~350 generations, we conducted temperature-dependent population growth assays on evolved selection lines. First, we sub-cultured all selection lines and acclimated sub-cultures to ten temperatures spanning the thermal niche for ~12 generations (days to acclimation ranged from ~10 d at near-optimal temperatures to more than a month at 3°C). Approximately 10^5 cells from each acclimated culture were then propagated into an identical flask containing fresh L1 medium, and the cell density was estimated daily at the acclimated temperature until stationary phase (5-10 d, depending on the temperature). Light conditions were as above. Culture density was estimated daily at all temperatures ≥16°C by placing the polystyrene culture flask in a Shimadzu UV-2401PC spectrophotometer (Shimadzu Corporation, Kyoto, Japan) and measuring Abs_{436} (the wavelength corresponding to the absorbance maximum of chlorophyll *a*: Neori et al., 1986); At 3 and 10°C, due to fogging of culture flasks, daily density estimates were conducted using the CASY counter instead; to make sure density estimation method did not bias estimates, we checked model residuals at 3 and 10°C against those from other temperatures, and found no indication of method-induced bias (see Appendix A, Figure A1). We calculated exponential growth rates by fitting regression lines to log-transformed population densities over time; with a minimum of three points that best represented exponential-phase growth (those that formed a straight line when log-transformed). Single cultures of each selection line were assayed at each temperature, except those at 16 and 31°C, which were assayed in triplicate to facilitate direct statistical comparison of growth rates (n = 14 total points per thermal reaction norm). This comparison serves as a "reciprocal transplant" experiment, a common approach to test for local adaptation (Kawecki & Ebert, 2004; Blanquart et al., 2013).

We derived temperature-dependent trait values by fitting a model proposed by Logan et al., (1976) and recently used by Thomas et al., (2017), in which birth and death are both exponential functions of temperature. The resulting curve is a unimodal, left-skewed thermal reaction norm. In the following double-exponential equation, the first term is the exponential birth term, the second term is the exponential mortality term:

$$\mu_{max} = b_1 e^{b_2 T} - d_1 e^{d_2 T} - d_0 \qquad (1),$$

where μ_{max} is the specific growth rate (d^{-1}), T is temperature, b_1 and d_1 are the pre-exponential constants for birth and death, respectively, b_2 and d_2 are the exponential rates of increase in both terms, and d_0 is the temperature-independent death rate. To facilitate fitting this model, we used an alternative parameterization of (1) that includes an explicit T_{opt} parameter, thus making it possible to directly compute 95% confidence intervals for this trait (see Appendix B); the two formulations are mathematically equivalent and yield similar fits. We determined the "sharpness" of the thermal reaction norm peaks by taking the second derivative of the thermal reaction norm with respect to temperature at T_{opt} ("Peak sharpness" [Figure 3b] is the negative of this number), and the upward-concavity below T_{opt} by computing the maxima in the second derivative across $0 \leq T \leq T_{opt}$. We estimated the inflection point of each thermal reaction norm by setting $\frac{\partial^2 \mu_{max}}{\partial T^2} = 0$ and solving for T within the range $0 \leq T \leq T_{opt}$.

Nitrate-dependent growth assays

Per-capita population growth as a function of external nitrate concentration can be described using the Monod equation (Monod, 1949):

$$\frac{1}{N}\frac{dN}{dt} = \frac{\mu_{max} aR}{\mu_{max} + aR} \quad (2),$$

where N is the population density, R is the resource (nitrate) concentration, μ_{max} is the resource-saturated (maximum) population growth rate, and a (liters μmol^{-1} d^{-1}) is the nitrate growth affinity (the initial slope of the Monod curve). Note that this formulation directly incorporates the affinity a, rather than the traditional formulation with the half-saturation constant for growth, K. Growth affinity is a more mechanistic parameter because it is more directly indicative of competitive ability (Healy, 1980). The two parameters are related by $K = \mu_{\max}/a$. For a full derivation of Equation 2, see Appendix B.

To determine if the nutrient-related traits changed as a result of adaptation to different temperatures, we estimated Monod growth curves for nitrate at 16 and 31°C after ~450 generations. The difference in the number of generations elapsed for the temperature and nutrient trait assays was due to the logistical infeasibility of running those experiments simultaneously. We investigated whether temperature selection had caused evolutionary divergence in nitrate growth affinities between lines from each temperature treatment when assayed at both selection temperatures, and whether this divergence corresponded to the tradeoff between the maximum growth rate and nitrate growth affinity. Selection lines were assayed in triplicate at each selection temperature and at ten nitrate concentrations (0, 2.5, 5 10, 20, 40, 60, 90, 180 and 882 µmol l^{-1}), the latter being the N concentration of undiluted L1 medium). Prior to the Monod assay, all lines were acclimated to assay temperatures as above, followed by a 5-day N-starvation period in which cultures were kept in modified N-free L1 medium. Population growth rates were estimated as for temperature-dependent growth assays. In some replicates, an opaque, white contaminant

was visible, which appeared under the microscope to be bacteria; these replicates were excluded from analyses.

Model fitting, trait estimation and statistical analysis

We conducted all statistical analyses using R statistical programming language, version 3.3.2. We fit Equation (1) to temperature-dependent growth data using the "mle2()" function from the "bbmle" package (Bolker et al., 2017). Due to high uncertainty in some growth rate estimates in Monod assays, we used weighted, nonlinear least squares regression to fit Equation (2) to nutrient-dependent growth data, weighting growth rate estimates by their inverse variances.

We compared traits derived from thermal reaction norms by conducting ANOVA on weighted least squares linear models. To quantify uncertainty in all trait estimates (except T_{opt}) for each selection line, we conducted 1000 residual bootstraps of the double-exponential fits using a procedure described in Listmann et al., (2016). We incorporated this uncertainty into linear models by weighting each trait estimate for each selection line by the inverse of the variance of its bootstrap distribution (see Appendix A, Model 1), except in the case of T_{opt}, where we were able to directly employ its variance, though T_{opt} variances estimated directly were nearly identical to those estimated via bootstrapping (Appendix A, Figure A3).

We used a nested ANOVA to compare maximum growth rates (μ_{max}) at the selection temperatures in a reciprocal transplant (all 16°C- and 31°C-selected lines assayed at both temperatures). Uncertainty in μ_{max} could be estimated directly (n = 3, no bootstraps), and we fit a *selection temperature* × *assay temperature* interaction and nested replicate selection line within selection temperature to test for local adaptation and strain-level selection temperature effects,

respectively (Appendix A, Model A2).

We compared μ_{max} and nitrate growth affinity (a_{NO3}) estimates derived from fits of the Monod equation to growth rates estimated across a nitrate gradient at the selection temperatures (reciprocal transplant scenario) using two-way ANOVA conducted on weighted, least squares linear models (Appendix A, Equation A3), as above. Uncertainties in these trait estimates were estimated directly when fitting the Monod equation, as its parameters are the traits being compared; uncertainties were incorporated into the linear model as weights ($1/\sigma^2$), as was done with bootstrap variances above. To test for a global tradeoff between μ_{max} and a_{NO3} within selection groups (pooled across assay temperatures), we used Deming regression, a form of orthogonal regression that allows for uncertainty in individual measurements and assumes unequal variances in x and y. We conducted this test using the "mcreg()" function in the "mcr" package in *R* (Manuilova et al., 2014). Note in the results below that we did not obtain *t*-statistics or *p*-values from the Deming regression, but that we used a bootstrapping option built into the mcreg() function to calculate 95% confidence intervals for slopes and intercepts. All data files and R code used in this study are included in the supporting information.

Results

Evolutionary change in thermal reaction norms

Growth for 350 generations at two different temperatures, below and above the temperature optimum for *T. pseudonana* (16 and 31°C), led to a significant divergence of the thermal reaction norms (Figure 1). T_{opt} was 1.87°C higher, on average, in selection lines evolved at 31°C than in those evolved at 16°C ($F_{1,8}$ = 17.02; P = 0.0033; Figure 2a; Appendix A, Table A1); the maximum growth rate at T_{opt} (μ_{opt}) was also ~0.1 d^{-1} higher in 31°C-selected lines ($F_{1,8}$ = 7.99; P

= 0.022; Figure 2b; Appendix A, Table A1). CT_{max} trended higher in 31°C-selected lines than in 16°C-selected lines, with one exception (replicate line 31_5), though the difference was not statistically significant ($F_{1,8} = 2.09$; P = 0.19; Figure 2c; Appendix A, Table A1).

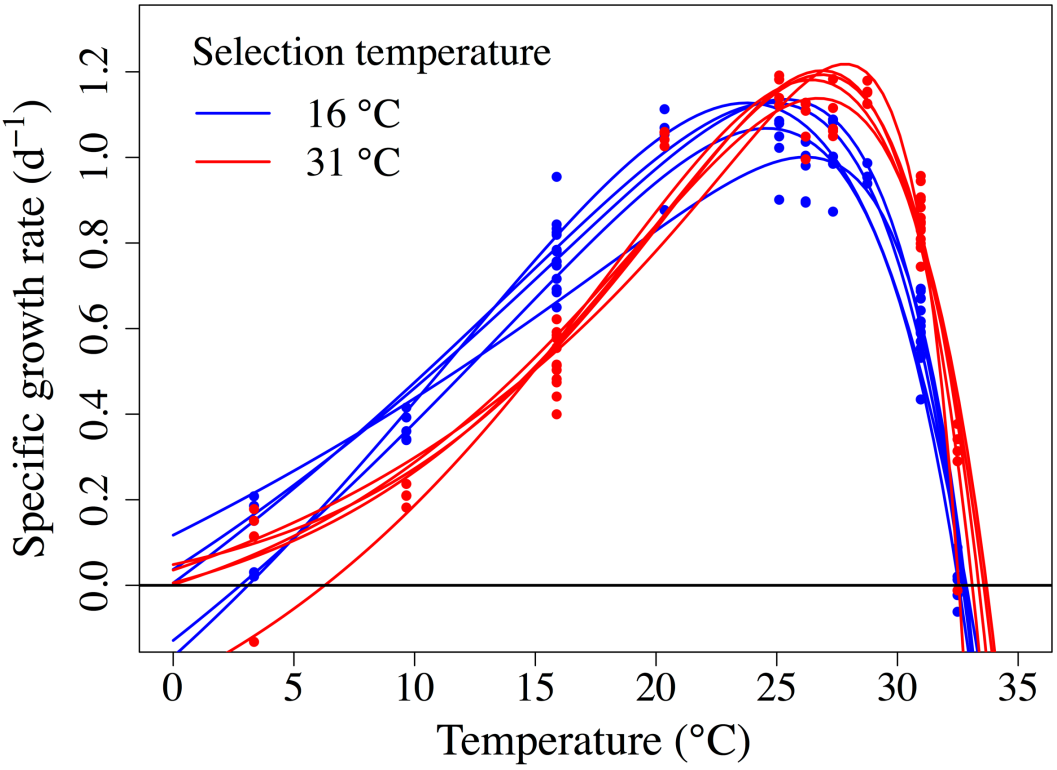

Figure 1: Thermal reaction norms for per-capita population growth of 10 *T. pseudonana* populations. Growth rates were measured at 10 temperatures for each replicate population (five selected at 16°C [red] and five selected at 31°C [blue]) after 350 generations of experimental selection. Growth rates were measured in triplicate at the selection temperatures (reciprocal transplant scenario). N = 14 for each curve.

A "reciprocal transplant" comparison between temperature treatments revealed that selection lines from each treatment had higher maximum growth rates (μ_{max}) in their "home" temperature environments than in "away" environments; "local" lines also had higher growth

rates than "foreign" lines (*assay temp.* × *selection temp.* interaction: $F_{1,8} = 254.82$; $P < 0.0001$; Figure 2d; Appendix A, Table A1; see Appendix A, Figure A2 for population-level effects). Taken together, these results are the signature of local adaptation to temperature (Kawecki & Ebert, 2004; Blanquart et al., 2013). While μ_{max} estimates differed slightly between 350 and 450 generations (measured for thermal reaction norm and Monod assays, respectively), differences were not directionally consistent across selection lines, and the overall pattern of local adaptation persisted (see next section; Appendix A, Figure A5a; Appendix A, Table A3).

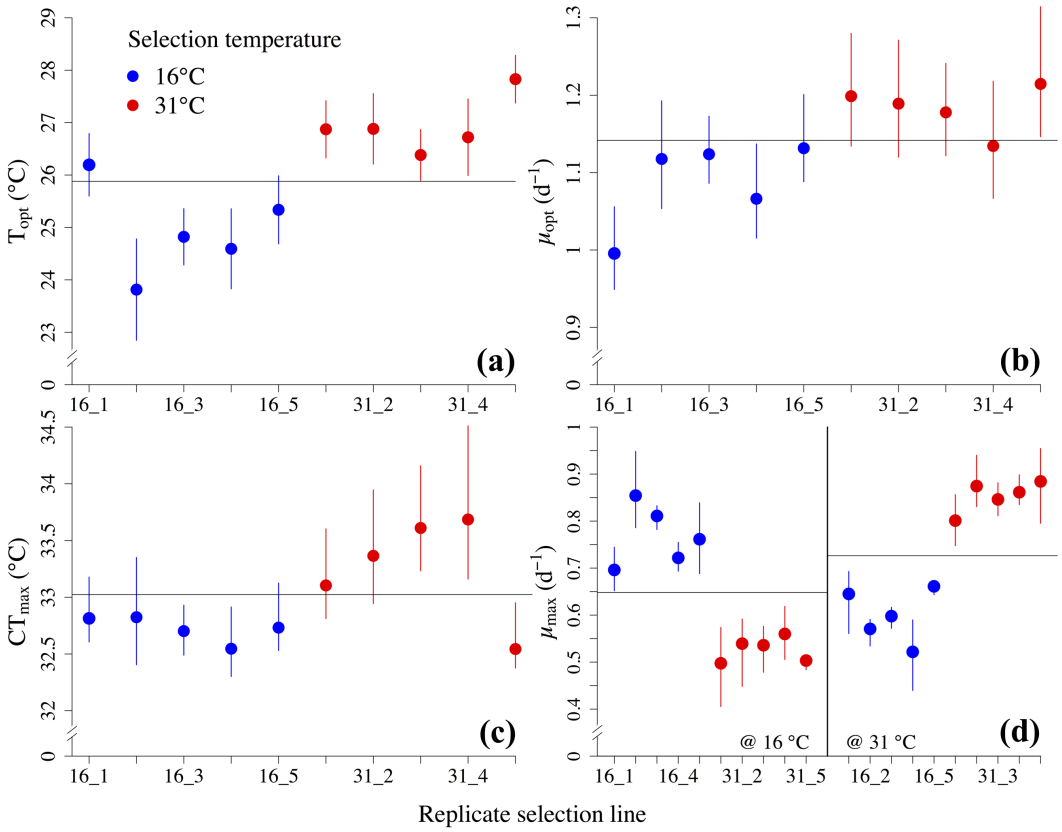

Figure 2: **Thermal performance traits of 16°C- and 31°C-selected populations. I.** (A) Thermal optimum (T_{opt}); (B) Maximum growth rates at T_{opt} (μ_{opt}); (C) Upper critical temperature (CT_{max}); (D) μ_{max} at the selection temperatures in the reciprocal transplant scenario (both selection groups assayed at both selection temperatures). All trait estimates in (B-C) were

derived numerically from fits of the double-exponential model. Bars in (A) are Fisher's 95% CI estimated directly from the standard errors of double-exponential T_{opt} parameter estimates. Bars in (B-C) are 95% CI estimated as 2.5%-97.5% quantiles of bootstrap distributions (n = 1000 bootstraps for each replicate population); bars in (D) are 95% CI directly from triplicate growth rate estimates (no bootstrapping). In (A-C), the horizontal line across the whole panel is the grand mean across trait estimates for all replicate populations; in (D), horizontal lines are grand means for assay temperature groups.

The peaks of the thermal reaction norms of 31°C-selected lines appeared sharper, and the left tails more deeply concave-up than those of 16°C -selected lines, both for the parametric (Figure 1) and nonparametric (Appendix A, Figure A6) thermal reaction norms. These observations, combined with the statistically nonsignificant difference in CT_{max} between the two selection regimes, led us to hypothesize that CT_{max} is less evolutionarily labile than T_{opt}, resulting in greater skew in thermal reaction norms of 31°C-selected lines, rather than a simple rightward shift of the thermal reaction norms along the temperature axis. The difficulty in reliably estimating CT_{min} prevented statistical comparisons of CT_{min} and of thermal niche width among selection lines, and also prevented estimation of skewness. However, we determined the distance between T_{opt} and CT_{max} for all bootstrapped thermal reaction norms; ideally, this distance would be scaled by thermal niche width, but absence of reliable thermal niche width estimates prevented scaling. The distance between T_{opt} and CT_{max} ("upper tail length") was smaller in 31°C-selected lines than in 16°C-selected lines ($F_{1,8} = 6.58$; $P = 0.033$; Figure 3a; Appendix A, Table A2), suggesting that the change in T_{opt} was greater than the change in CT_{max} at one or, possibly, both selection temperatures. 31°C-selected lines had sharper peaks at T_{opt} ($F_{1,8} = 26.77$;

P = 0.00085; Figure 3b; Appendix A, Table A2), were more deeply concave-up below T_{opt} ($F_{1,8}$ = 91.41; P < 0.0001; Figure 3c; Appendix A, Table A2), and had inflection points at higher temperatures than 16°C-selected lines ($F_{1,8}$ = 12.36; P = 0.0079; Figure 3d; Appendix A, Table A2), suggesting greater negative skew.

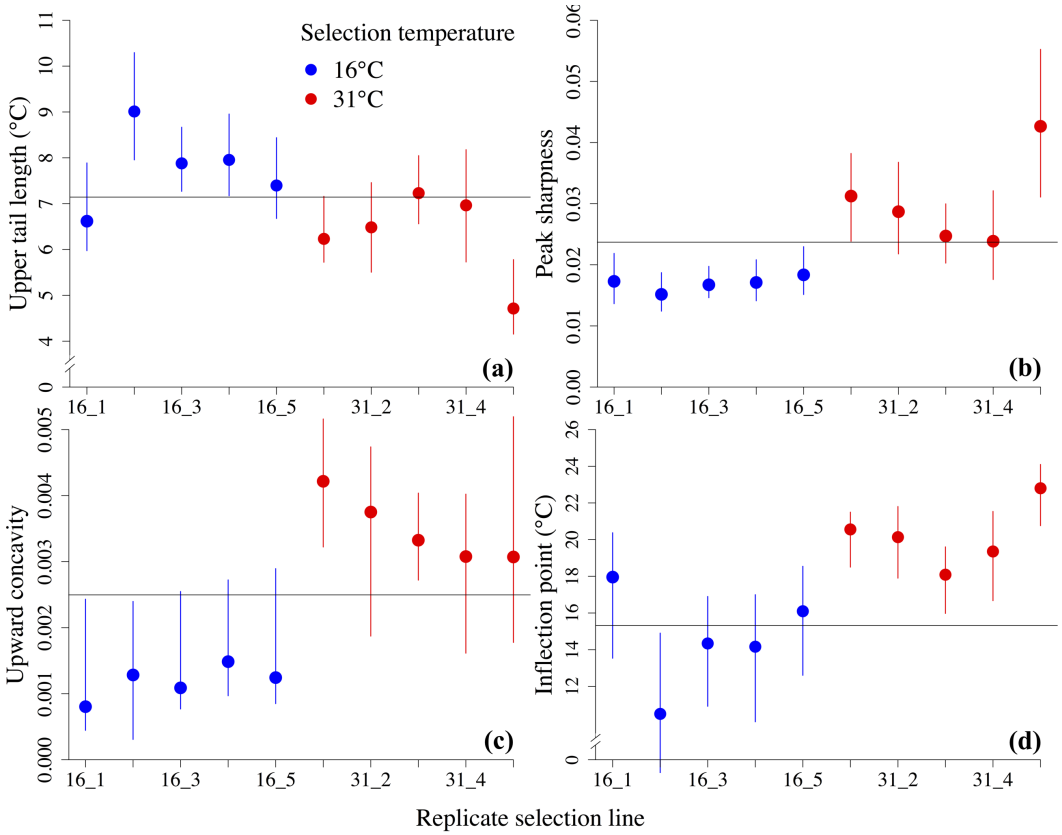

Figure 3: Thermal performance traits of 16°C- and 31°C-selected populations. II. (A) Upper tail lengths ($CT_{max} - T_{opt}$) derived numerically from double-exponential curves (n = 1000 bootstraps). (B) Peak sharpness of double-exponential curves. Sharpness is calculated as the negative of the second derivative of the double-exponential curve with respect to temperature at T_{opt} (larger values represent more negative gradients). (C) Upward concavity of double-exponential curves below T_{opt}, calculated as the maximum of the second derivative across $0 \leq T$

$\leq T_{opt}$. (D) The inflection point below T_{opt}, where $\frac{\partial^2 \mu_{max}}{\partial T^2} = 0$. Symbols are as in Figure 2.

Evolution of competitive ability for nitrate

Temperature selection did not lead to consistent evolutionary divergence in competitive ability for nitrate; there was no significant effect of assay temperature ($F_{1,16} = 0.27$; $P = 0.61$) or selection temperature ($F_{1,16} = 1.26$; $P = 0.28$) on nitrate growth affinity (a_{NO3}), nor was there an *assay temperature* × *selection temperature* interaction ($F_{1,16} = 0.12$; $P = 0.74$; Appendix A, Table A3; Appendix A, Figure A4; Appendix A, Figure A5). The differences in a_{NO3} among selection groups or assay temperatures appeared idiosyncratic, with estimates ranging over nearly an order of magnitude across replicate populations. However, as in the reciprocal transplant above, there was a significant *selection temperature* × *assay temperature* interaction effect on μ_{max} estimates derived from Monod fits ($F_{1,16} = 10.79$, $P = 0.0047$; Appendix A, Table A3; Appendix A, Figure A4; Appendix A, Figure 5). A tradeoff between the maximum growth rate and nitrate growth affinity was apparent in the 16°C-selected lines (Deming regression ± 95% CI: slope = -0.098 ± 0.075; intercept = 0.11 ± 0.074) but was not statistically significant in the 31°C-selected lines (slope = -0.21 ± 0.35; intercept = 0.24 ± 0.61), with replicates pooled across assay temperatures (Figure 4).

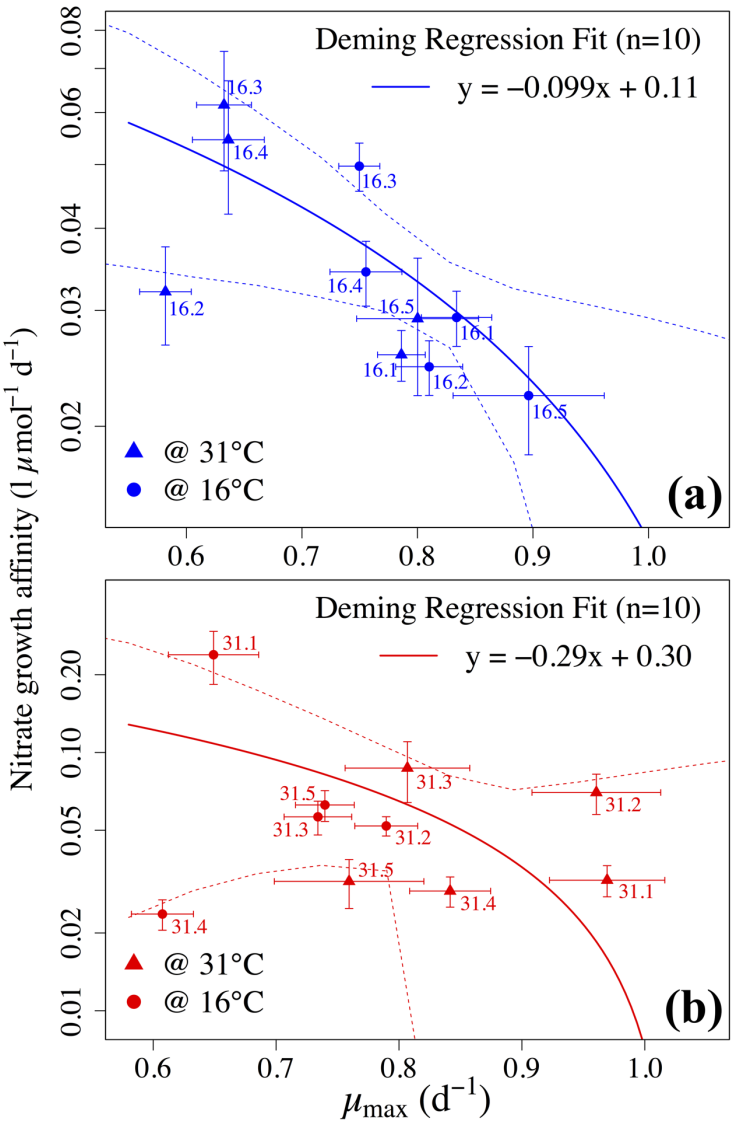

Figure 4: Deming regression plots for nitrate growth affinity (a_{NO3}) versus maximum growth rate (μ_{max}). Traits are estimated from maximum likelihood fits of the Monod equation to nitrate-dependent growth assay data. (A) 16°C-selected lines; (B) 31°C-selected lines. Curves are Deming regression fits. Confidence bands are calculated using a residual bootstrap of the regression fit (n = 1000 bootstraps), and account for uncertainty in each point, taken from Monod equation fits. All points are displayed with ±1 SEM from Monod parameter estimates. Note that y-axis scales differ between panels, and that y-axes in both panels are on a log scale, resulting in apparent curvature of linear fits.

Discussion

Evidence that phytoplankton can evolve rapidly in response to environmental change is mounting (Collins & Bell, 2004; Hutchins et al., 2015; Listmann et al., 2016), but the response even to a single, directional selection pressure can be multifaceted (Low-Décarie et al., 2013; Schlüter et al., 2014, Hutchins et al., 2015). We showed that adaptation to different temperatures not only changes the growth rate at the selection temperature, but also significantly alters the shape of the whole thermal reaction norm, a function-valued trait. The changes included shifts of a critical temperature trait, T_{opt}, and changes in the slope and curvature of the thermal reaction norm. Adaptation to high temperature resulted in a growth rate decline at low temperatures (a performance tradeoff). In contrast, despite some evidence for a tradeoff between maximum growth rate (μ_{max}) and competitive ability for nitrate (indicated by nitrate growth affinity, a_{NO3}) in the 16°C-selected populations (Figure 4), evolution of high μ_{max} did not consistently lead to a reduction in a_{NO3} under the selection conditions in this study. Pleiotropic effects (Elena & Lenski, 2003) or resource allocation or acquisition tradeoffs (Gilchrist, 1995; Angilletta et al., 2003) associated with nitrogen acquisition or utilization were apparently minimal or absent.

While we cannot be certain that selection was stronger and the degree of evolution greater in warm- versus cold-adapted populations or *vice versa* (we lack a common, ancestral thermal reaction norm for our *T. pseudonana* populations, as assays on ancestral strains were conducted in ESAW medium preventing direct comparisons to contemporary strains), we can confidently infer evolutionary divergence between 16°C- and 31°C-adapted populations from their measured derived traits (as in Huey et al., 1991). Selection at 31°C, well above the previously recorded T_{opt} for *T. pseudonana* (Boyd et al., 2013) led to a divergence in T_{opt} of ~2 °C, on average. Furthermore, at the conclusion of the evolution experiment, T_{opt} of 16°C-selected

were comparable to previously observed T_{opt} for *T. pseudonana* (Boyd et al. 2013), suggesting that the divergence between 16°C- and 31°C-selected populations was primarily driven by evolution of higher T_{opt} in 31°C-selected populations. Concurrent with this shift, the maximum growth rate at T_{opt} (μ_{opt}) diverged by ~0.1 d^{-1} ("vertical shift" [Kingsolver *et al.* 2005]); notably, the vertical shift also coincided with a narrowing of the region of the thermal reaction norm immediately adjacent to T_{opt} in 31°C-selected lines, such that less of the curve was in the near-optimal range (Figure 1). All strains but one (replicate line 16_1) met both the "local versus foreign" and "home versus away" criteria for demonstrating local adaptation at both 16°C and 31°C (Kawecki & Ebert, 2004; Blanquart et al., 2013).

The results suggest that the variation in *T. pseudonana*'s thermal reaction norm caused by thermal adaptation led to (or was driven by) a number of tradeoffs. First, while we could not precisely estimate CT_{min} or the thermal niche width, the performance tradeoff resulting from selection at 16°C versus at 31°C, combined with change in T_{opt} (and a suggestion of change in CT_{max}, though this was non-significant) suggest some horizontal shift in the thermal reaction norm (Izem & Kingsolver, 2005; Kingsolver, 2009), as previously observed in bacteriophages (Knies et al., 2006) and the marine coccolithophore *Emiliana huxleyi* (Listmann et al., 2016)—however, this tradeoff may also result from thermal reaction norms of 31°C-selected populations becoming more concave-up below T_{opt}, and from changes in their higher inflection points (Figure 3). In addition, both temperature "generalist-specialist" and resource allocation tradeoffs were apparent (Gilchrist 1995; Angilletta et al., 2003), leading to a "diagonal stretch" in thermal reaction norms toward the upper right. The higher, sharper peaks and compressed upper tails in the thermal reaction norm of 31°C-selected lines, accompanied by a reduction in fitness at 16°C, suggest greater specialization for growth at high temperatures in 31°C-selected lines and less

specialization in general in 16°C-selected lines.

We hypothesized that the evolutionary changes in the shape of the thermal reaction norm in response to selection at high temperature may be explained by increased allocation to cellular repair machinery. To test the plausibility of this hypothesis, we modified Equation (1) to include differential allocation to repair machinery, which provides the benefit of high-temperature tolerance while incurring the costs of increased nutrient requirements and reduced growth. In high-temperature adapted species, the thermodynamically predicted temperature of maximum enzyme stability falls well below the statistically fit T_{opt} (Ratkowsky et al., 1995; Corkrey et al., 2014), suggesting that it is rapid repair, rather than enhanced stability of enzymes that allows for positive growth at very high temperatures. The tradeoff in the following model assumes lack of plasticity in resource allocation to enzyme repair at high temperatures versus reproduction across temperatures (Angilletta et al., 2003).

$$f(T) = b_1 e^{b_2 T} - d_1 e^{d_2 T} - d_0, \quad (3.1)$$

$$d_1 = \frac{d_1'}{p} \quad (3.2)$$

$$q = q_0 + q_1 p \quad (3.3)$$

$$b_1 = \frac{b_1'}{q}, \quad (3.4)$$

Here, the exponential mortality term ($d_1 e^{d_2 T}$ in [3.1]) is weighted inversely by p, which represents investment in protection from heat-induced denaturation of enzymes (or the induction of repair enzyme activity) (3.2); q is the nutrient content of a cell (quota), which is linearly related to p (3.3). Thus, as investment in protection and repair increases, temperature-dependent mortality decreases. However, temperature-dependent birth is also negatively affected as resources are diverted from reproduction and allocated to protection (3.4). The modified double-exponential model can produce changes in the curvature of the thermal reaction norm similar to

those observed in our *T. pseudonana* selection experiment (Figure 5). The model predicts that peak sharpness at T_{opt}, upward concavity below T_{opt}, and the location of the inflection point are all positive, saturating functions of p (Appendix A, Figure A7).

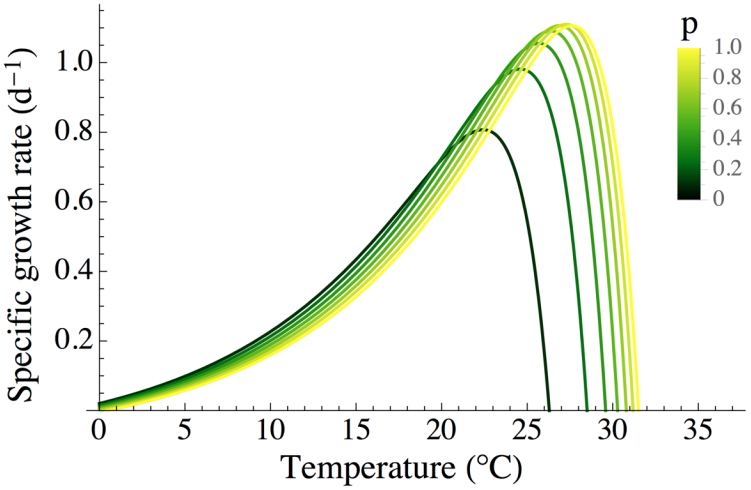

Figure 5: The modified double-exponential model with allocation to thermal protection (p) ranging from 0.1 to 1. Other parameter values are as follows: $b_1 = 0.124$, $b_2 = 0.1$, $d_0 = 0.1$, $d_1 = 3.059\times10^{-7}$, $d_2 = 0.5$, $q_0 = 1$, $q_1 = 0.3$.

There are two observed results that this model does not predict, though the second follows from the first. First, the model predicts comparable evolutionary lability of T_{opt} and CT_{max} (Appendix A, Figure A7a), while in experiments, the difference in CT_{max} between 31°C- and 16°C-selected populations was not statistically significant. Evolution of CT_{max} may thus be constrained by other physiological barriers not incorporated in the model. Second, the model predicts that upper tail length is a positive, saturating function of p, only changing appreciably where $p < 0.2$ (Appendix A, Figure A7b). In contrast, the upper tails of our experimentally derived thermal reaction norms were more compressed in 31°C-selected lines, compared to

16°C-selected lines (Figure 3a), and ranged in width from ~4°C to ~9°C. Although evolution of CT_{max} in response to temperature selection has been observed in the bacterium *Escherichia coli* (Mongold et al., 1996) and in the marine coccolithophore *Emiliana huxleyi* (Listmann et al., 2016), the lack of significant change in CT_{max} relative to T_{opt} in this study suggest that, at least in *T. pseudonana*, T_{opt} is more evolutionarily labile than CT_{max} (Araújo et al., 2013). However, the vast diversity in CT_{max} in nature (Thomas et al., 2012; Corkrey et al., 2014), and in diatoms in particular (Thomas et al., 2016), indicates that such constraints are not evolutionarily insurmountable. It is possible that on timescales relevant to the current rate of increase of global sea surface temperature, constraints on evolution of a higher CT_{max} may cause regional extinctions, contributing to diversity loss, especially at low latitudes (Thomas et al., 2012).

The tradeoff between μ_{max} and resource affinities may be a general trend in nature (Grover, 1991; Klausmeier et al., 2007), but the overall weak and idiosyncratic response of nitrate affinity to temperature selection in our experiment may imply that temperature selection acted most strongly on systems other than those involved in nitrate uptake and utilization. However, the apparent tradeoff in 16°C-selected lines but not in 31°C-selected lines (Figure 4) suggests that thermal adaptation to high temperature may make the tradeoff weaker. In the absence of persistent nutrient limitation (and thus any selection for enhanced nutrient competitive ability, as was likely the case here), selection at a constant temperature should favor high μ_{max} at that temperature. If a μ_{max}-a_{NO3} tradeoff were driven by temperature selection, we would predict a concomitant decrease in competitive ability for nitrate, but changes in a_{NO3} in response to temperature selection were not consistent and did not suggest a tradeoff driven by temperature selection. Here, μ_{max} at both "home" and "away" temperatures changed predictably in response to temperature selection, but a_{NO3} did not. The absence of an assay temperature effect

on a_{NO3} suggests that any μ_{max}-a_{NO3} tradeoff does not depend on the temperature environment in the short term, at least within the temperature range explored here, and that strong selection acted on μ_{max} alone, without pleiotropic effects on nitrate competitive ability in most replicates.

Thermal adaptation in the ocean would frequently occur under nitrogen limitation, at least in the temperate ocean where *T. pseudonana* is commonly found (Fong, 2008), and may thus produce changes in nitrogen affinities different from those we observed here. Therefore, we suggest that future temperature selection experiments should also account for nutrient limitation to reflect possible climate change scenarios in natural systems.

Evolution experiments are essential to enhancing our understanding of the effects of climate change on marine and freshwater food webs. Arguably, phytoplankton are among the highest-payoff organisms upon which we can conduct evolution experiments: they offer a unique combination of potential for rapid evolutionary responses to environmental change, tractability as experimental subjects, and global ecological importance (Reusch & Boyd, 2013). Eco-evolutionary responses to changes in temperature, ocean acidity, nutrient limitation and other environmental factors are complex, and are made more complex by interactions among these factors. Single-stressor evolution experiments are a valuable first step, but future evolution experiments must account for interactive effects of multiple stressors (e.g., temperature and nitrate limitation).

APPENDICES

APPENDIX A:

Chapter 1 supplemental figures, tables, and equations

A.1: Double-exponential residual plots

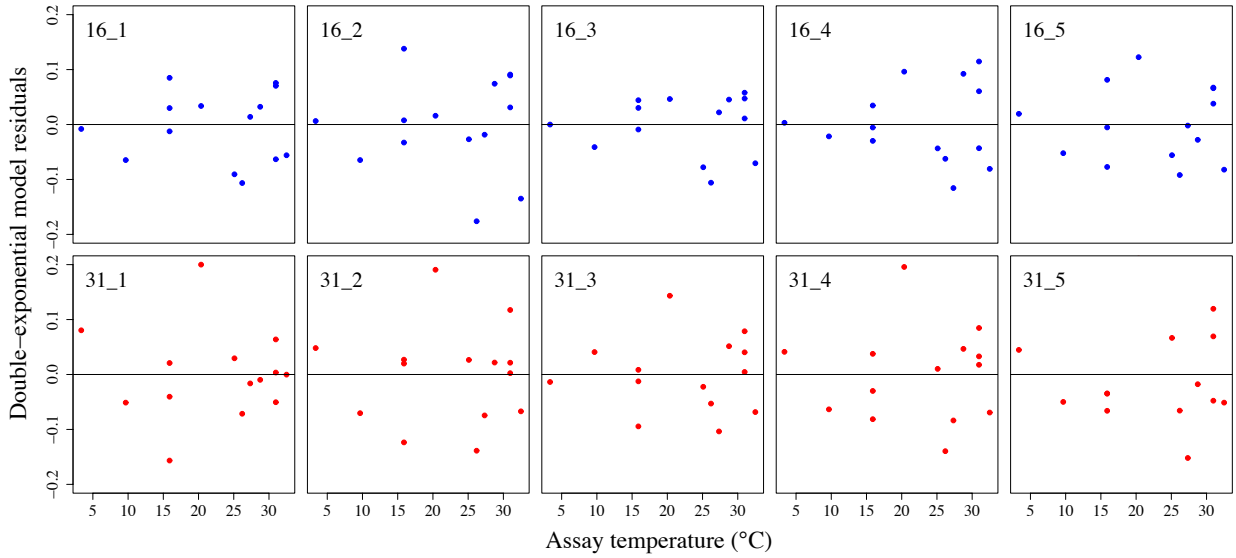

Figure A1: Residual plots for fits of the double-exponential model to data from temperature-dependent growth assays of all replicate *T. pseudonana* populations at 16 and 31°C. In each panel, note the two points farthest to the left (assays at 3°C and 10°C). n = 14 in each panel. Replicate population ID is indicted in the upper left of each panel.

A.2: Linear models and statistical output.

Models compare traits shown in Figure 1 and Figure 2.

Model A1. Thermal performance traits (Figures 2A-C)

$trait \sim N(\beta_0 + \beta_1 \times Selection\ temp.,\ \sigma^2/w)$,

where $w = 1/\sigma_b^2$; the subscript *b* indicates that this is the variance of the bootstrap distribution,

not to be confused with σ^2 of the linear model above.

Data fit to Model 1 are trait estimates numerically derived from the double-exponential model (Thomas et al. 2017). In Model 1, replicate selection lines are pooled within assay temperature, as there were insufficient degrees of freedom to test for strain-level effects. To quantify uncertainty in trait estimates compared in Model 1, we conducted 1000 residual bootstraps of the double-exponential fits using a procedure identical to that described in Listmann *et al.* (2016). We incorporated the uncertainty estimated from bootstrap distributions into linear models by weighting each trait estimate by the inverse of the variance of its bootstrap distribution.

Model A2: μ_{max} in a reciprocal transplant (Figure 2D)

$$\mu_{max} \sim N(\beta_0 + \beta_1 \times assay\ temp. + \beta_2 \times Selection\ temp. + \beta_3(assay\ temp \times Selection\ temp) + \beta_{1(4)} \times Strain,\ \sigma^2)$$

Note that this is *not* a weighted model. We used Model 2 to directly compare maximum growth rates (μ_{max}) at the selection temperatures in a reciprocal transplant (all 16°C- and 31°C-selected lines assayed at both temperatures). Uncertainty in μ_{max} could be estimated directly (n = 3, no bootstraps), and we fit a selection temperature × assay temperature interaction and nested replicate selection line within selection temperature to test for local adaptation and strain-level selection temperature effects, respectively.

Model A3: μ_{max} and a_{NO3} from Monod equation fits (Figure 5)

$$trait \sim N(\beta_0 + \beta_1 \times assay\ temp. + \beta_2 \times Selection\ temp. + \beta_3(assay\ temp \times Selection\ temp),\ \sigma^2/w)$$

Model 3 was applied to μ_{max} and nitrate growth affinity (a_{NO3}) estimates derived from fits of the Monod equation to growth rates estimated across a nitrate gradient (10 concentrations) at the selection temperatures, also in a reciprocal transplant scenario. Uncertainties in these estimates were estimated directly when fitting the Monod equation, as its parameters are the traits being compared; these uncertainties were incorporated into the linear model as weights (w = $1/\sigma_b^2$), as in Model 1.

ANOVA tables show statistical outputs of ANOVA conducted on linear models (Table A1; Table A2; Table A3). Following Table A1, Figure A1 shows within-group, replicate population-level effects of Model 2.

Table A1: ANOVA table for traits described in Figure 2: thermal optimum (T_{opt}), maximum growth rate at T_{opt} (μ_{opt}), upper critical temperature (CT_{max}) (all Model 1), and maximum growth rates at the selection temperatures (μ_{max}) in a reciprocal transplant (Model 2).

Trait *Source*	**Linear model coefficient (95% CI)**	**df**	**MS**	**F-value**	**P-Value**
T_{opt} (°C)					
Selection temperature	1.87 (0.83, 2.92)	1	6.48	17.02	0.0033
Residual		8	0.38	--	--
μ_{opt} (d^{-1})					
Selection temperature	0.095 (0.018, 0.17)	1	20.41	7.99	0.022
Residual		8	2.55	--	--
CT_{max} (°C)					
Selection temperature	0.30 (-0.18, 0.77)	1	6.57	2.09	0.19
Residual		8	3.15	--	--

Table A1 (cont'd)

μ_{max} (d^{-1}) at selection temps					
Assay temperature	-0.051 (-0.15, 0.048)	1	0.092	25.43	<0.0001
Selection temperature	-0.19 (-0.29, -0.094)	1	0.00058	0.16	0.69
Assay temp. × Selection temp	0.43 (0.29, 0.57)	1	0.92	254.82	<0.0001
Sel. temp. : Strain	See Figure A2	8	0.0069	1.89	0.052
Residual	--	40	0.0036	--	--

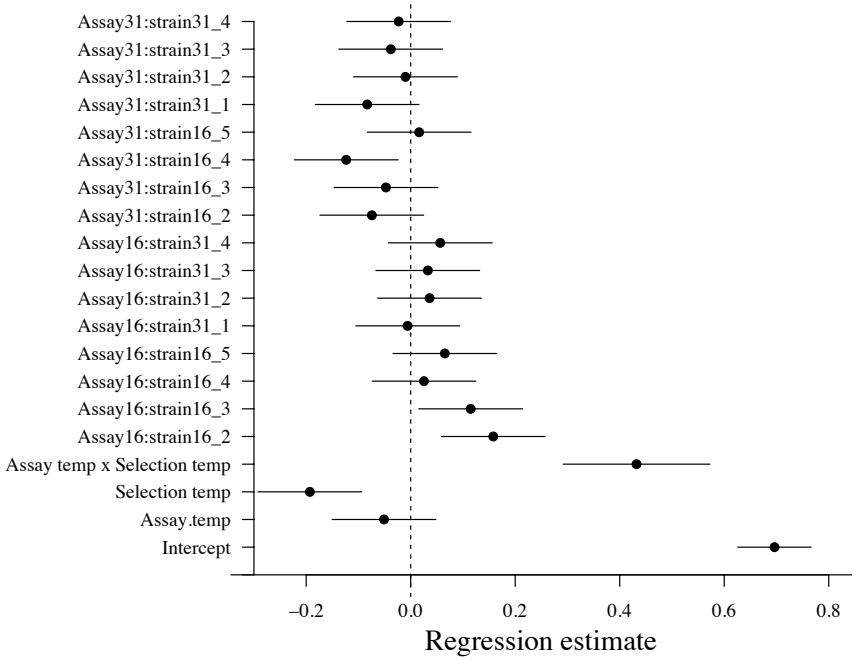

Figure A2: Regression coefficients from Model 2, describing μ_{max} at the selection temperatures in a reciprocal transplant (n = 3). For Assay temp : strain estimates, strains 16.1 and 31.5 are reference levels and thus do not appear on this plot. Bars are 95% CI.

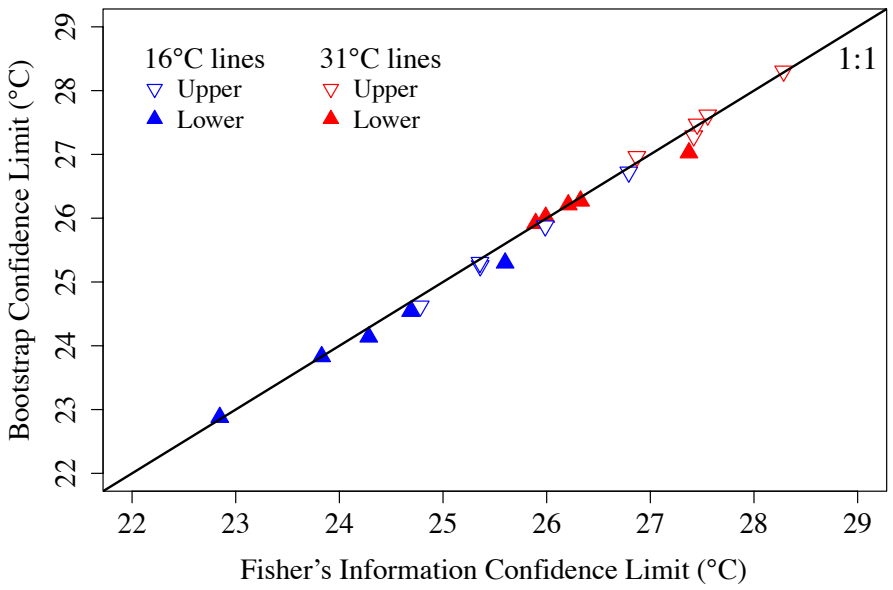

Figure A3: Comparison of Fisher's Information 95% confidence limits to bootstrap confidence limits for T_{opt} parameter in double-exponential model fits to temperature-dependent growth data.

Table A2: ANOVA tables comparing traits described in Figure 3. Traits compared between selection temperature groups: Upper tail length (CT_{max} -T_{opt}), Peak sharpness at T_{opt}, upper concavity below T_{opt}, and the inflection point of the thermal reaction norm (see Model A1).

Trait *Source*	**Linear model coefficient (95% CI)**	**df**	**MS**	**F-value**	**P-Value**
Upper tail length (°C)					
Selection temperature	-1.47 (-2.80, -0.1495)	1	28.50	6.58	0.033
Residual		8	4.33	--	--
Peak sharpness					
Selection temperature	0.011 (0.0060, 0.016)	1	38.39	26.77	0.00085
Residual		8	1.43	--	--
Upward concavity					
Selection temperature	0.0023 (0.0014, 0.0029)	1	45.66	91.41	< 0.0001
Residual		8	0.86	--	--
Inflection point (°C)					
Selection temperature	5.07 (1.75, 8.39)	1	32.15	12.36	0.0079
Residual		8	2.60	--	--

Table A3: ANOVA comparing maximum growth rates (μ_{max}) and nitrate affinities (a_{NO3}).

Traits are compared between temperature selection groups and between assay temperatures in the reciprocal transplant scenario (see Model A3). Strain-level effects could not be tested, due to insufficient degrees of freedom.

Trait *Source*	Coefficient (95% CI)	df	MS	F-value	P-Value
μ_{max} (d^{-1})					
Assay temperature	-0.12 (-0.21, -0.18)	1	0.00047	0.0018	0.97
Selection temperature	-0.088 (-0.18, -0.00085)	1	0.026	0.10	0.76
Assay temp. × Selection temp.	0.27 (0.11, 0.43)	1	2.83	10.79	0.0047
Residual		16	0.26	--	--
$ln[a_{NO3}$ (l μmol^{-1} d^{-1})]					
Assay temperature	-0.13 (-0.66, -0.41)	1	0.068	0.27	0.61
Selection temperature	0.31 (-0.18, 0.79)	1	0.32	1.26	0.28
Assay temp. × Selection temp.	-0.045 (-0.88, 0.79)	1	0.029	0.12	0.74
Residual		16	0.25	--	--

A.3: Figures A4-A6

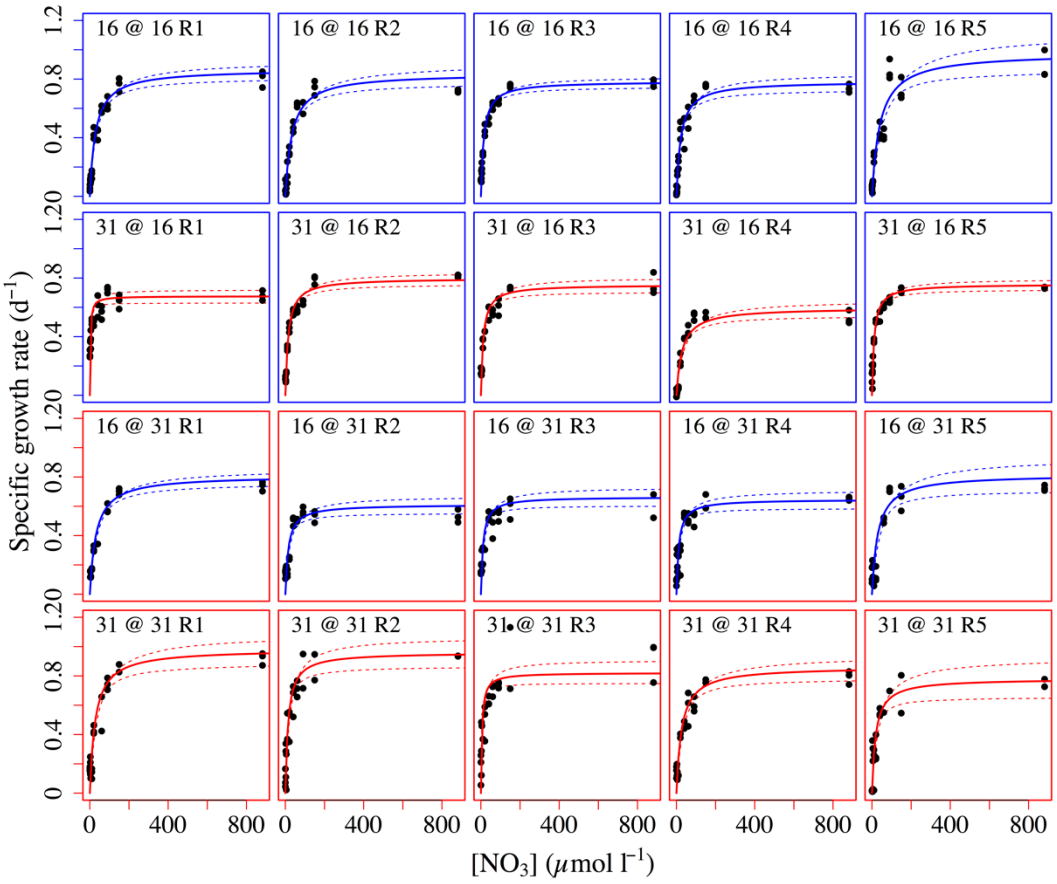

Figure A4: Nitrate-dependent growth (Monod) assays at 16°C (top, blue boxes) and 31°C (bottom, red boxes). Curves were fit to *T. pseudonana* exponential growth rates at ambient NO_3 concentrations ranging from 0 to 882 μmol l^{-1} (the NO_3 concentration in unaltered L1 marine medium). For each panel, $n \leq 30$ (see "Methods"). Confidence bands were generated from fits to 1000 residual bootstraps.

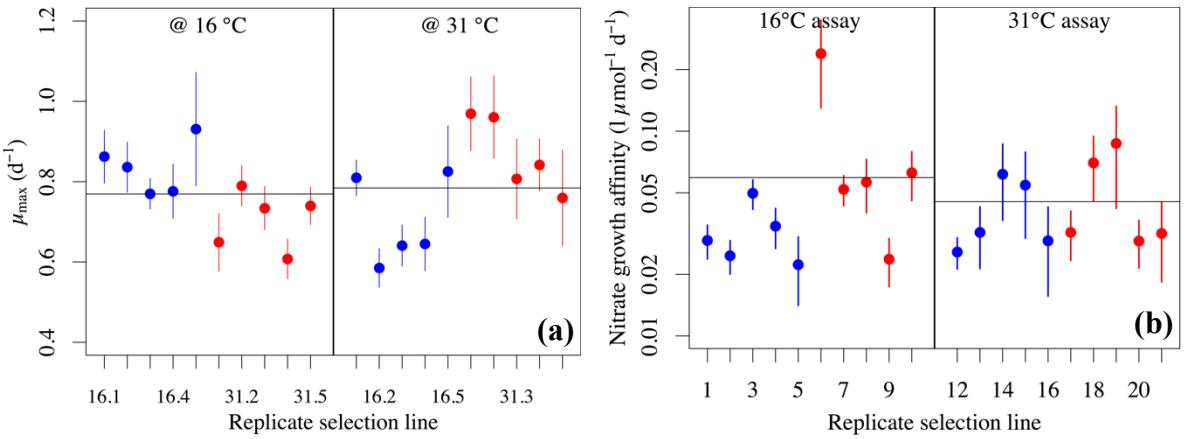

Figure A5: Nitrate-dependent growth (Monod) kinetic parameters at ~450 generations. (a) *T. pseudonana* maximum specific growth rates (μ_{max}) for 16°C- and 31°C-selected lines (blue and red, respectively) assayed at 31°C and at 16°C. (b) Nitrate growth affinity (a_{NO3}). Bars are 95% CI, based on uncertainties from bootstrap Monod parameter distributions (n = 1000). Note that the y-axis in panel B is on a log scale, hence the asymmetry in confidence intervals.

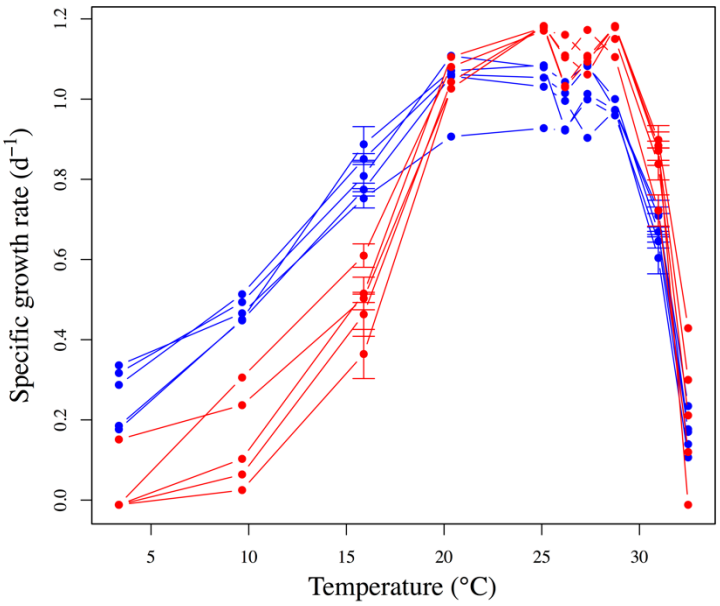

Figure A6: **Nonparametric plot of thermal reaction norms (n = 14 for each).** Bars on points at the two selection temperatures are ±1 SE (n = 3 at each temperature).

A.4: Graphical analysis of the modified double-exponential model (Eq. 3 and 4 in main text)

Panels show theoretical relationships between the traits estimated for *T. pseudonana* and the "protection" parameter, *p*, in the modified double-exponential model.

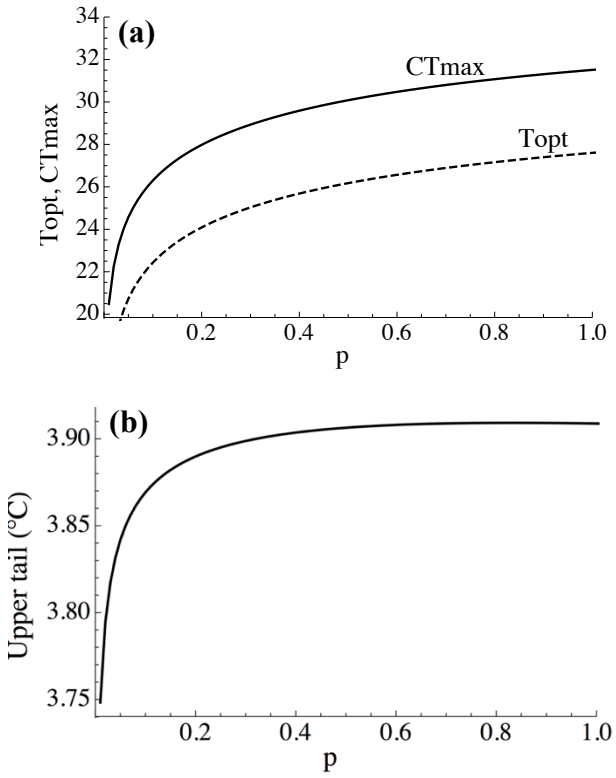

Figure A7: Relationships between thermal performance traits and the protection parameter (*p*) in Equations (3). (a) CT_{max} and T_{opt}, (b) upper tail length, (c) thermal niche width, (d) inflection point, and (e) peak sharpness, and (f) upward concavity as functions of protection, as defined in Equation (3).

Figure A7 (cont'd)

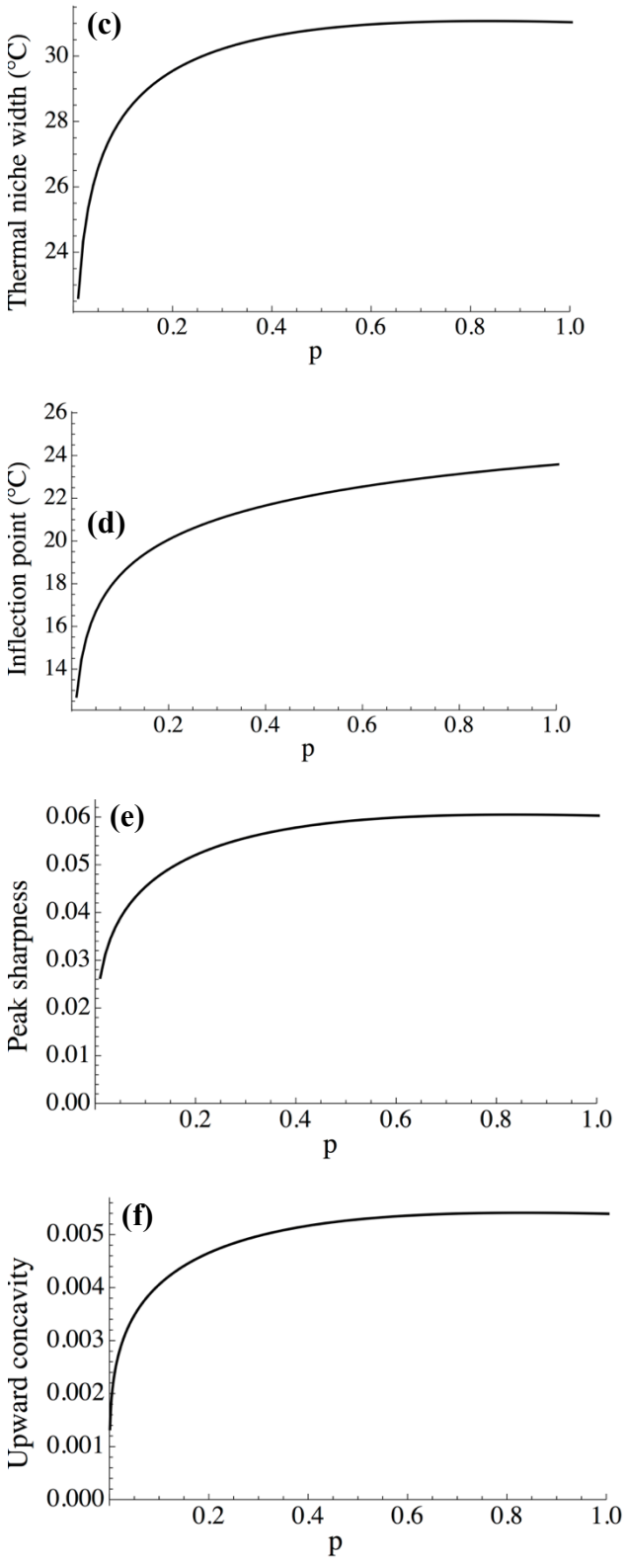

APPENDIX B:

Chapter 1 supplemental derivations

B.1: Analytical determination of T_{opt}

First, we derive T_{opt} for Equation (1) by taking its derivative with respect to temperature (T) and setting it equal to 0. Solving for T yields the solution for T_{opt}.

$$f(T) = b_1 e^{b_2 T} - d_1 e^{d_2 T} - d_0 \quad \text{(Equation 1)}$$

$$f'(T) = b_1 b_2 e^{b_2 T} - d_1 d_2 e^{d_2 T} = 0 \quad \text{(1')}$$

$$T_{opt} = \log(b_1 b_2 / d_1 d_2) / (d_2 - b_2) \quad \text{(B1)}$$

T_{opt} can likewise be derived from the modified double-exponential model.

$$f(T) = (1/q) b_1 e^{b_2 T} - (1/p) d_1 e^{d_2 T} - d_0 \quad \text{(B2)}$$

$$f'(T) = b_1 b_2 e^{b_2 T}/q - d_1 d_2 e^{d_2 T}/p = 0 \quad \text{(B2')}$$

$$T_{opt} = \log(d_1 d_2 q / b_1 b_2 p) / (b_1 - d_2) \quad \text{(B3)}$$

B.2: Re-parameterization of the double-exponential model with explicit T_{opt}

Equation (B3) can be solved for b_1:

$$b_1 = \frac{d_1 d_2}{b_2} e^{(d_2 - b_2) T_{opt}}, \quad \text{(B4)}$$

which can then be substituted into Equation (1) and simplified, yielding:

$$f(T) = \frac{d_1 d_2}{b_2} e^{b_2 \cdot T + (d_2 - b_2) T_{opt}} - (d_0 + d_1 e^{d_2 T}). \quad \text{(B5)}$$

Equation (B5) has the same number of parameters (5) as Equation (1), can be directly parameterized using Maximum Likelihood Estimation, and contains T_{opt} as an explicit parameter. This formulation both facilitates fitting by allowing "eyeballing" of the starting value for T_{opt}, and facilitates calculating confidence intervals for T_{opt} estimates based on properties of likelihood surfaces rather than requiring bootstrapping approaches. For Equation (B5) to produce a canonical unimodal thermal performance curve, $d_1 > d_2$. Additionally, $d_0 > 0$ for the function to cross zero below T_{opt}, ensuring a proper CT_{min} value.

B.3: Derivation of Equation 2 from Monod (1949)

The Monod (1949) equation describing per-capita population growth as a function of resource concentration is

$$\frac{1}{N}\frac{dN}{dt} = \frac{\mu_{max}R}{R+K}, \quad \text{(B6)}$$

where N is the population density, μ_{max} is the nutrient-saturated (maximum) Malthusian parameter, R is the resource concentration, and K is the half-saturation constant (the value of R at which growth is $0.5 \times \mu_{max}$. According to Healy (1980), $K = \frac{\mu_{max}}{a}$, so it follows that Equation (B6) can be written as

$$\frac{1}{N}\frac{dN}{dt} = \frac{\mu_{max}R}{R+(\frac{\mu_{max}}{a})} \quad \text{(B6')}$$

Multiplying the right side by $\frac{a}{a}$, we see that

$$\frac{1}{N}\frac{dN}{dt} = \frac{\mu_{max}R}{R+(\frac{\mu_{max}}{a})} \times \frac{a}{a} = \frac{\mu_{max}aR}{\mu_{max} + aR},$$ which is Equation (2).

REFERENCES

REFERENCES

Angilletta MJ, Wilson RS, Navas CA, James RS. 2003. Tradeoffs and the evolution of thermal reaction norms. *Trends in Ecology and Evolution* **18**:234-240.

Araújo M, Ferri-Yáñez F, Bozinovic F, Marquet PA, Valladares F, *et al.* 2013. Heat freezes niche evolution. *Ecology Letters* **16**:1206–1219.

Baker KG, Robinson CM, Radford DT, McInnes AS, Evenhuis C, *et al.* 2016. Thermal performance curves of functional traits aid understanding of thermally induced changes in diatom-mediated biogeochemical fluxes. *Frontiers in Marine Science* **3**:1–14.

Bell G. 2013. Evolutionary rescue and the limits of adaptation. *Philosophical Transactions of the Royal Society of London B: Biological Sciences* **368**:20120080.

Bennett AF, Lenski RE. 1993. Evolutionary adaptation to temperature II. Thermal niches of experimental lines of *Escherichia coli*. *Evolution* **47**:1-12.

Blanquart F, Kaltz O, Nuismer SL, Gandon S. 2013. A practical guide to measuring local adaptation. *Ecology Letters* **16**:1195–1205.

Bolker B, R Core Team. 2017. bbmle: tools for general maximum likelihood estimation. R package version 1.0.19. https://cran.r-project.org/web/packages/bbmle/index.html.

Boyce DG, Lewis MR, Worm B. 2010. Global phytoplankton decline over the past century. *Nature* **466**:591–596.

Boyd PW, Rynearson TA, Armstrong EA, Fu F, Hayashi K, *et al.* 2013. Marine phytoplankton temperature versus growth responses from polar to tropical waters – outcome of a scientific community-wide study. *PLoS One* **8**:e63091.

Bradford MA. 2013. Thermal adaptation of decomposer communities in warming soils. *Frontiers in Microbiology* **4**:1-16.

Collins S, Bell G. 2004. Phenotypic consequences of 1,000 generations of selection at elevated CO_2 in a green alga. *Nature* **431**:566–569.

Corkrey R, McMeekin TA, Bowman JP, Ratkowsky DA, Olley J, *et al.* 2014. Protein thermodynamics can be predicted directly from biological growth rates. *PloS One* **9**:e96100.

Crawfurd KJ, Raven JA, Wheeler GL, Baxter EJ, Joint I. 2011. The response of *Thalassiosira pseudonana* to long-term exposure to increased CO_2 and decreased pH. *PloS One* **6**:e26695.

Elena SF, Lenski RE. 2003. Evolution experiments with microorganisms: the dynamics and genetic bases of adaptation. *Nature Reviews Genetics* **4**:457–469.

Field CB, Behrenfeld MJ, Randerson JT, Falkowski PG. 1998. Primary production of the biosphere: integrating terrestrial and oceanic components. *Science* **281**:237–240.

Fong P. 2008. Macroalgal-dominated ecosystems. In: *Nitrogen in the Marine Environment*, 2nd ed. (eds Capone DG, Bronk DA, Mulholland MR, Carpenter EJ), pp. 917-947. Academic Press (Elsevier), Cambridge, MA, USA.

Gilchrist GW. 1995. Specialists and generalists in changing environments. I. Fitness landscapes of thermal sensitivity. *The American Naturalist* **146**:252–270.

Gomulkiewicz R, Holt RD. 1995. When does evolution by natural selection prevent extinction? *Evolution* **49**:201–207.

Grover JP 1991. Resource competition in a variable environment: phytoplankton growing according to the variable-internal-stores model. *The American Naturalist* **138**:811–835.

Guillard R, Hargraves P. 1993. *Stichochrysis immobilis* is a diatom, not a chrysophyte. *Phycologia* **32**:234-236.

Harrison P, Waters R, Taylor F. 1980. A broad spectrum artificial seawater medium for coastal and open ocean phytoplankton. *Journal of Phycology* **16**:28-35.

Healy FP. 1980. Slope of the Monod equation as an indicator of advantage in nutrient competition. *Microbial Ecology* **5**:281-286.

Hinners J, Kremp A, Hense I. 2017. Evolution in temperature-dependent phytoplankton traits revealed from a sediment archive: do reaction norms tell the whole story? *Proceedings of the Royal Society B* **284**:20171888.

Hoffmann AA, Sgrò CM. 2011. Climate change and evolutionary adaptation. *Nature* **470**:479-485.

Huey RB, Partridge L, Fowler K. 1991. Thermal sensitivity of *Drosophila melanogaster* responds rapidly to laboratory natural selection. *Evolution* **45**:751-756.

Hutchins DA, Walworth NG, Webb EA, Saito MA, Moran D, *et al*. 2015. Irreversibly increased nitrogen fixation in *Trichodesmium* experimentally adapted to elevated carbon dioxide. *Nature Communications* **6**:8155.

Izem R, Kingsolver JG. 2005. Variation in continuous reaction norms: quantifying directions of biological interest. *The American Naturalist* **166**:277–289.

Jiang H, Gao K. 2004. Effects of lowering temperature during culture on the production of polyunsaturated fatty acids in the marine diatom *Phaeodactylum tricornutum* (Bacillariophyceae). *Journal of Phycology* **40**:651–654.

Jin P, Gao K, Beardall J. 2013. Evolutionary responses of a coccolithophorid *Gephyrocapsa oceanica* to ocean acidification. *Evolution* **67**:1869–1878.

Kawecki TJ, Ebert D. 2004. Conceptual issues in local adaptation. *Ecology Letters* **7**:1225–1241.

Kingsolver JG, Gomulkiewicz R, Carter PA. 2001. Variation, selection and evolution of function-valued traits. *Genetica* **112**:87–104.

Kingsolver JG. 2009. The well-temperatured biologist. *The American Naturalist* **174**:755–768.

Klausmeier CA, Litchman E, Daufresne T, Levin SA. 2004. Optimal nitrogen-to-phosphorus stoichiometry of phytoplankton. *Nature* **429**:171–174.

Knies JL, Izem R, Supler KL, Kingsolver JG, Burch CL. 2006. The genetic basis of thermal reaction norm evolution in lab and natural phage populations. *PLoS Biology* **4**:e201.

Kutcherov D. 2016. Thermal reaction norms can surmount evolutionary constraints: comparative evidence across leaf beetle species. *Ecology and Evolution* **6**:4670–4683.

Listmann L, LeRoch M, Schlüter L, Thomas MK, Reusch TBH. 2016. Swift thermal reaction norm evolution in a key marine phytoplankton species. *Evolutionary Applications* **9**:1156–1164.

Litchman E, Klausmeier CA, Schofield OM, Falkowski PG. 2007. The role of functional traits and tradeoffs in structuring phytoplankton communities: scaling from cellular to ecosystem level. *Ecology Letters* **10**:1170–1181.

Litchman E, Edwards K, Klausmeier CA, Thomas MK. 2012. Phytoplankton niches, traits and eco-evolutionary responses to global environmental change. *Marine Ecology Progress Series* **470**:235–248.

Logan JA, Wollkind DJ, Hoyt SC, Tanigoshi LK. 1976. An analytical model for description of temperature dependent rate phenomena in arthropods. *Environmental Entomology* **5**:1133-1140.

Lohbeck KT, Riebesell U, Reusch TBH. 2012. Adaptive evolution of a key phytoplankton species to ocean acidification. *Nature Geosciences* **5**:346–351.

Low-Décarie E, Jewell MD, Fussmann GF, Bell G. 2013. Long-term culture at elevated atmospheric CO_2 fails to evoke specific adaptation in seven freshwater phytoplankton species. *Proceedings of the Royal Society B* **280**:20122598.

Manuilova E, Schuetzenmeister A, Model F. 2014. mcr: Method Comparison Regression. R package version 1.2.1. https://cran.r-project.org/package=mcr.

Martiny AC, Ma L, Mouginot C, Chandler JW, Zinser ER. 2016. Interactions between thermal acclimation, growth rate, and phylogeny influence *Prochlorococcus* elemental stoichiometry. *PLoS One* **11**:e0168291.

Mongold JA, Bennett AF, Lenski RE. 1996. Evolutionary adaptation to temperature. IV. Adaptation of Escherichia coli at a niche boundary. *Evolution* **50**:35-43.

Monod J. 1949. The growth of bacterial cultures. *Annual Reviews in Microbiology* **3**:371-394.

Nedwell D. 1999. Effect of low temperature on microbial growth: lowered affinity for substrates limits growth at low temperature. *FEMS Microbiology and Ecology* **30**:101–111.

Nelson DM, Tréguer P, Brzezinski MA, Leynaert A, Quéguiner B. 1995. Production and dissolution of biogenic silica in the ocean: revised global estimates, comparison with regional data and relationship to biogenic sedimentation. *Global Biogeochemical Cycles* **9**:359–372.

Neori A, Vernet M, Holm-Hansen O, Haxo FT. 1986. Relationship between action spectra for chlorophyll *a* fluorescence and photosynthetic O_2 evolution in algae. *Journal of Plankton Research* **8**:537-548.

Padfield D, Yvon-Durocher G, Buckling A, Jennings S, Yvon-Durocher G. 2015. Rapid evolution of metabolic traits explains thermal adaptation in phytoplankton. *Ecology Letters* **19**:133–142.

Ratkowsky DA, Olley J, Ross T. 2005. Unifying temperature effects on the growth rate of bacteria and the stability of globular proteins. *Journal of Theoretical Biology* **233**:351–362.

Redfield AC. 1958. The biological control of chemical factors in the environment. *American Scientist* **46**:205–221.

Reusch TBH, Boyd PW. 2013. Experimental evolution meets marine phytoplankton. *Evolution* **67**:1849–1859.

Rowan R. 2004. Thermal adaptation in reef coral symbionts. *Nature* **430**:742.

Schaum C-E, Barton S, Bestion E, Buckling A, Garcia-Carreras B, *et al*. 2017. Adaptation of phytoplankton to a decade of experimental warming linked to increased photosynthesis. *Nature Ecology Evolution* **1**:0094.

Schiffers K, Bourne EC, Lavergne S, Thuiller W, Travis JMJ. 2013. Limited evolutionary rescue of locally adapted populations facing climate change. *Philosophical Transactions of the Royal Society of London B: Biological Sciences* **368**:20120083.

Schlüter L, Lohbeck KT, Gutowska MA, Gröger JP, Riebesell U, *et al.* 2014. Adaptation of a globally important coccolithophore to ocean warming and acidification. *Nature Climate Change* **4**:1024–1030.

Schoener TW. 2011. The newest synthesis: understanding the interplay of evolutionary and ecological dynamics. *Science* **331**:426–429.

Thomas MK, Kremer CT, Klausmeier CA, Litchman E. 2012. A global pattern of thermal adaptation in marine phytoplankton. *Science* **338**:1085–1088.

Thomas MK, Kremer CT, Litchman E. 2016. Environment and evolutionary history determine phytoplankton temperature traits globally. *Global Ecology & Biogeography* **25**:71-86.

Thomas MK, Aranguren-Gassis M, Kremer CT, Gould MR, Anderson K, *et al.* 2017. Temperature-nutrient interactions exacerbate sensitivity to warming in phytoplankton. *Global Change Biology* **23**:3269-3280.

Thrane J-E, Hessen DO, Anderson T. 2017. Plasticity in algal stoichiometry: experimental evidence of a temperature-induced shift in optimal supply N:P ratio. *Limnology and Oceanography* **62**:1346-1354.

Tilman DA, Mattson M, Langer S. 1981. Competition and nutrient kinetics along a temperature gradient: an experimental test of a mechanistic approach to niche theory. *Limnology and Oceanography* **26**:1020-1033.

Yvon-Durocher G, Schaum C-E, Trimmer M. 2017. The temperature dependence of phytoplankton stoichiometry: investigating the roles of species sorting and local adaptation. *Frontiers in Microbiology* **8**:2003.

CHAPTER 2: Experimental evolution of fatty acid thermal reaction norms in a marine diatom

Introduction

Temperature affects practically every aspect of poikilotherms' physiology, from rates of respiration (Beamish & Mookherjii 1964; Caron *et al.* 1986; Bradford 2013) and photosynthesis (Neori & Holm-Hansen 1982; Robarts & Zohary 1987; Pastenes & Horton 1996) to reproductive rates (Knoblauch & Jorgensen 1999; Lee & Ahn 2000; Thomas *et al.* 2012) and body size (Montagnes & Franklin 2001; Peter & Sommer 2013; Lindmark *et al.* 2018). As body temperature rises, the physical properties of cellular structures change: proteins change conformation or denature (Ratkowsky *et al.* 2005; Corkrey *et al.* 2014) and membranes become more fluid and permeable to solutes (reviewed in Hazel 1995). These changes necessitate the evolution of physiological strategies to maintain cellular function in a thermally variable environment. Rates of resource acquisition, efficiencies of resource use (Bradford 2013), and strategies for storing resources such as carbon, nitrogen and phosphorus can lead to changes in relative resource requirements (Thrane *et al.* 2017), internal stoichiometry (Sakamoto & Bryant 1998; Thrane *et al.* 2017), and the content and composition of fatty acid (FA) molecules (Canvin 1965; James *et al.* 1989; Thompson *et al.* 1992b; Teoh *et al.* 2004).

One strategy for maintaining membrane function in a thermally variable environment is to change the FA composition of cellular membranes to maintain homeoviscosity of membranes across temperature within an organism's thermal niche (Sinensky 1975). FA in cell walls and organelle membranes may become increasingly unsaturated at low temperatures (Patterson 1970; Joh *et al.* 1993; Jiang & Gao 2004) as unsaturated FA (UFA) pack together more loosely, conferring greater membrane fluidity and permeability; conversely, membrane FA tend to be

more saturated at high temperatures (Quinn 1981; Wada *et al.* 1990; Murata & Los 1997; Zhu *et al.* 1997), as saturated FA (SFA) pack together tightly and in a more ordered fashion, conferring greater membrane rigidity (Quinn 1981; Murata & Los 1997; Renaud *et al.* 2002; Converti *et al.* 2009).

Plasticity in FA content and composition has been studied in a wide variety of taxa (Sinensky 1974; Bhakoo and Herbert 1979; reviewed in Neidleman 1987), however the FA content and composition of phytoplankton, in particular, has attracted extensive study, in part due to their potential utility as feedstock for production of biofuels (Hu *et al.* 2008; Converti *et al.* 2009; Williams & Laurens 2010) and to their global importance as the leading source of omega-3 FA (Litzow *et al.* 2006; Kang 2011; Hixson & Arts 2016). Published trends in algal FA profiles across temperature are extremely variable, even within a given functional group (e.g. diatoms); however, a number of generalities seem to exist. Specifically: 1) overall FA content is generally highest at the thermal niche boundaries (Patterson 1970; Thompson *et al.* 1992a; Van Wagenen *et al.* 2012), which results in an overall negative correlation between population growth rate and FA content. Notably, a negative correlation between growth rate and FA content in algae has also been observed when the former was controlled by factors other than temperature, such as irradiance (Shifrin & Chisolm 1991; Thompson *et al.* 1990; Williams & Laurens 2010) or nutrients (Yang *et al.* 2018). 2) As has been observed in other organisms, % SFA tends to increase with temperature, especially below the thermal optimum for population growth (T_{opt}). 3) Below T_{opt}, % polyunsaturated FA (PUFA) tends to decrease with temperature. 4) Trends in % monounsaturated FA (MUFA) across temperature are variable and often non-significant (Patterson 1970; Sato *et al.* 1979; Thompson *et al.* 1992b; Renaud *et al.* 2002; Rousch *et al.* 2003; Pasquet *et al.* 2014). Exceptions to these trends can be found in most of the studies

cited here.

While plasticity in FA profiles has been characterized for many phytoplankton species (see previous paragraph), the aim of this study is to investigate evolutionary change in temperature-dependent reaction norms for total FA content, FA composition (representation of FA classes as a percentages of total FA), and overall saturation/unsaturation of FA in response to long-term experimental selection at low (16°C) and high (31°C) temperatures. Evolutionary adaptation to an extreme temperature may lead to a temperature-specialized FA profile (a hot-cold tradeoff). While an increase in temperature can lead to greater FA saturation over the short term via physiological plasticity (Wada *et al.* 1990; Murata & Los 1997; Zhu *et al.* 1997), prolonged exposure (over many generations) to high temperature may cause an evolutionary reduction in the ability to maintain homeoviscosity through production of UFA should the temperature drop (a tradeoff). A similar tradeoff may be predicted in the opposite direction for cold-adapted populations. Alternatively, thermal adaptation may simply lead to increased plasticity in the FA profile, contributing to (or resulting from) the broadening of the thermal niche (see Izem & Kingsolver 2005; Kingsolver 2009).

Thermal reaction norms for per-capita population growth have been shown to evolve rapidly in response to experimental selection in phytoplankton (Listmann *et al.* 2016; Padfield *et al.* 2016; O'Donnell *et al.* 2018) and other organisms (Mongold *et al.* 1996; Knies *et al.* 2006; Geerts *et al.* 2013). However, only a few studies have examined the metabolic, stoichiometric or biochemical causes and consequences of these changes (Schlüter *et al.* 2014; Padfield *et al.* 2016; O'Donnell *et al.* 2018). Knowledge of evolutionary changes in the temperature dependence of cellular chemistry in poikilotherms is crucial to achieving a comprehensive understanding of the effects of temperature selection at the level of the organism. This study is

among the first to examine the effects of experimental thermal adaptation on the fatty acid profile of a phytoplankton species.

Materials and Methods

500 generation temperature selection experiment

The temperature-dependent growth assays described here were conducted after ~500 generations of thermal adaptation at 16°C and 31°C, a detailed account of which can be found in O'Donnell *et al.* (2018). Briefly, we maintained five replicate populations of *Thalassiosira pseudonana* CCMP1335 (Hustedt) Hasle et Heimdal (obtained from the Provasoli-Guillard National Center for Culture of Marine Phytoplankton (CCMP), Maine, USA) in exponential growth under cool, white, fluorescent bulbs at a photon flux density of 110 μmol photons m^{-2} s^{-1} on a 14:10 light:dark cycle, transferring 10^6 cells into fresh L1 marine culture medium (Guillard & Hargraves 1993; modified by O'Donnell *et al.* 2018) every four days, with occasional deviations of ±1 day. After the selection experiment, all populations were cryopreserved in liquid nitrogen until they were needed, at which point they were revived for assays (see below).

Cryopreservation and revival

To cryopreserve *T. pseudonana* populations, we first grew them to late log-phase in their selection ("home") temperature environments before placing 1 ml of culture in a 2 ml cryogenic vial. We then added 1 ml of 24% dimethyl sulfoxide (mixed with 76% L1 marine medium), for a final DMSO concentration of 12%. After 20 minutes, cryogenic vials were placed in a passive freezer unit (Mr. Frosty, Thermo Scientific, USA) containing 250 ml isopropyl alcohol, and cooled to -80°C at ~1 °C min^{-1}, after which vials were plunged and stored in liquid nitrogen (-

196 °C).

We revived cultures two weeks prior to beginning acclimation for temperature-dependent assays. We thawed cryogenic vials by floating them in 500 ml beakers full of 20°C tap water. We preformed this operation in the dark. Once thawed, each vial was immediately emptied into a 20 ml scintillation vial containing 10 ml of L1 marine medium, also at 20°C. Scintillation vials were loosely capped and placed in a light-proofed cardboard box at 20°C for 36 h (as in Hipkin *et al.* 2013), after which they were placed under cool, white fluorescent lights at 110 µmol photons m^{-2} s^{-1} on a 14:10 light:dark cycle. Each vial was gently inverted daily to keep cells in suspension. As soon as a revived culture grew to a visible density, it was transferred to a 50 ml tissue culture flask containing 20 ml of L1 marine medium. Starting at this point, all cultures were maintained at 20 °C for 10 generations prior to acclimation at assay temperatures.

Algal growth and harvesting

We assayed all five replicate *T. pseudonana* populations from each experimental selection temperature group (16°C and 31°C) in triplicate at 10, 16, 26 and 31°C (2 selection temperatures x 4 assay temperatures x 5 populations x 3 replicates = 120 total cultures). We chose these temperatures to achieve broad coverage of *T. pseudonana*'s physiology at temperatures spanning the majority of its thermal tolerance range, and to include the two selection temperatures and one temperature (26°C) approximating *T. pseudonana'*s optimal temperature for population growth (Boyd *et al.* 2013; O'Donnell *et al.* 2018). We conducted acclimations and assays in temperature-controlled growth chambers, under cool, white fluorescent grow lights at 110 µmol photons m^{-2} s^{-1} on a 14:10 light:dark cycle. Each replicate population was maintained in exponential growth for a 10-generation acclimation period at each

assay temperature prior to the assay. From each replicate population, 10^5 cells were transferred to each of three 50 ml polystyrene tissue culture flasks containing 40 ml of sterile-filtered L1 marine culture medium. We monitored relative change in cell densities daily by placing each tissue culture flask in a spectrophotometer (Shimadzu UV-2401PC; Shimadzu Corporation, Kyoto, Japan) and measuring Abs_{436}, corresponding to the absorbance peak of chlorophyll-*a* (Neori *et al.* 1986).

We harvested all 120 cultures in late log-phase; time to harvest varied by temperature. We filtered 15 ml of culture through a Whatman GF/B glass fiber filter for fatty acid analysis and froze these samples at -20°C. We retained 25 μl for population density and mean cell size (μm^3) measurements using a CASY particle counter (Schärfe System GmbH, Reutlingen, Germany); the remaining ~25 ml of each culture was filtered for analyses not addressed here.

Fatty Acid Methyl Ester reaction and Gas Chromatography

To analyze the fatty acid profiles of replicate *T. pseudonana* populations, we extracted neutral lipids from the frozen, filtered samples described above and performed fatty acid methyl ester (FAME) reactions on each according to the protocol by Wang and Benning (2011) and adapted for algae by Boyle *et al.* (2012). We first extracted lipids from Whatman GF/B glass fiber filters using a solution of chloroform, methanol and formic acid (10:20:1). After washing with a buffer (0.2M H_3PO_4 + 1M KCl), we spun samples down for three minutes at 2000 x g, transferring the remaining chloroform layer to a fresh tube and dried the samples with a stream of N_2 gas. After drying, we added 100 µl of internal 15:0 standard (50 µg ml^{-1} pentadecanoic acid), then proceeded with the FAME protocol (Wang *et al.* 2011; Boyle *et al.* 2012) and quantified fatty acids using an Agilent Technologies 7890A Gas Chromatography system

(Agilent Technologies, Santa Clara, CA, USA).

Calculations

All percentages presented here are calculated based on molar masses of fatty acid molecules on a per-biovolume basis (μm^{-3}). Individual fatty acids are presented as percentages of total fatty acid weight (molar). Mean chain length (*MCL*) is calculated as $MCL = \sum_{i=1}^{16} \frac{mol\ FA_i}{mol\ FA_{tot}} \times\ lc_i$, where $mol\ FA_i$ is the weight in moles of a given fatty acid, $mol\ FA_{tot}$ is the total weight of all fatty acids, and lc_i is the length, (number of carbon atoms) of FA_i (Renaud *et al.* 2002). Degree of unsaturation ("unsaturation", hereafter) is calculated as $WUnSat = \sum_{i=1}^{16} \frac{mol\ FA_i}{mol\ FA_{tot}} \times\ ndb_i$, where the first term is as above, and ndb_i is the number of double bonds in FA_i (Thompson *et al.* 1992b).

Linear mixed-effects models

All linear mixed models describing unsaturation, chain length, etc. are nested versions of the same model, fit using the "lme" function from R package "nlme" (Pinheiro & Bates 2018). The full model includes the main effects *selection temperature* and *assay temperature* as factors, plus an interaction between these two factors. For each replicate selection line, we included random intercepts and slopes to account for repeated measures across assay temperatures. Finally, the full model includes two identity variance functions (which allow for different variances by factor level: Pinheiro & Bates 2018) to account for unequal variances between selection temperature levels and among assay temperature levels. These variance functions are included as weights in the model using the "varIdent" function from nlme (Pinheiro and Bates 2018). To include two varIdent functions simultaneously, the "varComb" function (also from

nlme) was used. In some cases, weights and/or *selection temperature × assay temperature* interaction terms did not improve model fits and were dropped from the model. We used likelihood ratio tests to select models; formal models can be found in Appendix C.

Results

As observed in other marine diatoms (see, e.g., Harwood and Jones 1989), *T. pseudonana* contains FA ranging in length from C_{14} to C_{22}, with substantial representation of longer (C_{20} and C_{22}) FA molecules. The dominant fatty acid in both 16°C- and 31°C-selected populations was $16{:}1^{\Delta 3}$ at all four assay temperatures (Figure 11). Total fatty acid content per biovolume (μm^3) trended higher on average in 31°C-selected populations than in 16°C-selected populations, though not significantly (Table 1; Figure 7A), and total fatty acid content was lowest in both groups at 10°C and highest at 31°C (Table 1; Figure 7A). The percentage of total FA represented by saturated fatty acids (SFA) was higher in 16°C-selected populations than in 31°C-selected populations, though not at the 10°C assay temperature; the difference in % SFA was especially pronounced at the 31°C assay temperature, where % SFA in 31°C-selected populations was ~20% lower than in 16°C-selected populations (Table 1; Figure 7B). The percentage of total FA represented by monounsaturated FA (MUFA) was ~10% higher in 31°C-selected populations than in 16°C-selected populations, but did not vary across assay temperatures (Table 1; Figure 7C). Percent polyunsaturated FA (% PUFA) was not different between the two selection groups at 10, 16, and 26°C, however 16°C-selected populations experienced a ~14% decrease in % PUFA between 26°C and 31°C, leading to a significant difference in % PUFA between the two groups at the 31°C assay temperature (Table 1; Figure 7D).

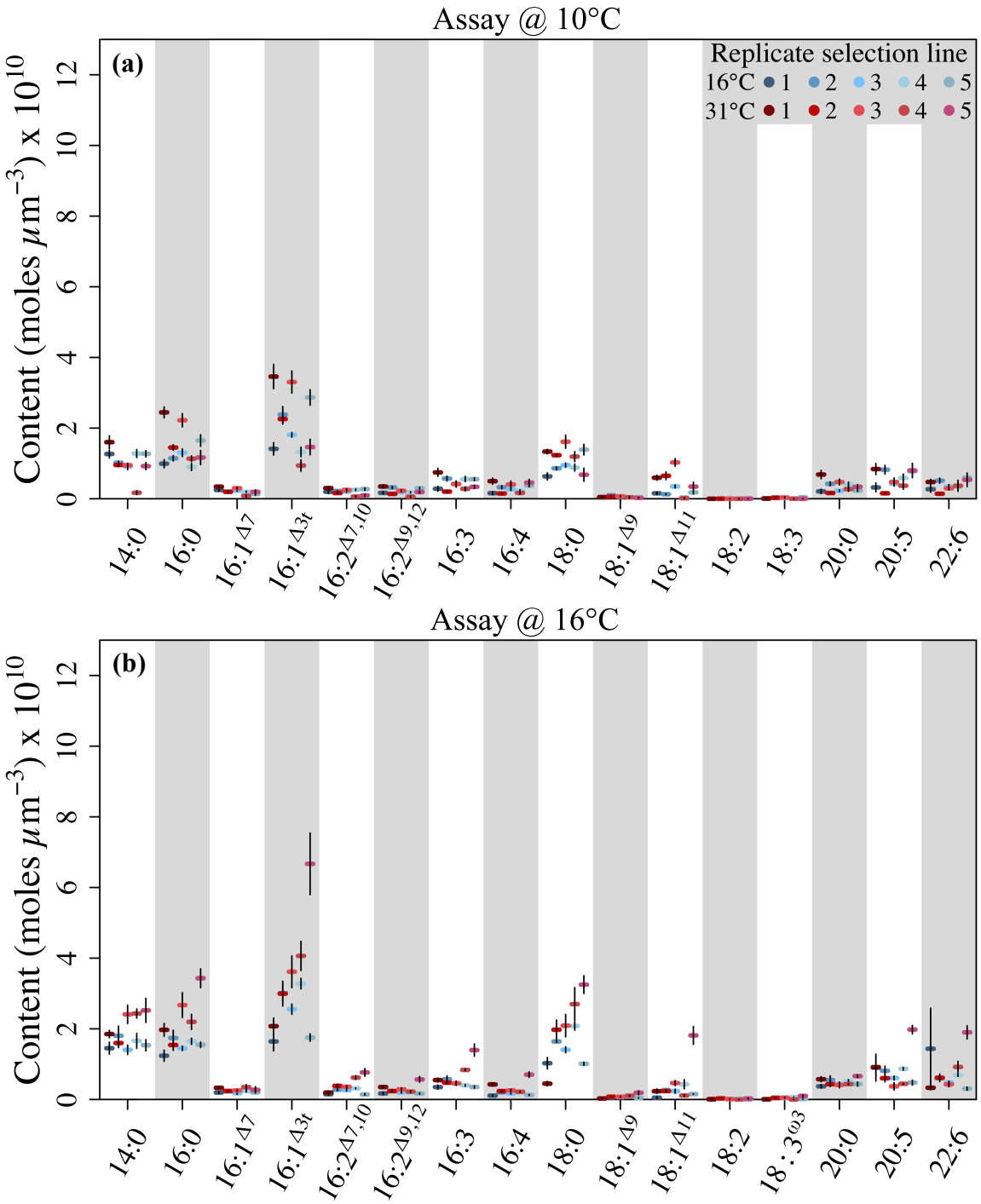

Figure 6: Total content of 16 fatty acid classes in *T. pseudonana* selected at 16 °C (blue shades) and 31°C (red shades) and grown at (**a**) 10°C; (**b**) 16°C; (**c**) 26°C; and (**d**) 31°C. error bars are ±1 SE. Y-axis values are multiplied by 10^{10} for clarity.

Figure 6 (cont'd)

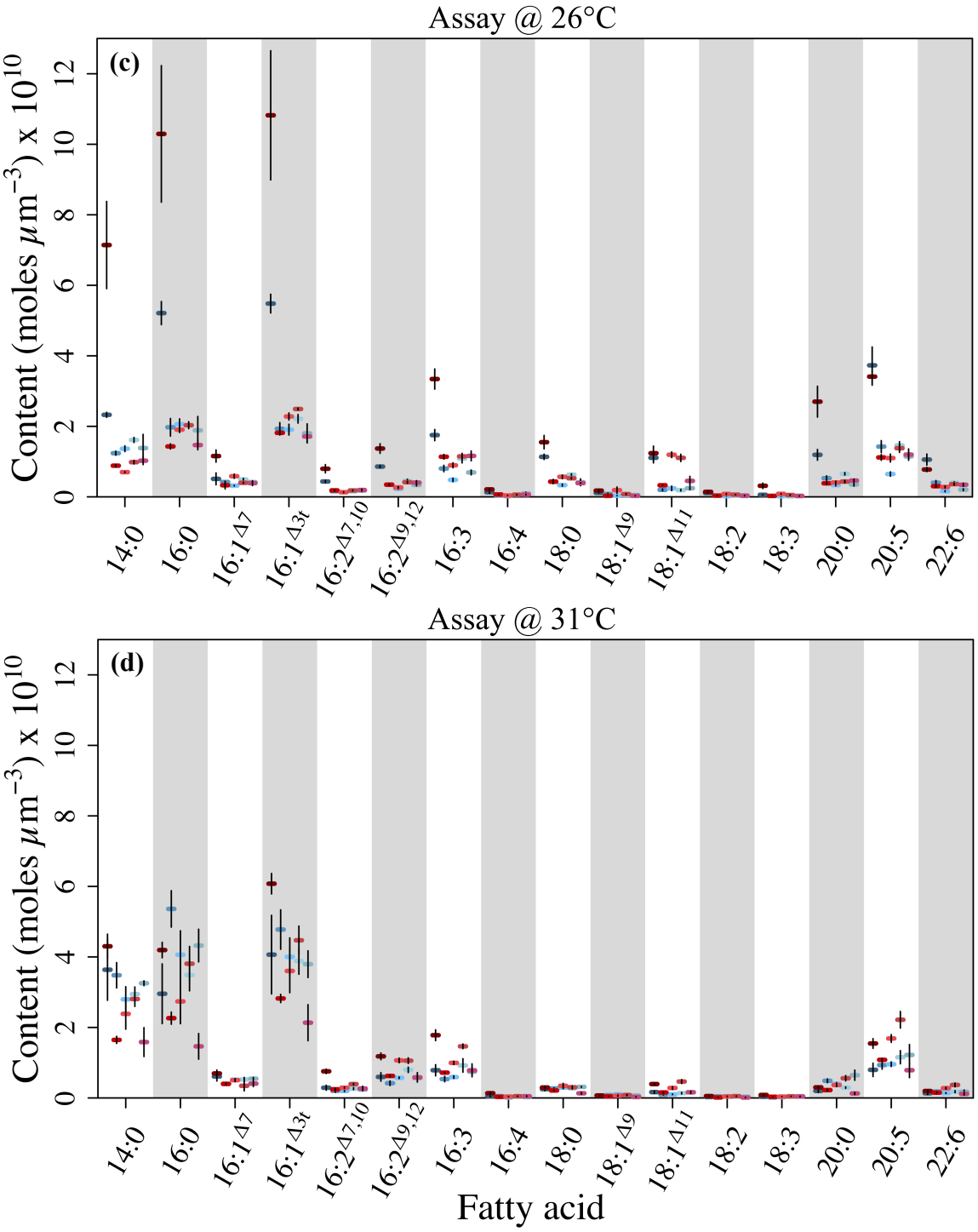

Table 1: RM-ANOVA testing effects of selection temperature and assay temperature on *T. pseudonana* mean chain length (*MCL*), unsaturation (*WUnSat*), total fatty acids (Total FA), percent saturated FA (% SFA), percent monounsaturated FA (% MUFA), percent polyunsaturated FA (% PUFA), and percentages of individual FA classes.

Trait	Effect	df	MS	F-statistic	P-value
MCL	Assay temp.	3,12	2.98	33.31	<0.0001
	Selection temp.	1,96	0.32	3.61	0.060
	Error	112	0.089	--	--
WUnSat	Assay temp.	3,12	0.87	24.97	<0.0001
	Selection temp.	1,93	0.24	7.01	0.0093
	Assay temp. × Sel. Temp.	3,93	0.24	6.83	0.0003
	Error	112	0.035	--	--
Total FA (mol)	Assay temp.	3,12	0.027	5.04	0.0026
	Selection temp.	1,93	0.012	2.21	0.14
	Error	109	0.0053	--	--
% SFA	Assay temp.	3,12	329.3	9.71	<0.0001
	Selection temp.	1,94	467.7	13.79	0.0003
	Assay temp. × Sel. Temp.	3,94	244.8	7.22	0.0002
	Error	110	33.9	--	--
% 14:0	Assay temp.	3,12	343.6	24.03	<0.0001
	Selection temp.	1,97	276.6	19.35	<0.0001
	Error	113	14.30	--	--
% 16:0	Assay temp.	3,12	267.47	22.89	<0.0001
	Selection temp.	1,94	38.55	3.30	0.072
	Assay temp. × Sel. Temp.	3,94	146.04	12.50	<0.0001
	Error	110	11.68	--	--
% 18:0	Assay temp.	3,12	1017.0	102.46	<0.0001
	Selection temp.	1,97	8.30	0.83	0.36
	Error	113	9.90	--	--
% 20:0	Assay temp.	3,12	28.29	21.43	<0.0001
	Selection temp.	1,97	2.77	2.10	0.15
	Error	113	1.32	--	--
% MUFA	Assay temp.	3,12	24.90	1.13	0.34
	Selection temp.	1,97	163.00	15.22	0.0076
	Error	113	22.06	--	--
% 16:1$^{\Delta 7}$	Assay temp.	3,12	20.56	13.03	<0.0001
	Selection temp.	1,97	0.004	0.002	0.96
	Error	113	1.58	--	--
% 16:1$^{\Delta 3}$	Assay temp.	3,12	132.85	12.97	<0.0001
	Selection temp.	1,97	1.55	0.14	0.71
	Error	113	10.92	--	--
% 18:1$^{\Delta 9}$	Assay temp.	3,12	0.25	0.97	0.41
	Selection temp.	1,97	0.0002	0.001	0.98
	Error	113	0.26	--	--

Table 1 continued on next page

Table 1 (cont'd)

% 18:1$^{\Delta 11}$	Assay temp.	3,12	58.29	11.04	<0.0001
	Selection temp.	1,94	133.88	25.36	<0.0001
	Assay temp. × Sel. Temp.	3,94	15.01	2.84	0.041
	Error	110	5.28	--	--
% PUFA	Assay temp.	3,12	337.7	6.34	0.0005
	Selection temp.	1,94	78.50	1.47	0.23
	Assay temp. × Sel. Temp.	3,94	305.8	5.74	0.0011
	Error	110	51.30	--	--
% 16:2$^{\Delta 7,10}$	Assay temp.	3,12	3.72	9.81	<0.0001
	Selection temp.	1,94	1.67	4.41	0.038
	Assay temp. × Sel. Temp.	3,94	6.36	16.78	<0.0001
	Error	110	0.38	--	--
% 16:2$^{\Delta 9,12}$	Assay temp.	3,12	55.64	57.81	<0.0001
	Selection temp.	1,94	6.78	7.05	0.0091
	Assay temp. × Sel. Temp.	3,94	12.93	13.43	<0.0001
	Error	110	0.96	--	--
% 16:3$^{\Delta 7,10,13}$	Assay temp.	3,12	125.08	41.51	<0.0001
	Selection temp.	1,94	45.45	15.09	0.0002
	Assay temp. × Sel. Temp.	3,94	34.32	11.39	<0.0001
	Error	110	3.01	--	--
% 16:4$^{\Delta 4,7,10,13}$	Assay temp.	3,12	59.92	110.08	<0.0001
	Selection temp.	1,94	3.41	6.26	0.014
	Assay temp. × Sel. Temp.	3,94	1.01	1.85	0.14
	Error	110	0.54	--	--
* *% 18:2$^{\Delta 9,12}$*	--	--	--	--	--
* *% 18:3$^{\Delta 9,12,15}$*	--	--	--	--	--
% 20:5$^{\Delta 5,8,11,14,17}$	Assay temp.	3,12	219.89	27.37	<0.0001
	Selection temp.	1,94	0.010	0.002	0.97
	Assay temp. × Sel. Temp.	3,94	33.17	4.13	0.0081
	Error	110	8.03	--	--
% 22:6$^{\Delta 4,7,10,13,16,19}$	Assay temp.	3,12	131.55	7.32	0.0002
	Selection temp.	1,94	17.29	0.96	0.33
	Assay temp. × Sel. Temp.	3,94	13.20	0.74	0.53
	Error	110	17.96	--	--

* No model fit, due to zero inflation.

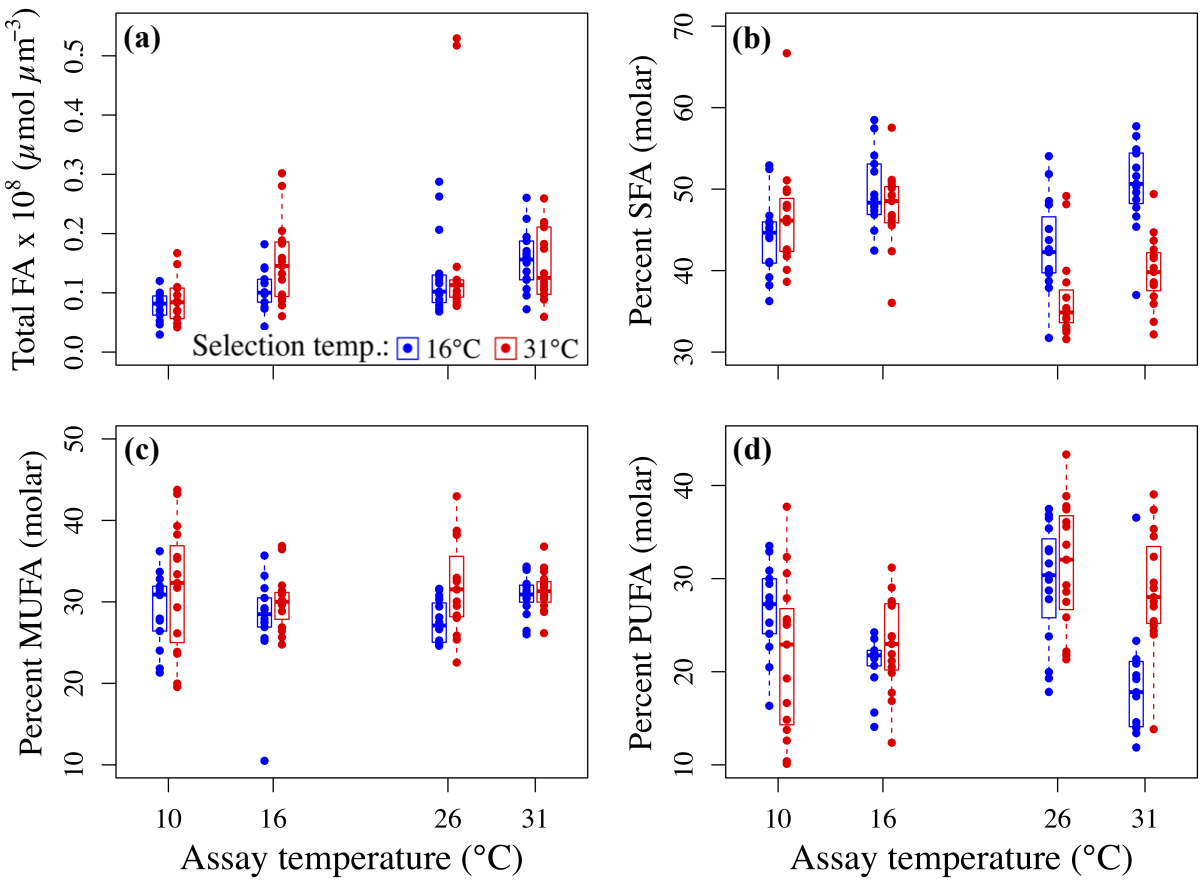

Figure 7: (a) Total fatty acid (FA) content per biovolume in 16°C-selected (blue) and 31°C-selected (red) populations at 10, 16, 26, and 31°C; (b) Saturated FA as a fraction of total FA; (c) Monounsaturated FA as a fraction of total FA; (d) Polyunsaturated FA as a fraction of total FA. n = 3 for each replicate population. Lines across boxes indicate the median of each group, with the lower and upper bounds indicate the 25th and 75th quartiles, respectively. Points beyond the lower and upper whiskers are outliers, falling outside the 0th and 100th quartiles.

The composite metric of FA unsaturation (*WUnSat*) was largely driven by % PUFA. Unsaturation was higher overall in 31°C-selected populations (Table 1; Figure 8A), with the greatest difference in unsaturation at the 31°C assay temperature (Table 1 Figure 8A). Mean

chain length (C atoms per FA molecule) was also higher in 31°C-selected populations overall (Table 1; Figure 8B).

c

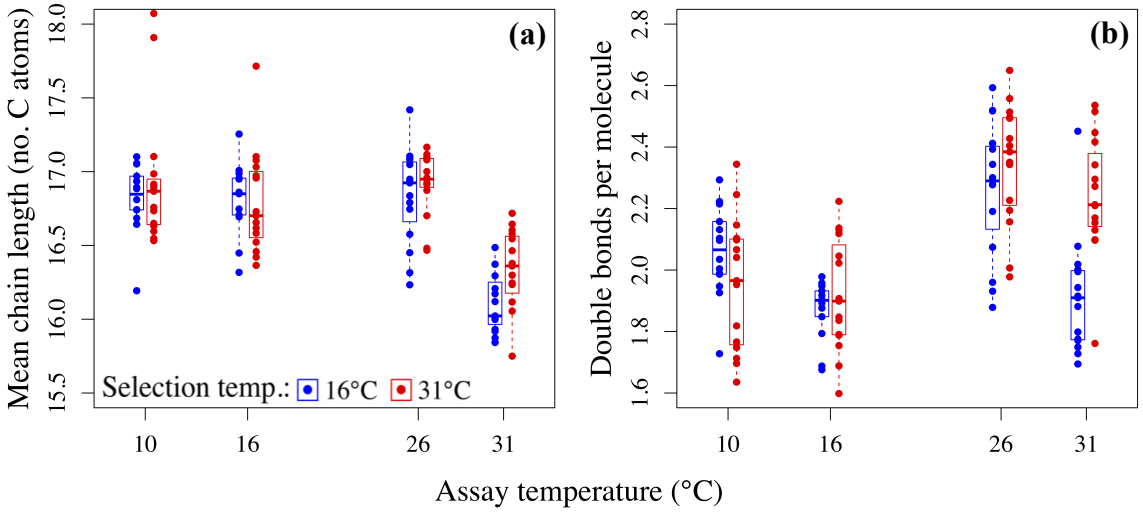

Figure 8: (a) Mean chain length (C atoms per molecule); (b) degree of unsaturation (double bonds per molecule) in 16°C-selected (blue) versus 31°C-selected (red) *T. pseudonana* populations at 10, 16, 26, and 31°C. n = 3 for each replicate population. Symbols are as above.

While composite metrics of FA content and unsaturation differed between selection groups primarily at the 31°C assay temperature, these metrics mask some underlying divergence (or lack thereof) in thermal reaction norms between selection groups for key FA classes. We will highlight a few notable FA classes in the text; for all others, refer to Table 1 and Figures 4-6.

Among the SFA, 16:0 FA were notable in that, at the 10°C assay temperature, 31°-selected populations had higher % 16:0, while at 16°C there was little difference between selection groups and at 26 and 31°C, 31°C-selected populations had the highest % 16:0 (Table 1; Figure 9b). Percent 18:0 FA decreased ~60% between the 16°C and 26°C assay temperatures in both selection groups, dropping an additional ~25% between 26°C and 31°C (Table 1; Figure

9c); % 18:0 FA was the only SFA that was consistently higher in 31°C selected populations across assay temperatures, with the greatest difference observed at 10°C (Table 1; Figure 9c).

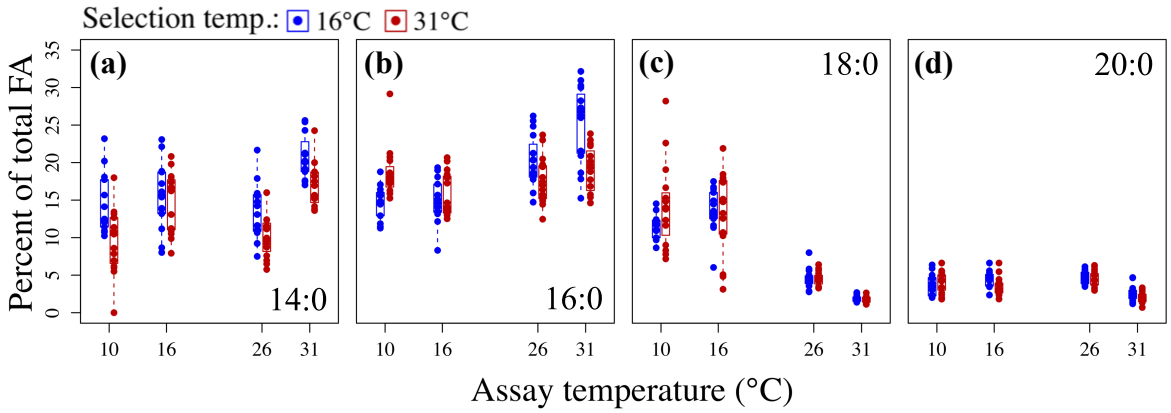

Figure 9: Saturated fatty acids as percentages of total fatty acids in 16°C-selected (blue) versus 31°C-selected (red) *T. pseudonana* populations at 10, 16, 26, and 31°C. n = 3 for each replicate population. Numbers in the lower (a,b) and upper right corners indicate the fatty acid classes shown in each panel; for example, "14:0" is a FA with 14 C atoms and no double bonds. Other symbols are as above.

Among the MUFA, $16{:}1^{\Delta 7}$ and $16{:}1^{\Delta 3}$ FA represented between 20 and 30% of total FA in both selection groups and at all assay temperatures. However, these two FA classes differed the least between the two temperature selection groups. Thermal reaction norms for % $16{:}1^{\Delta 7}$ FA classes were parallel and differed by << 1% at every assay temperature (Table 1; Figure 10a). Percent $16{:}1^{\Delta 3}$ reaction norms were effectively identical (Table 1; Figure 10b). *Assay temperature × selection temperature* interaction effects were non-significant, did not improve model fits, and were dropped from both % 16:1 FA models altogether, as was also the case for % $18{:}1^{\Delta 9}$. Percent $18{:}1^{\Delta 11}$ was ~3x higher in 31°C-selected populations than in 16°C-selected

populations across assay temperatures (Table 1; Figure 10d). Percent $18{:}1^{\Delta 11}$ was lowest for both selection groups at the 31°C assay temperature (*assay temperature × selection temperature* interaction Table 1; Figure 10d).

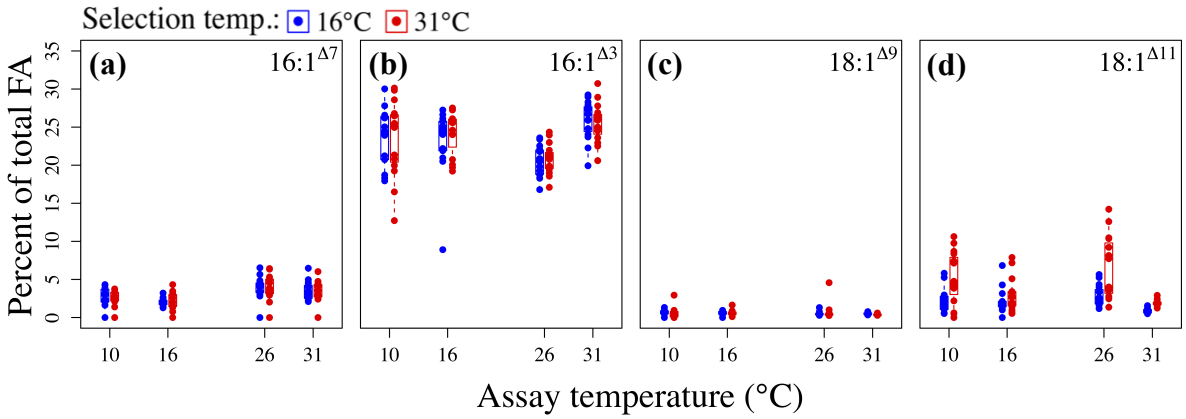

Figure 10: Monounsaturated fatty acids as percentages of total fatty acids in 16°C-selected (blue) versus 31°C-selected (red) *T. pseudonana* populations at 10, 16, 26, and 31°C. n = 3 for each replicate population. Numbers in the lower (a,b) and upper right corners indicate the fatty acid classes shown in each panel. "Δ" indicates the position, from the carboxyl end, of the double bond; for example, "Δ3" indicates a double bond in the third position form the carboxyl end. Other symbols are as above.

Percent $16{:}3^{\Delta 7,10,13}$ FA was higher in 16°C-selected populations than in 31°C-selected populations at 10°C, while the reverse was true at 16, 26, and 31°C (Table 1; Figure 11c). Percent $16{:}4^{\Delta 4,7,10,13}$ FA was consistently higher in 31°C-selected populations than in 16°C-selected populations (Table 1; Figure 11d), but decreased by roughly an order of magnitude between 10°C and 31°C assay temperatures in both selection groups (Table 1; Figure 11d). $18{:}2^{\Delta 9,12}$ and $18{:}3^{\Delta 9,12,15}$ FA were notable in their near-absence. Combined, they rarely exceeded

1% of total FA, and were often undetectable, preventing statistical analysis. 20:5$^{\Delta5,8,11,14,17}$ and 22:6$^{\Delta4,7,10,13,16,19}$ FA were the two longest (most C atoms) FA classes, and each was notable in its relative abundance, representing between 1% and 10% of total FA. Percent 20:5$^{\Delta5,8,11,14,17}$ and % 22:6$^{\Delta4,7,10,13,16,19}$ did not differ between selection groups overall, but was higher in 31°C-selected populations at the 31°C assay temperature (*assay temperature × selection temperature* interaction: Table 1; Figure 11g,h). Percent 20:5$^{\Delta5,8,11,14,17}$ was highest overall for both selection groups at 26°C (Table 1; Figure 11g), while % 22:6$^{\Delta4,7,10,13,16,19}$ peaked for both groups at 16°C, then declined by nearly an order of magnitude between 16°C and 31°C (Table 1; Figure 11h).

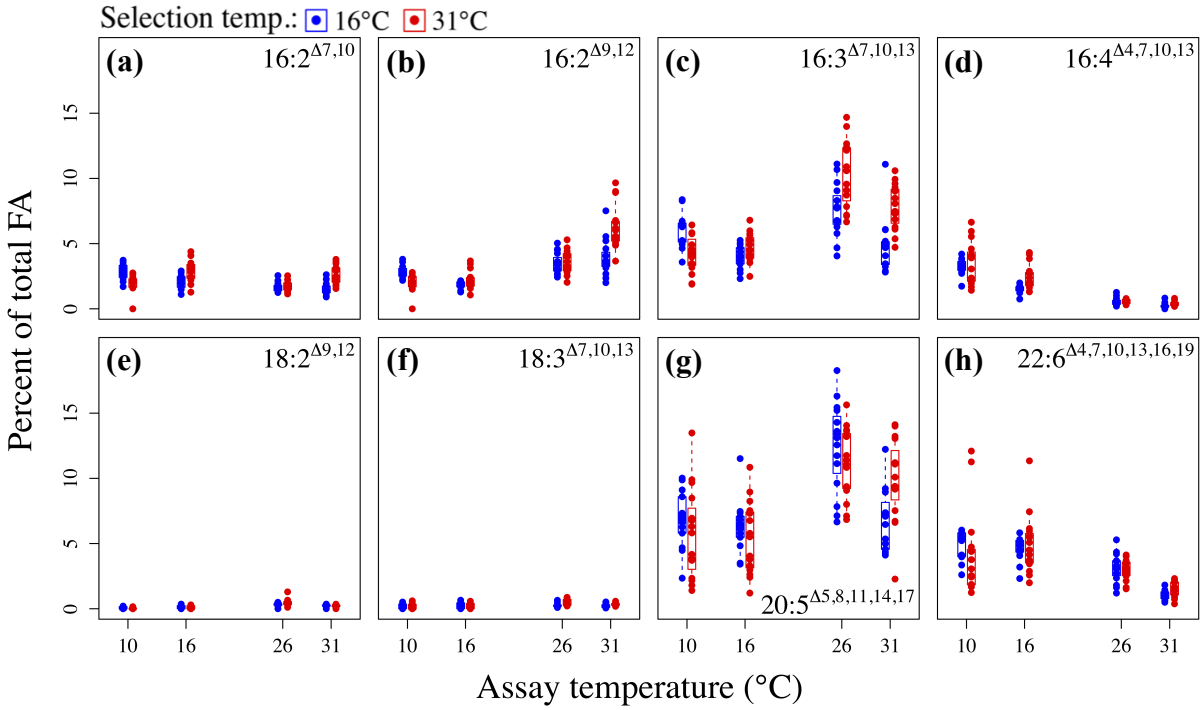

Figure 11: Polyunsaturated fatty acids as percentages of total fatty acids in 16°C-selected (blue) versus 31°C-selected (red) *T. pseudonana* populations at 10, 16, 26, and 31°C. n = 3 for each replicate population. Symbols are as above.

Discussion

Previous studies have suggested that many poikilotherms increase levels of FA saturation with increasing temperature to maintain homeoviscosity of membranes (Patterson 1970; Sinensky 1974; Joh *et al.* 1993; reviewed in Neidleman *et al.* 1987; Jiang & Gao 2004). Indeed, Thompson *et al.* (1992b) observed a strong negative trend in the ratio of unsaturated to saturated FA in *T. pseudonana* between 10 and 25°C. We therefore predicted that 1) *T. pseudonana* in our study would exhibit a similar negative trend in unsaturation across temperature, and 2) selection of *T. pseudonana* populations for ~500 generations at 16°C would lead to a greater predisposition to FA unsaturation at low temperatures, and possibly across all assay temperatures if plasticity in FA unsaturation was low. Conversely, 31°C-selected populations should evolve enhanced production of saturated FA to maintain membrane rigidity at high temperatures, or across all temperatures if the same tradeoff applied. Many of our results were nearly exactly opposite these predictions.

We showed that the temperature dependence of fatty acid profiles in *Thalassiosira pseudonana* can evolve rapidly in response to experimental temperature selection. Replicate *T. pseudonana* populations that underwent ~500 generations of experimental natural selection at low (16°C) and high (31°C) temperatures exhibited marked divergence in FA saturation at the four assay temperatures (10, 16, 26, and 31°C), driven by major divergence in thermal reaction norms of a few key FA classes. However, the temperature-dependent responses of fatty acid content and composition in both *T. pseudonana* temperature selection groups were complex, idiosyncratic, and often opposite what we predicted based on prior research (Patterson 1970; Sinensky 1975; Jiang & Gao 2004; Wada *et al.* 1990); for example, SFA were higher at low temperatures and UFA were higher at high temperatures in many cases. We note that unexpected

and idiosyncratic responses of phytoplankton FA to temperature seem to be common among previous studies of the topic (Thompson *et al.* 1992a,b; Rousch *et al.* 2003; Jiang & Gao 2004).

Average total FA per biovolume varied little across assay temperatures, but was lowest at 10°C and highest at 31°C for both selection groups, on average. In contrast, Patterson (1970) showed that FA as a percentage of dry weight in the chlorophyte *Chlorella sorokiniana* increased toward the thermal niche boundaries, and was lowest near T_{opt}. Van Wagenen *et al.* (2012) showed a similar pattern for the ochrophyte *Nannochloropsis salina*. In eight species of phytoplankton including *T. pseudonana,* Thompson *et al.* (1992a) found thermal reaction norms for lipid cell^{-1} to be highly variable, ranging from concave up to concave down between 10 and 25°C; of particular note, however, the reaction norm for *T. pseudonana* was distinctly concave-up. While it is possible that our assay temperature range simply failed to adequately capture the temperature regions closest to the niche boundaries, we would point out that assay temperatures in Thompson *et al.* (1992a) ranged from 10°C to 25°C, and that ours matched (on the low end) or exceeded (on the high end) this range.

Percent SFA decreased slightly between 10 and 31°C in 16°C-selected populations, with a dramatic drop between 16 and 26°C; % SFA decreased dramatically in 31°C-selected populations between 10°C and 31°C; and % SFA was significantly higher in 16°C-selected populations than in 31°C-selected populations at all assay temperatures except 10°C. These unexpected trends are not unprecedented. Teoh *et al.* (1994) observed increased unsaturation at low temperatures in only one of six phytoplankton species studied. There were some indications, however, that *T. pseudonana* adjusted percentages of certain PUFA as a means of maintaining homeoviscosity across temperature, and that thermal reaction norms for these PUFA evolved in response to temperature selection in the direction predicted. First, % PUFA, and, consequently,

WUnSat (average double bonds per FA molecule) were slightly higher in 16°C-selected populations than in 31°C-selected populations at 10°C. Second, the most highly unsaturated fatty acids, $20{:}5^{\Delta 5,8,11,14,17}$ and $22{:}6^{\Delta 4,7,10,13,16,19}$, which ranged roughly from 1% to 10% of total FA in both 16 and 31°C-selected populations, were significantly higher in 16°C-selected populations than in 31°C-selected populations at 10, 16 and 26°C, but were significantly lower at 31°C. It would appear, therefore, that in addition to evolving enhanced production of these highly-unsaturated FA (HUFA), 16°C-selected populations were also more plastic in their ability to regulate the amount of HUFA produced, depending on temperature. Percent $22{:}6^{\Delta 4,7,10,13,16,19}$ decreased overall in both groups between 10 and 31°C, but $20{:}5^{\Delta 5,8,11,14,17}$ did not, in contrast to previous studies (Jiang & Gao 2004; Pasquet *et al.* 2014).

Besides unsaturation, FA chain length (C atoms per molecule) has been suggested to play a role in regulating membrane fluidity (Sinensky 1974; Hochachka & Somero 1984). These authors suggest that, as temperature increases, microbes tend to incorporate longer-chain FA into their membranes, as shorter FA molecules (especially SFA) "melt" at lower temperatures (Sinensky 1974; Hochachka & Somero 1984). Incorporation of short-chain SFA (14:0 and 16:0 FA, in this case) into membranes when cold and long-chain SFA (18:0 and 20:0 here) when warm may thus be considered a strategy for maintaining homeoviscosity across temperature. However, 14:0 and 16:0 FA have melting points of 53.9 and 63.1°C, respectively (Hochachka & Somero 1984), both of which lie well outside the thermal niche of *T. pseudonana*. No SFA detected in our study were thus ever in liquid phase. The longest-chain SFA in our study were 18:0 and 20:0, both of which decreased their % abundances dramatically between 10 and 31°C. Mean chain length (*MCL*), which incorporates both SFA and UFA, was fairly constant between 10 and 26°C in both *T. pseudonana* temperature selection groups and dropped significantly from

26 to 31°C. *MCL* was also significantly higher in 31°C-selected populations than in 16°C-selected populations at the 31°C assay temperature. While % 14:0 FA was higher in 16°C-selected populations than in 31°C-selected populations across assay temperatures, both 14:0 and 16:0 FA increased by ~50% in 16°C-selected populations between 10 and 31°C, indicating a tendency for cold-adapted *T. pseudonana* to increase production of short, saturated FA at high, rather than at low temperatures. This is consistent with some studies more recent than Sinensky (1974) and Hochachka & Somero (1984), which have shown non-significant (Thompson *et al.* 1992b; Renaud *et al* 1995; Renaud *et al.* 2002) or negative (Renaud *et al* 1995; Renaud *et al.* 2002) trends in *MCL* with increasing temperature. In sum, favoring shorter or longer *MCL* does not appear to be a strategy for maintaining homeoviscosity across temperature in *T. pseudonana* populations in either of our temperature selection groups, nor does this strategy appear to be the rule in other phytoplankton species.

Some well-targeted follow-up research could shed a great deal of light on temperature dependence of FA saturation and desaturation in temperature-selected populations of *T. pseudonana*, and in phytoplankton in general. For example, a study of mechanisms of FA desaturation at the cellular level in temperature-selected *T. pseudonana* populations combined with information on underlying molecular evolution would be a powerful and illuminating follow-up to this study. Seven desaturases were identified in *T. pseudonana* (Tonon *et al.* 2005) using the draft genome sequenced by Armbrust *et al.* (2004). Assays of the activities of these desaturases in cold- and warm-adapted *T. pseudonana* populations across a broad temperature range could be combined with the amino acid sequences of the desaturases themselves to better understand the role of FA profile evolution in *T. pseudonana*'s thermal adaptation.

Phytoplankton, especially diatoms, are a vital source of fatty acids for marine organisms at higher trophic levels, and are the primary source of long-chain HUFA in the world's marine (Kang 2011; Hixson & Arts 2016) and freshwater (Kainz *et al.* 2004) systems. Marine-derived HUFA are also a direct and essential link between marine phytoplankton and human health (Kang 2011), and global production of HUFA by marine phytoplankton may be declining as a result of rising sea surface temperatures (Hixson & Arts 2016); climate effects on HUFA production in phytoplankton must therefore be considered of global human interest. Studies of the effect of warming on the content and composition of FA in marine and freshwater phytoplankton communities have primarily focused on multi-species responses (Hixson & Arts 2016) or shifts in phytoplankton assemblages leading to changes in the availability of vital HUFA to higher trophic levels (Litzow *et al.* 2006; Kang 2011). Here, we showed that FA content and composition within a species of marine diatom, *Thalassiosira pseudonana*, is sensitive to temperature on both short (physiological) and long (evolutionary) timescales, and that thermal reaction norms of key FA are evolutionarily labile. Importantly, *T. pseudonana* populations experimentally adapted to 16°C and 31°C for ~500 generations exhibited different responses to medium temperature by three highly unsaturated omega-3 FA, $16{:}4^{\Delta 4,7,10,13}$, $20{:}5^{\Delta 5,8,11,14,17}$, and $22{:}6^{\Delta 4,7,10,13,16,19}$. 16:4 and 22:6 FA declined sharply between 10 and 31°C in all experimental populations, but 31°C-selected populations were significantly higher in all three omega-3 HUFA at the highest assay temperature, 31°C. Thus, while warming may lead to a decrease in production of some key HUFA, *T. pseudonana* may be able to recover some HUFA production through rapid evolutionary responses to warming seas. Long-term implications of evolutionary adaptation to warming in phytoplankton for availability of HUFA to higher trophic levels, including humans, are worthy of extensive future research.

REFERENCES

REFERENCES

Armbrust EV, Berges JA, Bowler C, Green BR, Martinez D, *et al.* 2004. The genome of the diatom *Thalassiosira pseudonana*: ecology, evolution, and metabolism. *Science* **306**:79–86.

Beamish FWH, Mookherjii PS. 1964. Respiration of fishes with special emphasis on standard oxygen consumption. I. Influence of weight and temperature on respiration of goldfish, *Carassius auratus* L. *Canadian Journal of Zoology* **50**:161-175.

Bhakoo M, Herbert RA. 1979. The effects of temperature on fatty acid and phospholipid composition of four obligately psychrophilic *Vibrio* spp. *Archives of Microbiol*ogy **121**:121-127.

Boyle NR, Page MD, Liu B, Blaby IK, Casero D, *et al.* 2012. Three acyltransferases and nitrogen-responsive regulator are implicated in nitrogen starvation-induced triacylglycerol accumulation in *Chlamydomonas*. *Journal of Biological Chemistry* **287**:15811–15825.

Boyd PW, Rynearson TA, Armstrong EA, Fu F, Hayashi K, *et al.* 2013. Marine phytoplankton temperature versus growth responses from polar to tropical waters—outcome of a scientific community-wide study. *PLoS One* **8**:e63091.

Bradford M. 2013. Thermal adaptation of decomposer communities in warming soils. *Frontiers in Microbiology* **4**:1-16.

Canvin DT. 1965. The effect of temperature on the oil content and fatty acid composition of the oils from several oil seed crops. *Canadian Journal of Botany* **43**:63-69.

Caron DA, Goldman JC, Dennett MR. 1986. Effect of temperature on growth, respiration, and nutrient regeneration by an omnivorous microflagellate. *Applied Environmental Microbiology* **52**:1340-1347.

Chen M, Tang H, Ma H, Holland TC, Ng KYS, *et al.* 2011. Effect of nutrients on growth and lipid accumulation in the green algae *Dunaliella tertiolecta*. *Bioresource Technology* **102**:1649–1655.

Converti A, Casazza AA, Ortiz EY, Perego P, Del Borghi M. 2009. Effect of temperature and nitrogen concentration on the growth and lipid content of *Nannochloropsis oculata* and *Chlorella vulgaris* for biodiesel production. *Chemical Engineering and Processing: Process Intensification* **48**:1146–1151.

Corkrey R, McMeekin TA, Bowman JP, Ratkowsky DA, Olley J, *et al.* 2014. Protein thermodynamics can be predicted directly from biological growth rates. *PLoS One* **9**:e96100.

Dean AP, Sigee DC, Estrada B, Pittman JK. 2010. Using FTIR spectroscopy for rapid

determination of lipid accumulation in response to nitrogen limitation in freshwater microalgae. *Bioresource Technology* **101**:4499–4507.

Gardner R, Peters P, Peyton B, Cooksey KE. 2011. Medium pH and nitrate concentration effects on accumulation of triacylglycerol in two members of the chlorophyta. *Journal of Applied Phycology* **23**:1005–1016.

Geerts AN, Vanoverbeke J, Vanschoenwinkel B, Van Doorslaer W, Feuchtmayr H, *et al.* 2015. Rapid evolution of thermal tolerance in the water flea *Daphnia*. *Nature Climate Change* **5**:665-669.

Guillard R, Hargraves P. 1993 *Stichochrysis immobilis* is a diatom, not a chrysophyte. *Phycologia* **32**:234–236.

Guschina IA, Harwood JL. 2006. Lipids and lipid metabolism in eukaryotic algae. *Progress in Lipid Research* **45**:160-186.

Harwood JL, Jones AL. 1989. Lipid metabolism in algae. *Advances in Botanical Research* **16**:1-53.

Hazel JR. 1995. Thermal adaptation in biological membranes: is homeoviscous adaptation the explanation? *Annual Review of Physiology* **57**:19-42.

Hipkin R, Day JG, Rad-Menéndez C, Mock T. 2013. The first evidence for genotypic stability in a cryopreserved transgenic diatom. *Journal of Applied Phycology* **26**:65-71.

Hixson SM, Arts MT. 2016. Climate warming is predicted to reduce omega-3, long-chain, polyunsaturated fatty acid production in phytoplankton. *Global Change Biology* **22**:2744-2755.

Hochachka PW, Somero GN. 1984. Temperature Adaptation. *In: Biochemical Adaptation,* Hochachka PW, Somero GN [Authors]. Princeton University Press, Princeton, NJ, USA. pp. 355-449.

Hu Q, Sommerfeld M, Jarvis E, Ghirardi M, Posewitz M, *et al*. 2008. Microalgal triacylglycerols as feedstocks for biofuel production: Perspectives and advances. *The Plant Journal* **54**:621-639.

Jiang H, Gao K. 2004. Effects of lowering temperature during culture on the production of polyunsaturated fatty acids in the marine diatom *Phaeodactylum tricornutum* (Bacillariophyceae). *Journal of Phycology* **40**:651–654.

Joh T, Yoshida T, Yoshimoto M, Miyamoto T, Hatano S. 1993. Composition and positional distribution of fatty acids in polar lipids from *Chlorella ellipsoidea* differing in chilling susceptibility and frost hardiness. *Physiologia Plantarum* **89**:285–290.

Kainz M, Arts MT, Mazumder A. 2004. Essential fatty acids in the planktonic food web and their ecological role for higher trophic levels. *Limnology and Oceanography* **49**:1784-1793.

Kang JX. 2011. Omega-3: A link between global climate change and human health. *Biotechnology Advances* **29**:388-390.

Knies JL, Izem R, Supler KL, Kingsolver JG, Burch CL. 2006. The genetic basis of thermal reaction norm evolution in lab and natural phage populations. *PLoS Biology* **4**:e201.

Knoblauch C, Jorgensen B. 1999. Effect of temperature on sulphate reduction, growth rate and growth yield in five psychrophilic sulphate-reducing bacteria from Arctic sediments. *Environmental Microbiology* **1**:457-467.

Lee J-H, Ahn JJ. 2000. Temperature effects on development, fecundity, and life table parameters of *Amblyseius womersleyi* (Acari: Phytoseiidae). *Environmental Entomology* **29**:265-271.

Lindmark M, Huss M, Ohlberger J, Gårdmark A. 2018. Temperature-dependent body size effects determine population responses to climate warming. *Ecology Letters* **21**:181-189.

Listmann L, LeRoch M, Schlüter L, Thomas MK, Reusch TBH. 2016. Swift thermal reaction norm evolution in a key marine phytoplankton species. *Evolutionary Applications* **9**:1156-1164.

Litzow MA, Bailey KM, Prahl FG, Heintz R. 2006. Climate regime shifts and reorganization of fish communities: The essential fatty acid limitation hypothesis. *Marine Ecology Progress Series* **315**:1-11.

Lynn SG, Kilham SS, Kreeger DA, Interlandi SJ. 2000. Effect of nutrient availability on the biochemical and elemental stoichiometry in freshwater diatom *Stephanodiscus minutulus* (Bacillariophyceae). *Journal of Phycology* **36**:510–522.

McLachlan JL, Curtis JM, Boutilier K, Keusgen M, Seguel MR. 1999. *Tetreutreptia pomquetensis* (Euglenophyta), a psychrophilic species: growth and fatty acid composition. *Journal of Phycology* **35**:280-286.

Mongold JA, Bennett AF, Lenski RE. 1996. Evolutionary adaptation to temperature. IV. Adaptation of *Escherichia coli* at a niche boundary. *Evolution* **50**:35-43.

Montagnes DJS, Franklin DJ. 2001. Effect of temperature on diatom volume, growth rate, and carbon and nitrogen content: reconsidering some paradigms. *Limnology and Oceanography* **46**:2008-2018.

Mortensen SH, Børsheim KY, Rainuzzo JR, Knutsen G. 1988. Fatty acid and elemental composition of the marine diatom *Chaetoceros gracilis* Schütt. Effects of silicate deprivation, temperature and light intensity. *Journal of Experimental Marine Biology and Ecology* **122**:173-185.

Murata N, Los D. 1997. Membrane fluidity and temperature perception. *Plant Physiology* **115**:875-859.

Neidleman SL. 1987. Effects of temperature on lipid unsaturation. *Biotechnology and Genetic Engineering Reviews* **5**:245-268.

Neori A, Holm-Hansen O. 1982. Effect of temperature on rate of photosynthesis in Antarctic phytoplankton. *Polar Biology* **1**:33-38.

Neori A, Vernet M, Holm-Hansen O, Haxo FT. 1986 Relationship between action spectra for chlorophyll a fluorescence and photosynthetic O_2 evolution in algae. *Journal of Plankton Research* **8**:537–548.

O'Donnell DR, Hamman CR, Johnson EC, Klausmeier CA, Litchman E. 2018. Rapid thermal adaptation in a marine diatom reveals constraints and trade-offs. *Global Change Biology* doi: 10.1111/gcb.14360. **[Epub ahead of print]**

Padfield D, Yvon-Durocher G, Buckling A, Jennings S, Yvon-Durocher G. 2015. Rapid evolution of metabolic traits explains thermal adaptation in phytoplankton. *Ecology Letters* **19**:133-142.

Pasquet V, Ulmann L, Mimouni V, Guihéneuf F, Jacquette B, *et al*. 2014. Fatty acids profile and temperature in the cultured marine diatom *Odontella aurita*. *Journal of Applied Phycology* **26**:2265–2271.

Pastenes C, Horton P. 1996. Effect of high temperature on photosynthesis in beans. I. Oxygen evolution and chlorophyll fluorescence. *Plant Physiology* **112**:1245-1251.

Peter KH, Sommer U. 2013. Phytoplankton cell size reduction in response to warming mediated by nutrient limitation. *PLoS One* **8**:e71528.

Pinheiro J, Bates D, R Core Team. 2017. nlme: linear and nonlinear mixed effects models. R package version 3.1-131. https://cran.r-project.org/web/packages/nlme/nlme.pdf.

Quinn PJ. 1981. The fluidity of cell membranes and its regulation. *Progress in Biophysics and Molecular Biology* **38**:1-104.

Ratkowsky DA, Olley J, Ross T. 2005. Unifying temperature effects on the growth rate of bacteria and the stability of globular proteins. *Journal of Theoretical Biology* **233**:351-362.

Reitan KI, Rainuzzo JR, Olsen Y. 1994. Effect of nutrient limitation on fatty acid and lipid content of marine microalgae. *Journal of Phycology* **30**:972–979.

Renaud SM, Zhou HC, Parry DL, Thinh L-V, Woo KC. 1995. Effect of temperature on the growth, total lipid content and fatty acid composition of recently isolated tropical microalgae

Isochrysis sp., *Nitzschia closterium*, *Nitzschia paleacea*, and commercial species *Isochrysis* sp. (clone T.ISO). *Journal of Applied Phycology* **7**:595-602.

Renaud SM, Thinh L-V, Lambrinidis G, Parry DL. 2002. Effect of temperature on growth, chemical composition and fatty acid composition of tropical Australian microalgae grown in batch cultures. *Aquaculture* **211**:195–214.

Robarts R, Zohary T. 1987. Temperature effects on photosynthetic capacity, respiration, and growth rates of bloom-forming cyanobacteria. *New Zealand Journal of Marine and Freshwater Research* **21**:391-399.

Sakamoto T, Bryant D. 1998. Growth at low temperature causes nitrogen limitation in the cyanobacterium *Synechococcus* sp . PCC 7002. *Archives of Microbiology* **162**:10-19.

Sato N, Murata N, Yoshiro M, Ueta N. 1979. Effect of growth temperature on lipid and fatty acid compositions in the blue-green algae, *Anabaena variabilis* and *Anacystis nidulans*. *Biochimica et Biophysica Acta* **572**:19-28.

Schlüter L, Lohbeck KT, Gutowska MA, Gröger JP, Riebesell U, *et al*. 2014. Adaptation of a globally important coccolithophore to ocean warming and acidification. *Nature Climate Change.* **4**:1024-1030.

Sharma KK, Schuhmann H, Schenk PM. 2012. High lipid induction in microalgae for biodiesel production. *Energies* **5:**1532–1553.

Shifrin N, Chisolm SW. 1981. Phytoplankton lipids-Interspecific differences and effects of nitrate, silicate and light-dark cycles. *Journal of Phycology* **17**:374-384.

Sinensky M. 1974. Homeoviscous adaptation—A homeostatic process that regulates the viscosity of membrane lipids in *Escherichia coli*. *Proceedings of the National Academy of Sciences of the United States of America* **571**:522-525.

Teoh M, Chu W, Marchant H, Phang S. 2004. Influence of culture temperature on the growth, biochemical composition and fatty acid profiles of six Antarctic microalgae. *Journal of Applied Phycology* **16**:421-430.

Thomas MR, Kremer CT, Klausmeier CA, Litchman E. 2012. A global pattern of thermal adaptation in marine phytoplankton. *Science* **338**:1085-1088.

Thompson PA, Harrison PJ, Whyte JNC. 1990. Influence of irradiance on the fatty acid composition of phytoplankton. *Journal of Phycology* **26**:278–288.

Thompson PA, Guo M, Harrison PJ. 1992a. Effects of variation in temperature. I. On the biochemical composition of eight species of marine phytoplankton. *Journal of Phycology* **8**:481-488.

Thompson PA, Guo M, Harrison PJ, Whyte JNC. 1992b. Effects of variation in temperature. II. On the fatty acid composition of eight species of marine phytoplankton. *Journal of Phycology* **8**:488-497.

Thrane J-E, Hessen DO, Andersen T. 2017. Plasticity in algal stoichiometry: experimental evidence of a temperature-induced shift in optimal supply N:P ratio. *Limnology and Oceanography* **62**:1346-1354.

Tonon T, Sayanova O, Michaelson LV, Qing R, Harvey D, *et al.* (2005). Fatty acid desaturases from the microalga *Thalassiosira pseudonana*. *FEBS Journal* **272**:3401-3412.

Van Wagenen J, Miller TW, Hobbs S, Hook P, Crowe B, *et al*. 2012. Effects of light and temperature on fatty acid production in *Nannochloropsis salina*. *Energies* **5**:731-740.

Wada H, Gombos Z, Murata N. 1990. Enhancement of chilling tolerance of a cyanobacterium by genetic manipulation of fatty acid desaturation. *Nature* **307**:200-203.

Wada H, Murata N. 1990. Temperature-Induced Changes in the Fatty Acid Composition of the Cyanobacterium, *Synechocystis* PCC6803. *Plant Physiology* **92**:1062-1069.

Wang Z, Benning C. 2011. *Arabidopsis thaliana* polar glycerolipid profiling by thin layer chromatography (TLC) coupled with gas-liquid chromatography (GLC). *Journal of Visualized Experiments.* **49**:e2518.

Williams PJB, Laurens LML. 2010. Microalgae as biodiesel & biomass feedstocks: review & analysis of the biochemistry, energetics & economics. *Energy and Environmental Science* **3**:554-590.

Yang L, Chen J, Qin S, Zeng M, Jiang Y, *et al.* 2018. Growth and lipid accumulation by different nutrients in the microalga *Chlamydomonas reinhardtii*. *Biotechnology for Biofuels* **11**, 1-12.

Zhu CJ, Lee YK, Chao TM. 1997. Effects of temperature and growth phase on lipid and biochemical composition of *Isochrysis galbana* TK1. *Journal of Applied Phycology* **9**:451–457.

CHAPTER 3: Evolution of C:N:P elemental stoichiometry, cell size and cell morphology in a marine diatom in response to temperature

Introduction

Temperature is a well-known control on carbon-nitrogen-phosphorus (C:N:P) stoichiometry and cell size in phytoplankton (Montagnes & Franklin 2001; Edwards *et al.* 2011; Toseland *et al.* 2013). Competitive abilities for N and P often correlate negatively with cell volume (Edwards *et al.* 2011) due to biophysical constraints (reduced surface area-to-volume ratio). The same biophysical constraints apply to the uptake of C, the demand for which is higher in larger cells due to the size-dependence of metabolic rate (reviewed in Finkel *et al.* 2010). Cell size also depends indirectly on temperature, as all biological processes involve the expenditure of nutrients, and all biological rates, including those involved in the uptake of nutrients, depend directly on temperature according to a unimodal, left-skewed function (Ratkowsky *et al.* 2005; Corkrey *et al.* 2014). Nutrient-driven selection on cell size and temperature-driven selection on nutrient (C, N, P) uptake and utilization traits may act synergistically to increase or decrease cell size, or they may be act antagonistically, depending on the nutrient and temperature environments a population experiences. As global temperatures rise and cause greater stratification of oceans and lakes, a combination of nutrient depletion and warm temperatures (Sarmiento *et al.* 2004; Polovina *et al.* 2008; Weber & Deutch 2012) are predicted to drive a decrease in phytoplankton cell size, through a combination of species turnover and intraspecific morphological change (Hare *et al.* 2007; Winder *et al.* 2009; Finkel *et al.* 2010; Craig *et al.* 2013). The extent to which the latter will be attributable to rapid evolution in response to warming, rather than simple phenotypic plasticity, is not known.

The relationship between temperature and C:N:P stoichiometry of phytoplankton cells is far from settled, though a great deal of research has been done on the subject. Thompson *et al.* (1992a) estimated C:N ratios in 8 diverse species of phytoplankton at 4 temperatures between 10°C and 25°C and found 8 different relationships, from positive and linear to unimodal to slightly negative. Montagnes & Franklin (2001) found no clear relationship between temperature and either cellular C or N in 8 species of marine diatoms and 2 species of flagellates grown in the lab.

On a global scale, however, evidence is mounting that phytoplankton C:P and N:P ratios increase with temperature (Martiny *et al.* 2013; Toseland *et al.* 2013; Yvon-Durocher *et al.* 2015b), which may also be true of terrestrial plants (Reich & Oleksyn 2004). Martiny *et al.* (2013) Yvon-Durocher *et al.* (2015b) both showed clear latitudinal patterns in N:P and C:P ratios, which were largely reflective of sea surface temperature. Toseland *et al.* (2013) showed that translation efficiency in the marine diatom *Thalassiosira pseudonana* is nearly 3x higher at 20°C than at 11°C, the implication being that at higher temperatures, fewer P-rich ribosomes are needed per unit protein (N-rich) produced in the cell. Toseland and colleagues then used a highly integrative ecosystems model to suggest that warming oceans may lead to a reduced demand for P relative to N and thus higher cellular N:P ratios in phytoplankton, leading to greater N limitation in the surface ocean. In contrast, in a long-term mesocosm warming experiment, Yvon-Durocher *et al.* (2017) found that warming led to an increase in seston N:P and C:P ratios due to species turnover, though C:N ratios were unaffected; notably, at least one chlorophyte species, *Chlamydomonas reinhardtii*, showed evidence of local adaptation resulting in N:P and C:P ratios that closely resembled those of the seston. To our knowledge, Yvon-Durocher *et al.*

(2017) is the first study to directly examine rapid, temperature-dependent evolution of N:P stoichiometry in a phytoplankton species, albeit a freshwater one.

In phytoplankton and other aquatic ectotherms, one remarkably repeatable trend exists in body size as it relates to temperature ("body size" includes the sizes of single-celled organisms in this context): as temperature increases, body size decreases (Atkinson 1994; Atkinson 1995; Montagnes & Franklin 2001; Atkinson *et al.* 2003). This relationship has come to be known as the "temperature-size rule" (TSR) (Atkinson 1994; Atkinson *et al.* 2003). A few notable exceptions to this rule have been reported (Fawley 1984; reviewed in Atkinson 1995), but such cases are rare in the literature. In a meta-analysis of temperature-size data from an eclectic collection of protists, Atkinson *et al.* (2003) found evidence to support two mechanistic hypotheses for the TSR. 1) Resource limitation: large cells have small surface-are-to-volume ratios (SA:V) compared to smaller cells, due to the 2/3 exponent of SA:V scaling (see Aksnes & Egge 1991). Resource limitation is thus a challenge for large cells, as they must transfer resources across a smaller relative membrane area to support greater metabolic demands (Gilooly *et al.* 2001), and they may be limited by the diffusion rate CO_2; compounding this challenge is the decreased solubility of CO_2 in water with increasing temperature. 2) Reproductive rate: as temperature increases, so too does the rate of cell division. At a higher rate of cell division, cells may divide earlier, before they reach their full size (see Jørgensen 1966,1968), thus reducing the mean cell size of the population.

A possible mechanism linking the temperature dependence of cellular C:N and cell size is the temperature dependence of photosynthetic efficiency. Chlorophyll *a* (Chl *a*) contains 4 N atoms, but rates of C assimilation per Chl *a* molecule (C/Chl *a*) can vary greatly in response to temperature—though not always in the same direction (Eppley & Sloan 1966; Jørgensen 1968;

Rhee & Gotham 1981; Thompson *et al.* 1992a). C/Chl *a* has been shown to be negatively correlated with cell volume (Eppley & Sloan 1966; Thompson 1992a), possibly as a result of reduced surface area for light absorption and C uptake per unit volume. Thus, temperature-driven selection for smaller cell size may increase photosynthetic efficiency, boosting cellular C and therefore C:N and C:P ratios.

Diatoms are unique among the phytoplankton in that they are incased in a glass (SiO_2) frustule which poses a challenge to exchanging C, N, P and other materials with their environments. Diatoms can only take up nutrients through their "valves", areas of the frustule consisting mostly of holes ("punctae"). Each diatom frustule has two valves pointing in opposite directions, joined in the middle by the "girdle band", an impermeable belt of glass. In centric diatoms, the valve faces are circular, giving the frustule a nearly perfectly cylindrical shape in many cases. For physiological purposes, surface area-to-volume ratio in diatoms must be calculated based only on the combined area of the valve faces, excluding the area of the girdle. Evolution and plasticity of the length-width relationship (length-diameter in centric diatoms) thus becomes a problem of geometry. While high temperature overwhelmingly leads to smaller cells in diatoms and most other phytoplankton, diatoms may also combat challenges of resource acquisition—caused by either nutrient depletion or by temperature—by simply adjusting the ratio of valve area to girdle area (Harrison *et al.* 1977; Joint *et al.* 1987; Cortese & Gersonde 2007).

The aim of this study is to elucidate the effects of 500 generations of experimental evolution at low (16°C) and high (31°C) temperatures on the C:N:P stoichiometry, C assimilation rate per unit chlorophyll *a*, cell size, and cell morphology of a marine species, the model centric diatom *Thalassiosira pseudonana*. The replicate *T. pseudonana* populations used

in this study—5 experimentally adapted to 16°C, 5 adapted to 31°C—were shown by O'Donnell *et al.* (2018) to have diverged markedly in their temperature-dependent population growth functions (thermal reaction norms) after 350 generations of temperature selection. After an additional 150 generations, we explored some of the physiological causes and consequences of thermal adaptation, with an eye toward implications of evolutionary adaptation to warming for persistence of phytoplankton species in the face of global change, and for phytoplankton-mediated biogeochemical change in the sea (Field *et al.* 1998; Toseland *et al.* 2013).

Materials and Methods

We tested the effects of 500 generations of experimental natural selection at 16°C and 31°C on *Thalassiosira pseudonana*'s thermal reaction norms for carbon (C), nitrogen (N), and phosphorus (P) elemental stoichiometry, chlorophyll *a* content and frustule morphology. A detailed account of the methods of the long-term selection experiment can be found in O'Donnell *et al.* (2018). After 500 generations of selection, we grew replicate 16°C-selected populations and 31°C-selected populations (five each) at 10°C, 16°C, 26°C and 31°C—these temperatures represent, respectively, a temperature at the lower extreme of *T. pseudonana*'s thermal niche, the low-temperature selection environment, a temperature near *T. pseudonana*'s thermal optimum for per-capita population growth, and the high-temperature selection environment.

Temperature assay

To acclimate the replicate selection lines (n = 5 for each selection temperature) to the four assay temperatures pre-assay, we transferred 10^5 cells from each (determined by a CASY particle counter [Schärfe System GmbH, Reutlingen, Germany]) into 4 polystyrene tissue culture

flasks (Greiner Bio- One GmbH, Frickenhausen, Germany) containing 40 ml of L1 marine culture medium (Guillard & Hargraves 1993; modified by O'Donnell *et al.* 2018) and allowed each to grow for 5 generations at its respective assay temperature under cool, white fluorescent grow lights (110 μmol photons m^{-2} s^{-1}) on a 14:10 light:dark cycle, agitating daily to maintain cells in suspension. We then transferred 10^5 cells and allowed an additional 5 generations of growth, for a total of 10 generations of temperature acclimation.

After acclimation, we transferred 10^5 cells from each acclimated culture into triplicate tissue culture flasks (2 selection temperatures × 5 selection lines × 4 assay temperatures × 3 replicates = 120 total cultures), each containing 40 ml of L1 medium. We grew experimental cultures until late log-phase, estimating relative change in population daily by optical density, using a spectrophotometer (Shimadzu UV-2401PC; Shimadzu Corporation, Kyoto, Japan) set to 436 nm (the absorbance peak for chlorophyll *a* [Neori et al., 1986]), with filtered L1 medium serving as the blank. Time to late log-phase ranged from 4 days at 26°C to nearly two weeks at 10°C.

Particulate chemical analysis

From each experimental culture, we filtered 10 ml through a pre-combusted (4 hours at 480°C) Whatman GF/B glass fiber filter for C and N analysis, 5ml through a second GF/B for P analysis, and 10 ml through a Whatman GF/F glass fiber filter for chlorophyll analysis. GF/B filters containing samples were frozen at -20°C until needed for analysis. We retained the remaining 15 ml for final cell counts (CASY counter) and other analyses not addressed here. We analyzed samples for C and N via combustion gas chromatography using a Costech Elemental

Combustion System 4010 (Costech Analytical Technologies, Valencia, CA, USA). A complete protocol for this CN analysis can be found at https://lter.kbs.msu.edu/protocols/148.

To analyze filtered cultures for particulate phosphorus, we used the persulfate oxidation method (Menzel & Corwin 1965). To analyze chlorophyll *a*, we extracted the GF/F filters overnight in 95% ethanol in the dark at 4°C, then read samples at 436 nm in the spectrophotometer described above, using 95% ethanol as a blank.

Thalassiosira pseudonana *morphometry*

After GF/B filters were digested for P analysis, many clean *T. pseudonana* frustules in each sample remained at the bottoms of the glass test tubes, affording an opportunity for morphometric analysis. We transferred each sample from its glass test tube into a 15 ml conical tube, simultaneously filtering the sample through a 62 μ mesh to remove large GF/B fibers. We allowed samples to settle for at least 24h. We then achieved blind sampling by haphazardly drawing each tube from the box, obscuring the label in our fist, and quickly placing the tube upright in an opaque bottle, with only the conical tube's cap exposed. Keeping the conical tube in the bottle, we drew a ~0.1 ml aliquot from the bottom of the tube using a long, glass Pasteur pipette and placed it on a standard glass microscope slide with a glass coverslip. Only after counting was complete for a given sample did we reveal the tube's label for data collection.

We measured the lengths and widths of 10 *T. pseudonana* frustules from each sample under 1000x oil immersion on a Nikon Eclipse 80i compound microscope with a Photometrics CoolSNAP EZ camera, and used Image-Pro Plus v4 image processing software (Media Cybernetics, Rockville, MD, USA) to photograph and measure each frustule. *T. pseudonana* is nearly perfectly cylindrical in shape; viewed laterally, a frustule appears rectangular, with a

distinct thinning of its outline indicating the location of the girdle. We measured each outside diameter at the girdle, and each outside length bisecting the frustule up the middle, perpendicular to the diameter measurement. Each slide contained very few frustules, some of which were ill-positioned for measurement; it was thus usually necessary to view multiple aliquots per sample to achieve the 10-cell quota. Sampling was quasi-random, as we simply measured the first 10 measurable frustules encountered.

Calculations and statistical analysis

Estimates of surface area and volume of *T. pseudonana* frustules were based on length and diameter measurements (microns) using basic geometry. We first calculated the circumference of the valve face by multiplying the measured diameter by π, and the valve surface area as πr^2, where r is the radius (diameter/2). Girdle surface area was calculated as measured frustule length × valve circumference. Volume of the cell was calculated as the volume of a cylinder, $\pi r^2 h$, where h (height) is the frustule length. Data used in statistical analyses were averages of the 10 cells measured from each experimental replicate. Models were fit to pooled replicate selection lines by temperature.

Eppley (1972) showed that photosynthetic efficiency in phytoplankton can be expressed in terms of particulate C/Chl *a*, i.e. the amount of carbon (by mass) per unit of chlorophyll *a* (referred to henceforth as the carbon assimilation number). Furthermore, population growth rate, μ, (doublings per day) can be expressed in terms of the assimilation number *per day* (ΔC/Chl *a*), i.e. the carbon assimilation rate (Eppley 1972, Equation 5):

$$\mu = \frac{1}{\Delta t} log_2 \frac{\mathrm{C/Chl}\ a + \Delta \mathrm{C/Chl}\ a}{\mathrm{C/Chl}\ a}, \qquad (4)$$

Where Δt is change in time. Rearranging algebraically, if Δt = 1 day, we find that

$$\Delta \mathrm{C/Chl}\ a = \mathrm{C/Chl}\ a \times 2^{\mu} - \mathrm{C/Chl}\ a. \quad (5)$$

A significant negative correlation between μ and C/Chl *a* (see Results) led us to substitute a linear equation for C/Chl *a* as a function of temperature, such that

$$\Delta \mathrm{C/Chl}\ a = (a\mu + b)(2^{\mu} - 1), \quad (6)$$

Where *a* is the slope and *b* is the intercept of C/Chl *a* as a function of μ. Thus, Equation (6) can be fit to ΔC/Chl *a* as a function of specific growth rate, μ (d^{-1}). We did this for 16°C- and 31°C-selected populations separately (pooled assay temperature groups) using nonlinear least squares. We used the function "gnls()" from the R package "nlme" version 3.1-137 (Pinheiro *et al.* 2018). A preliminary fit to 16°C-selected data revealed severely funneled residuals (increasing variance with increasing μ), which led us to weight the nonlinear regression for 16°C-selected populations using the "varExp()" function to allow for the variance to increase exponentially as a function of μ. The exponential variance function significantly improved the model (dAIC = 24.2; LRT $P < 0.0001$).

All data analyses were conducted using R statistical programming language, version 3.5.0. All stoichiometric ratio data were log-transformed to meet the normality assumptions of analyses. We analyzed stoichiometry and morphometric data using nested versions of a weighted linear mixed-effects model using the "lme()" function from the "nlme" R package. In the full model, *selection temperature*, *assay temperature* and *selection temperature* × *assay temperature* were the fixed effects. We fit a random intercept and slope for each replicate population

(*selection replicate*) across assay temperatures to account for repeated measures (each replicate population was assayed at four different temperatures). We used the "varIdent()" and "varComb()" functions in the nlme package to weight each level of *selection temperature* and *assay temperature* by its inverse variance, as unequal variances by factor level violated the assumptions of the linear models in some cases. For each data set, we performed model selection on nested models using likelihood ratio tests; in some cases, *temperature* × *assay temperature* interaction effects and/or weights did not improve model fits (based on likelihood ratio tests), and were dropped. We derived ANOVA tables from each mixed model, which were in effect repeated-measures ANOVA (RM-ANOVA) because of the random effects. We performed pairwise comparisons of *selection temperature* and *assay temperature* groups with Tukey's Honestly Significant Difference (Tukey HSD), using the "lsmeans()" function from the R package "lsmeans" version 2.27-62 (Lenth 2016).

Results

Particulate C, N, P and Chlorophyll a

Thalassiosira pseudonana populations experimentally evolved at 16°C and 31°C for 500 generations diverged significantly in their thermal reaction norms for chemistry. On a per-cell basis, particulate C in 16°C-selected populations was higher than in 31°C-selected populations, and increased across assay temperatures; In 31°C-selected populations, particulate C per cell increased between the 10°C and 26°C assay temperatures, but was lowest at 31°C (*selection temp* × *assay temp* interaction; Figure 12; Table 2). An increase in 16°C-selected populations and a decrease in 31°C-selected populations at the 31°C assay temperature resulted in a significant *selection temperature* × *assay temperature* interaction (Figure 12; Table 2), however there was

no main effect of selection temperature or assay temperature on particulate N per cell, but. As with C, particulate P per cell generally increased across assay temperatures, but was lowest in 31°C-selected populations at the 31°C assay temperature (*selection temp.* × *assay temp.* interaction; Figure 12; Table 2). Trends across assay temperature in chlorophyll *a* per cell generally mirrored those in Chl *a* per biovolume, but unlike Chl *a* per biovolume, Chl *a* on a per-cell basis was significantly lower in 31°C-selected populations than in 16°C-selected populations (Figure 12; Table 2).

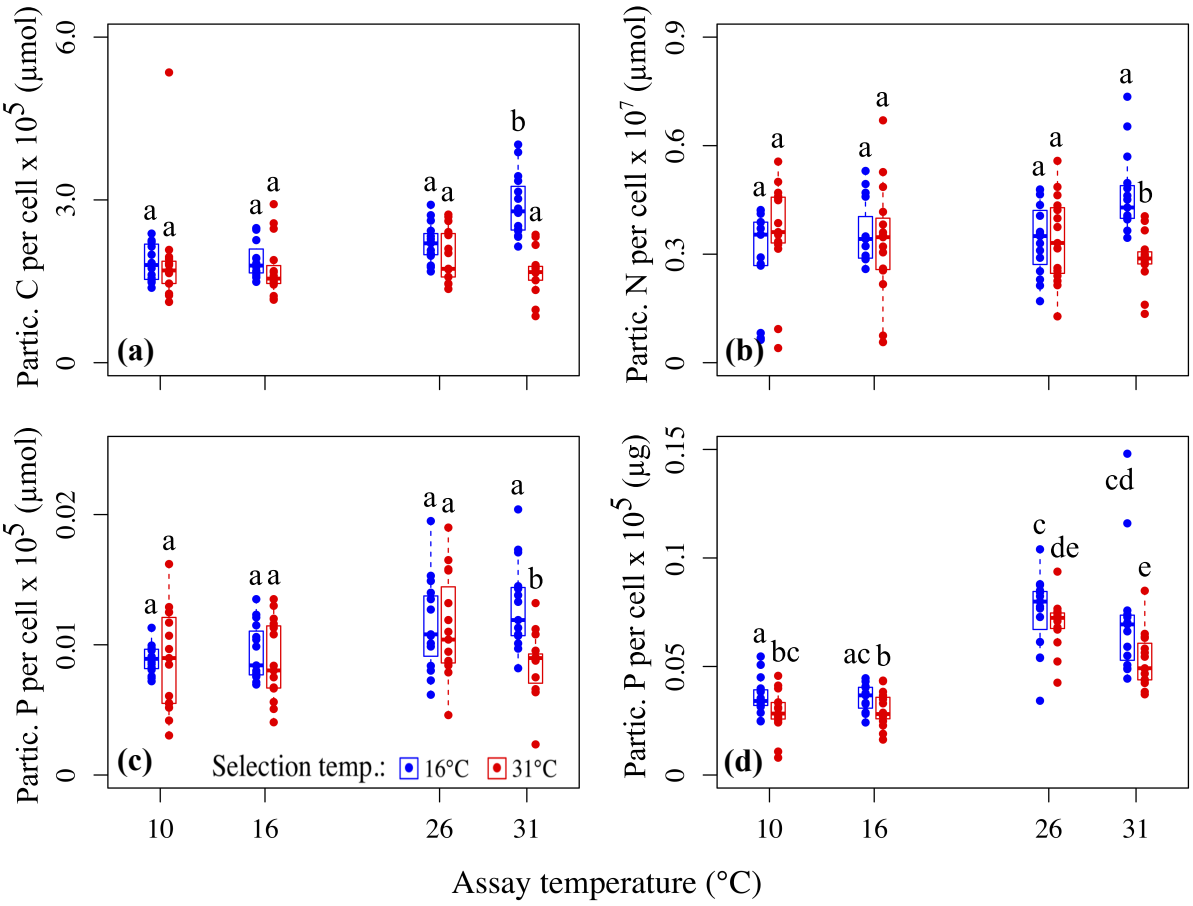

Figure 12: Particulate C, N, P (molar) and chlorophyll *a* (*µ*g) per cell in 16°C-selected (blue) and 31°C-selected (red) *T. pseudonana*, assayed at 10, 16, 26 and 31°C. (a) Particulate carbon; **(b)** particulate nitrogen; **(c)** particulate phosphorus; and **(d)** particulate chlorophyll.

Letters at the top of each panel indicate statistical significance: if a letter is not shared between two groups, those groups are significantly different (Tukey HSD; $\alpha = 0.95$). Lines across boxes indicate the median of each group, with the lower and upper bounds indicate the 25th and 75th quartiles, respectively. Points beyond the lower and upper whiskers are outliers, falling outside the 0th and 100th quartiles. All data are multiplied by 10^5.

Table 2: RM-ANOVA testing effects of selection temperature and assay temperature on *T. pseudonana* particulate C, N, P and chlorophyll *a* per-cell (μmol μm^{-3}) and all molar ratios thereof, and particulate chlorophyll *a* (μg μm^{-3}). Ratio data were log-transformed to meet the normality assumption of RM-ANOVA. Post-hoc, pairwise comparisons (Tukey HSD) are shown in Appendix D, Tables D1-D4.

Trait	Effect	df	MS	F-statistic	P-value
Particulate C cell^{-1}	Assay temp.	3	1.42	4.72	0.0039
	Selection temp.	1	4.50	14.95	0.0002
	Assay temp. × Sel. Temp.	3	2.36	7.85	<0.0001
	Error	106	0.30	--	--
Particulate N cell^{-1}	Assay temp.	3	0.016	1.11	0.35
	Selection temp.	1	0.034	2.38	0.13
	Assay temp. × Sel. Temp.	3	0.078	5.50	0.0015
	Error	106	0.014	--	--
Particulate P cell^{-1}	Assay temp.	3	5.6×10^{-5}	7.21	0.00019
	Selection temp.	1	4.1×10^{-5}	5.29	0.023
	Assay temp. × Sel. Temp.	3	2.8×10^{-5}	3.60	0.016
	Error	106	7.7×10^{-6}	--	--
Partic. Chl a *cell^{-1}*	Assay temp.	3	0.012	60.09	<0.0001
	Selection temp.	1	0.0021	10.15	0.0019
	Error	109	0.0002	--	--

Trends in C, N, P and chlorophyll *a* on a *per-biovolume* basis where markedly different from those estimated *per cell.* 31°C-selected populations had higher particulate carbon (Figure 13a; Table 2), nitrogen (Figure 13b; Table 3) and phosphorus (Figure 13c; Table 3) per

biovolume than 16°C-selected populations at all four assay temperatures (10, 16, 26, and 31°C); however, only the reaction norm for particulate P varied significantly across assay temperatures, with the highest particulate P μm^{-2} at 26°C in 16°C-selected populations and at 31°C in 31°C-selected populations (Figure 13c; Table 3; see Appendix D, Table D7 for Tukey HSD pairwise comparisons). Chlorophyll *a* per biovolume was also higher in 31°C-selected populations than in 16°C-selected populations, significantly so at 3 out of 4 assay temperatures (Figure 13d; Table 3). Chl *a* was lowest at the 10 and 16°C assay temperatures in both selection groups, and increased two- (in 16°C-selected populations) or threefold (31°C-selected populations) between 16°C and 26°C, then decreased by ~50% between 26°C and 31°C in both groups (Figure 13d; Table 3; Tukey pairwise comparisons in Appendix D, Table D8). The resulting thermal reaction norms for Chl *a* appeared left-skewed and unimodal, resembling the generic thermal reaction norm for any biological rate (see, e.g., Corkrey *et al.* 2014).

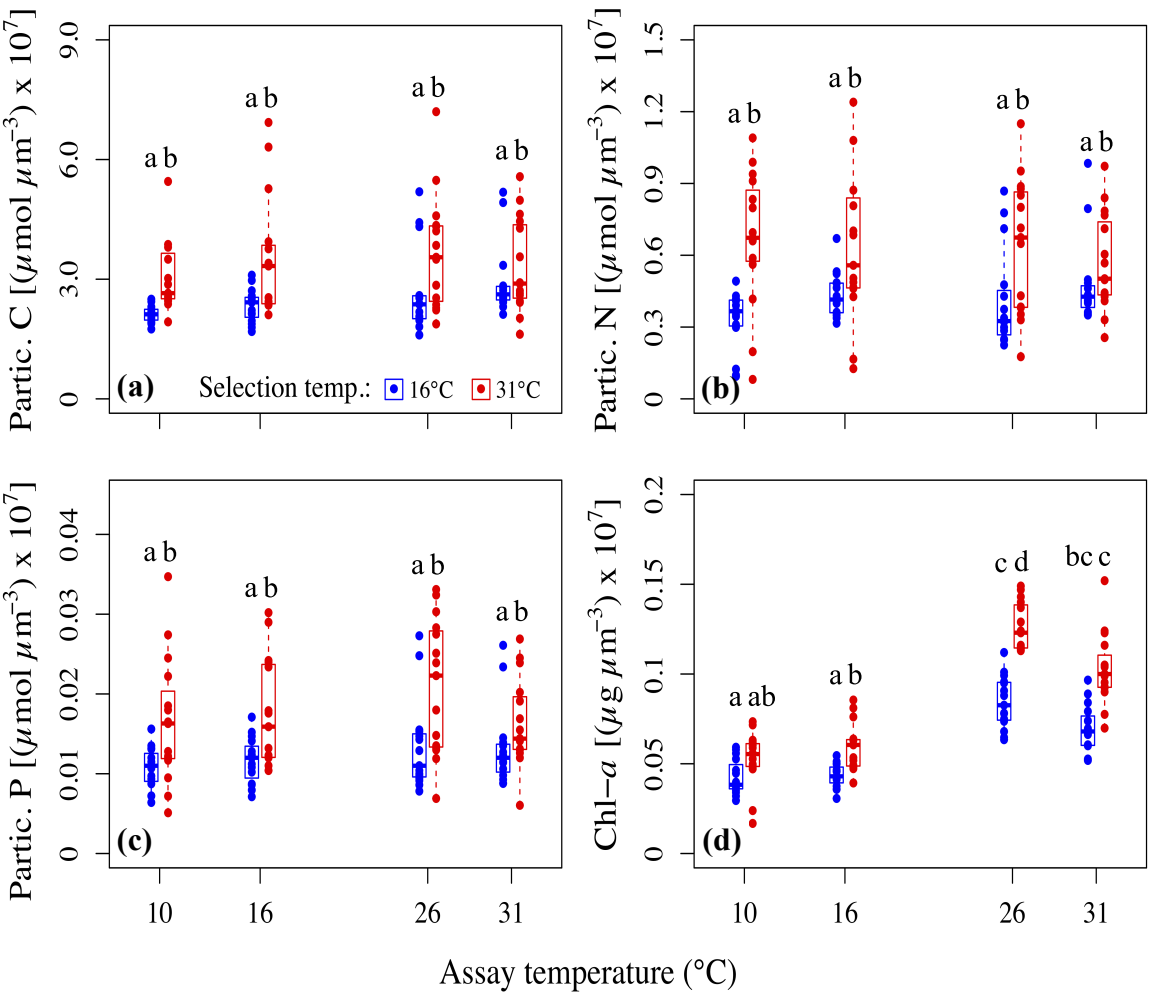

Figure 13: Particulate C, N, P (molar) and chlorophyll *a* (*μ*g) per biovolume in 16°C-selected (blue) and 31°C-selected (red) *T. pseudonana*, assayed at 10, 16, 26 and 31°C. (a) Particulate carbon; **(b)** particulate nitrogen; **(c)** particulate phosphorus; and **(d)** particulate chlorophyll. Letters at the top of each panel indicate statistical significance: if a letter is not shared between two groups, those groups are significantly different (Tukey HSD; $\alpha = 0.95$). Lines across boxes indicate the median of each group, with the lower and upper bounds indicate the 25th and 75th quartiles, respectively. Points beyond the lower and upper whiskers are outliers, falling outside the 0th and 100th quartiles. All data are multiplied by 10^7.

Stoichiometric ratios

The particulate C:P molar ratio was ~200 in both selection groups; C:N was between 5 and 10; and N:P was between 20 and 50 in both selection groups (Figure 14). Due to several large outliers, there were no detectable effects of selection temperature or assay temperature on stoichiometric ratios (Figure 14; Table 3).

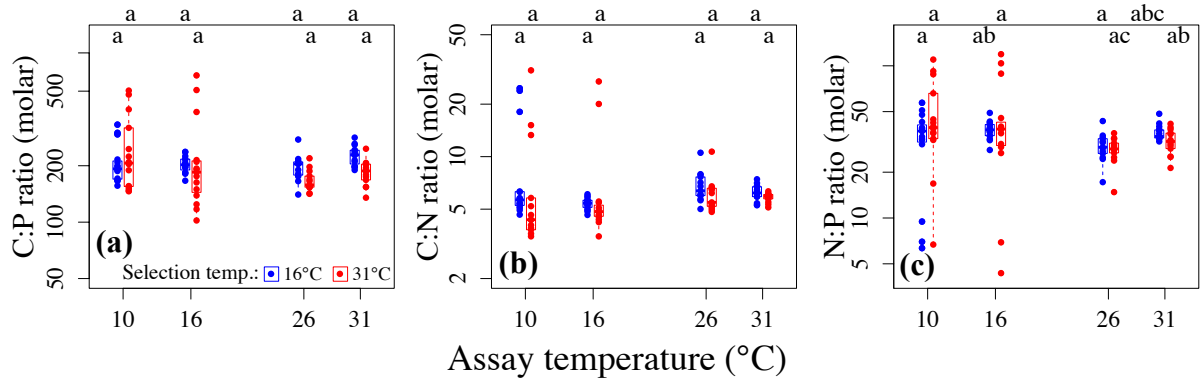

Figure 14: Particulate molar C:N:P ratios in 16°C-selected (blue) and 31°C-selected (red) *T. pseudonana*, assayed at 10, 16, 26 and 31°C. All ratios are calculated on a per biovolume (μm^3) basis. **(a)** C:P ratio; **(b)** C:N ratio; **(c)** N:P ratio. Symbols are as above. Note that y-axes are on a log scale.

Table 3: RM-ANOVA testing effects of selection temperature and assay temperature on *T. pseudonana* particulate C, N, P per biovolume (μmol μm^{-3}) and all molar ratios thereof, and particulate chlorophyll *a* (μg μm^{-3}). Ratio data were log-transformed to meet the normality assumption of RM-ANOVA. Post-hoc, pairwise comparisons (Tukey HSD) for particulate C, N, P and Chl *a* are shown in Appendix D, Tables D5-D7.

Trait	Effect	df	MS	F-statistic	P-value
Particulate C bv^{-1}	Assay temp.	3,12	0.24	0.121	0.95
	Selection temp.	1,93	28.63	14.344	0.0003
	Error	109	2.00	--	--

Table 3 (cont'd)

Particulate N bv^{-1}	Assay temp.	3,12	0.027	0.49	0.69
	Selection temp.	1,93	1.33	24.29	<0.0001
	Error	109	0.055	--	--
Particulate P bv^{-1}	Assay temp.	3,12	0.0003	3.26	0.024
	Selection temp.	1,93	0.0009	28.52	<0.0001
	Error	109	3.1×10^{-5}	--	--
Partic. C:P ratio	Assay temp.	3,12	0.16	2.03	0.11
	Selection temp.	1,90	0.12	1.51	0.22
	Assay temp. × Sel. Temp.	3,90	0.15	1.98	0.12
	Error	106	0.078	--	--
Partic. C:N ratio	Assay temp.	3,12	0.12	0.74	0.53
	Selection temp.	1,93	0.20	1.24	0.27
	Error	109	0.16	--	--
Partic. N:P ratio	Assay temp.	3,12	0.27	1.08	0.36
	Selection temp.	1,93	0.099	0.039	0.84
	Error	109	0.25	--	--
Partic. Chl a *bv^{-1}*	Assay temp.	3,12	0.022	115.38	<0.0001
	Selection temp.	1,90	0.018	92.45	<0.0001
	Assay temp. × Sel. Temp.	3,90	0.0016	8.44	<0.0001
	Error	106	0.0002	--	--

Photosynthetic efficiency

Carbon assimilation number (C/Chl *a*) (g C g Chl a^{-1}) generally decreased by as much as 50% between the 10°C and 31°C assay temperatures, but did not differ between 16°C- and 31°C-selected populations (Figure 15a; Table 4). C/Chl *a* was negatively correlated with specific growth rate, μ (d^{-1}), in both 16°C-selected (Pearson's correlation: R = -0.38; t_{58} = -3.11; P = 0.0029) and 31°C-selected (Pearson's correlation: R = -0.37; t_{58} = -3.00; P = 0.0040) populations (Figure 15b). Carbon assimilation rate, that is the rate of photosynthetic C assimilation per unit Chl *a* per day (ΔC/Chl *a*) (g C g Chl a^{-1} d^{-1}) varied across assay temperature, but did not differ between selection temperature groups (Figure 15c; Table 4). As with particulate Chl *a*, ΔC/Chl *a* was highest at intermediate temperatures and lowest at 10°C and 31°C (Figure 15c; Table 3). Equation 3 explained a significant amount of the variation in ΔC/Chl *a* as a function of specific growth rate (d^{-1}) for both temperature selection groups (Figure 15d; Table 5), but 95%

confidence intervals for both *a* and *b* overlapped between selection groups; the nonlinear regression fits for the two selection groups therefore did not differ significantly (Table 5).

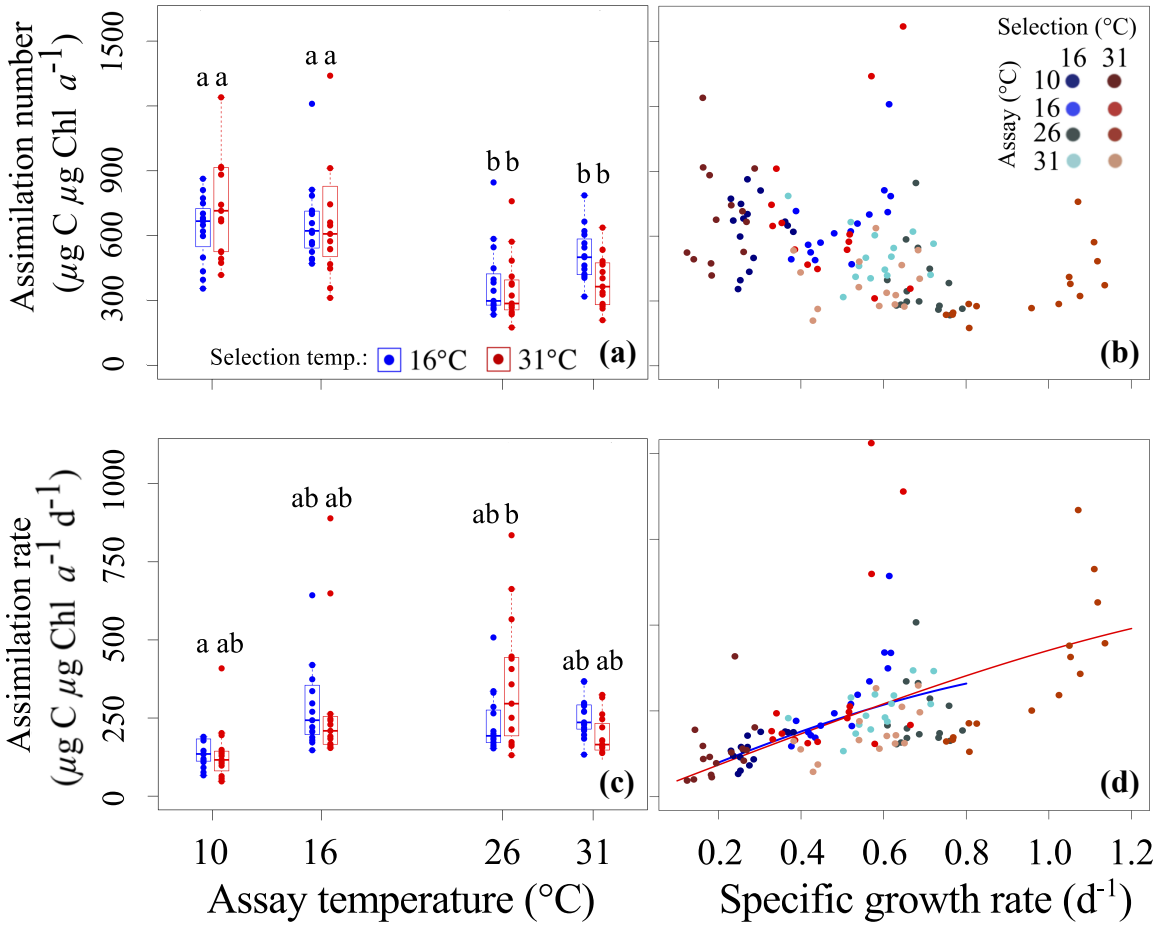

Figure 15: (a) Carbon assimilation number, C/Chl *a* (*μ*g C *μ*g Chl a^{-1}), of 16°C- (blue) and 31°C-selected (red) *T. pseudonana* populations grown at 10, 16, 26 and 31°C, determined from final C and Chl *a* samples. Symbols are as above. **(b)** Carbon assimilation number plotted against specific growth rate (d^{-1}); different shades of blue (16°C-selected) and red (31°C-selected) dots denote assay temperatures. **(c)** Carbon assimilation rate (*μ*g C *μ*g Chl a^{-1} d^{-1}) across assay temperatures at the time of harvest. Symbols are as in (a). **(d)** Carbon assimilation rate as a function of specific growth rate. Curves are Equation (6) fit separately to pooled selection group data using nonlinear least squares. Symbols are as in (b).

Table 4: RM-ANOVA testing effects of selection temperature and assay temperature on *T. pseudonana* carbon assimilation number (C/Chl *a*) (μg C μg Chl a^{-1}) and assimilation rate (μg C μg Chl a^{-1} d^{-1}). Pairwise contrasts (Tukey HSD) can be found in Appendix D, Tables D9 and D10.

Trait	Effect	df	MS	F-statistic	P-value
C/Chl a	Assay temp.	3,12	11.2×10^5	12.94	<0.0001
	Selection temp.	1,90	8.4×10^4	0.97	0.33
	Assay temp. × Sel. Temp.	3,90	2.2×10^5	2.53	0.061
	Error	106	8.7×10^4	--	--
ΔC/Chl a	Assay temp.	3,12	1.7×10^5	8.51	<0.0001
	Selection temp.	1,90	7894	0.40	0.53
	Assay temp. × Sel. Temp.	3,90	3.3×10^4	1.69	0.18
	Error	106	2.1×10^4	--	--

Table 5: Nonlinear regression fits of Equation (6) to carbon assimilation rate per unit Chl *a* (ΔC/Chl *a*) (μg C μg Chl a^{-1} d^{-1}) as a function of specific growth rate (d^{-1}). Equation (6) was fit separately to data from each selection group, pooled across assay temperatures. The regression fit to data from 16°C-selected was weighted using an exponential variance function, to account for heteroscedasticity.

Model	df	Model P-val.	R^2	RSE	Parameter	Value	95% CI
*16°C-selected**	58	<0.0001	0.29	11.96			
					a	-374.14	(-1055.92— -274.05)
					b	744.11	(662.3223—1154.4621)
31°C-selected	58	<0.0001	0.26	176.6			
					a	-244.9	(-562.13—72.27)
					b	671.5	(386.36—956.61)

*Variance function exponent = 3.43

Thalassiosira pseudonana *frustule size and morphology*

T. pseudonana frustule size and morphology were strongly affected by both selection temperature (16°C vs 31°C) and assay temperature (10, 16, 26, 31°C). Both frustule diameter

(measured across the circular valve face) and frustule length were ~25% larger in 16°C-selected populations than in 31°C-selected populations (Figure 16; Figure 17a,b; Table 6); frustule volumes differed between selection groups by a factor of 2-3 (Figure 16; Figure 17c; Table 6). Frustule diameter and frustule length also increased across assay temperatures in both selection groups (Figure 16; Figure 17a,b; Table 6), though frustule volume was only marginally affected by assay temperature ($F_{3,115} = 2.26$; $P = 0.085$; Figure 16; Figure 17c; Table 6).

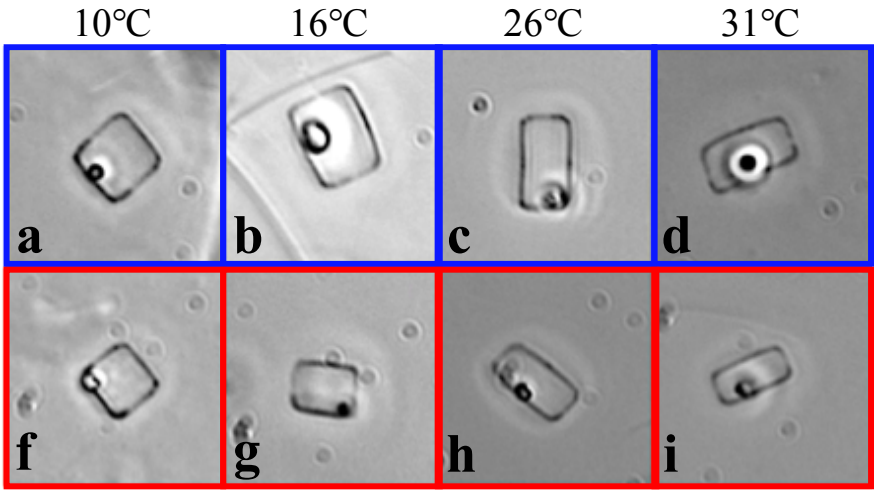

Figure 16: 16°C-selected (blue boxes) and 31°C-selected (red boxes) *Thalassiosira pseudonana* frustules photographed in lateral view under 1000x oil immersion. Frustules are from **(a,f)** 10°C; **(b,g)** 16°C; **(c,h)** 26°C and **(d,i)** 31°C assay temperatures. These images were chosen as exceptional representations of the statistical trends observed in length and diameter, and do not necessarily represent averages. Images have been sharpened and brightened slightly to improve quality but are otherwise unchanged.

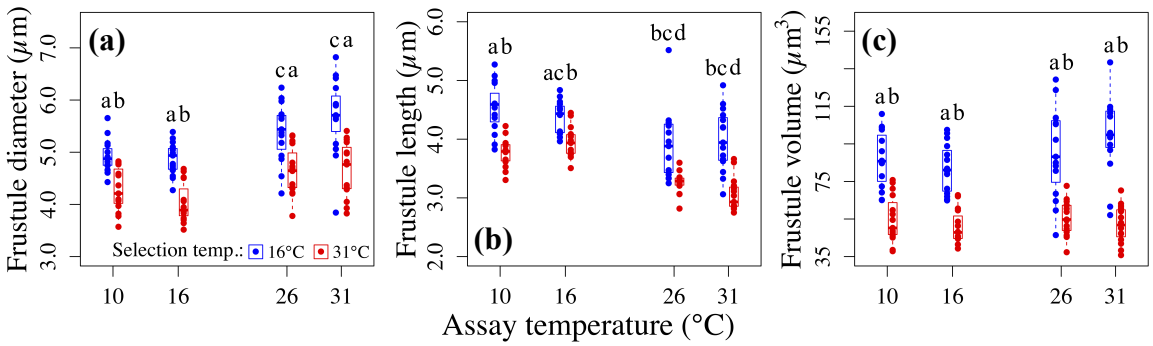

Figure 17: Frustule dimensions in 16°C (blue) and 31°C (red) selected *T. pseudonana* populations grown at 10, 16, 26 and 31°C. (a) Frustule diameter (μm); **(b)** frustule length (μm); **(c)** frustule volume (μm^3). Symbols are as above.

Total surface area-to-volume ratio (SA_{tot}:V) was ~20% higher in 31°C-selected populations than in 16°C-selected populations but was unaffected by assay temperature (Figure 16; Figure 18a; Table 6). The ratio of valve surface area to frustule volume (SA_{valve}:V) was >25% greater in 31°C-selected lines than in 16°C-selected lines, with the greatest difference at the 10°C and 31°C assay temperatures (Figure 16; Figure 18b; Table 6; see Appendix D, Table D15 for Tukey HSD pairwise comparisons). The ratio of girdle surface area to frustule volume (SA_{girdle}:V) was also as much as 25% greater in 31°C-selected populations than in 16°C-selected populations, and decreased by ~15% between the 16°C and 31°C assay temperatures in both groups (Figure 16; Figure 18c; Table 5; Tukey pairwise comparisons in Appendix D, Table D16). SA_{valve}:SA_{girdle} did not differ between selection groups, but was as much as 40% higher at the 26°C and 31°C assay temperatures than at 10°C and 16°C (Figure 16; Figure 18d; Table 6).

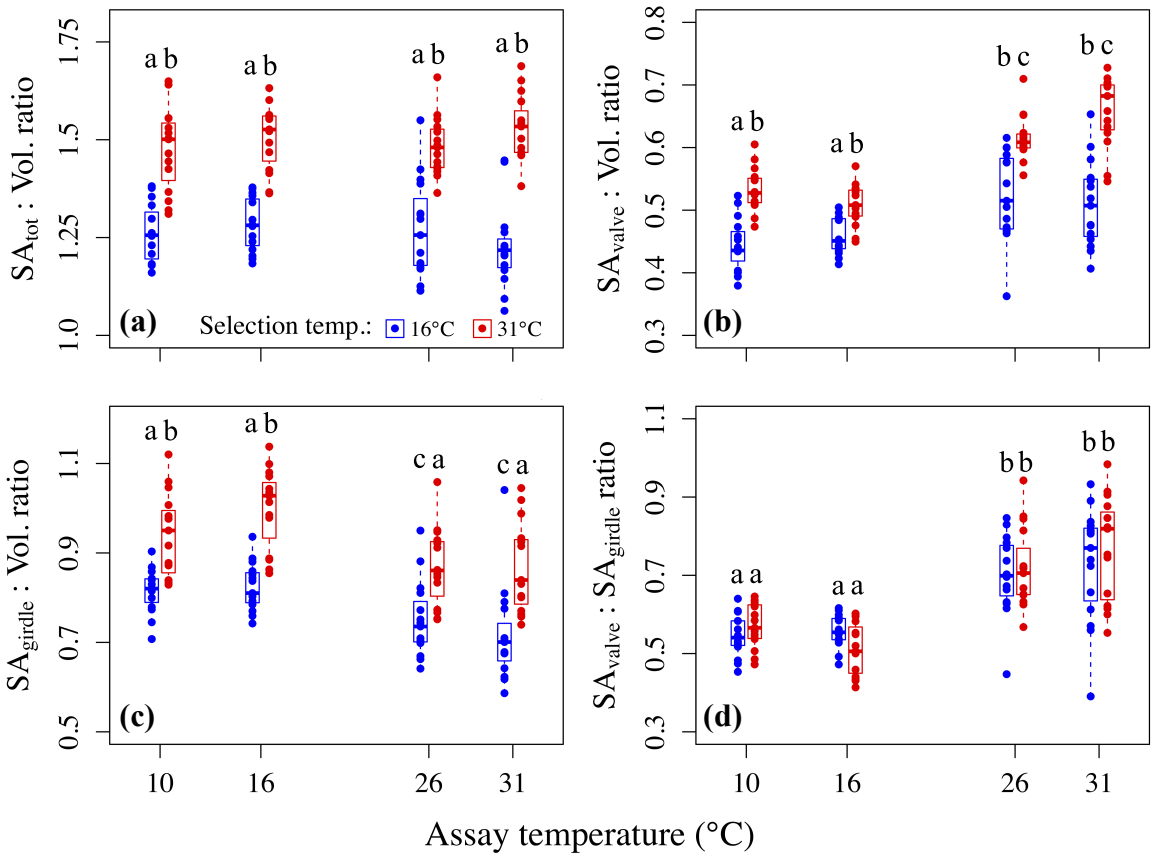

Figure 18: *T. pseudonana* whole frustule (a), valve only (b), and girdle only (c) surface-area-to-volume ratios (SA:V), and (d) valve SA:girdle SA in populations selected at 16°C (blue) and 31°C (red) and grown at 10, 16, 26 and 31°C. Symbols are as above. Surface area is in units of μm^2, and volume is in μm^3.

Table 6: RM-ANOVA testing effects of selection temperature and assay temperature on *T. pseudonana* frustule diameter, frustule length, frustule volume, valve surface area-to-frustule volume ratio, girdle surface area-to-frustule volume ratio, and the ratio of valve surface area to girdle surface area. Linear measurements are in units of μm, areas are μm^2, volumes are μm^3. Post-hoc, pairwise comparisons (Tukey HSD) are shown in Appendix D, Tables D11-D17.

Trait	Effect	df	MS	F-statistic	P-value
Frustule diameter	Assay temp.	3,12	3.47	15.03	<0.0001
	Selection temp.	1,99	19.76	85.58	<0.0001
	Error	115	0.23	--	--
Frustule length	Assay temp.	3,96	3.71	26.37	<0.0001
	Selection temp.	1,96	14.32	101.81	<0.0001
	Assay temp. × Sel. Temp.	3,96	0.35	2.51	0.062
	Error	112	0.141	--	--
Frustule volume	Assay temp.	3,12	582	2.26	0.085
	Selection temp.	1,99	40871	158.72	<0.0001
	Error	115	257	--	--
SA_{total} *: Volume ratio*	Assay temp.	3,12	0.0038	0.439	0.73
	Selection temp.	1,99	1.70	196.67	<0.0001
	Error	115	0.0086	--	--
SA_{valve} *: Volume ratio*	Assay temp.	3,12	0.0038	0.45	0.72
	Selection temp.	1,96	1.70	200.49	<0.0001
	Assay temp. × Sel. Temp.	3,96	0.015	1.75	0.16
	Error	112	0.0085	--	--
SA_{girdle} *: Volume ratio*	Assay temp.	3,12	0.0.096	13.11	<0.0001
	Selection temp.	1,99	0.61	84.13	<0.0001
	Error	115	0.0073	--	--
SA_{valve} *:* SA_{girdle} *ratio*	Assay temp.	3,12	0.35	38.44	<0.0001
	Selection temp.	1,96	0.0026	0.28	0.60
	Assay temp. × Sel. Temp.	3,96	0.011	1.19	0.32
	Error	112	0.0090	--	--

When regressed against frustule volume, the slopes of total surface are-to-volume ratio (SA_{total}:V), SA_{valve}:V and SA_{girdle}:V differed between selection groups and among assay temperatures (Figure 19; Table 7). While similar at 10°C and 16°C, the slopes of SA:V_{total} in

16°C-selected populations were more strongly negative than those of 31°C-selected populations at 26°C and 31°C (Figure 19a; Table 7). Slopes of SA_{valva}:V as a function of frustule volume were also smaller (by value, not magnitude) at all temperatures in 16°C-selected populations at all assay temperatures, but generally increased across assay temperatures in both groups (Figure 19b; Table 7). The effects of selection temperature, assay temperature, and frustule volume on $SA:V_{girdle}$ were exactly opposite those of SA_{valve}:V (Figure 19c; Table 7)—these effects offset one another to produce the trends in SA_{total}:V.

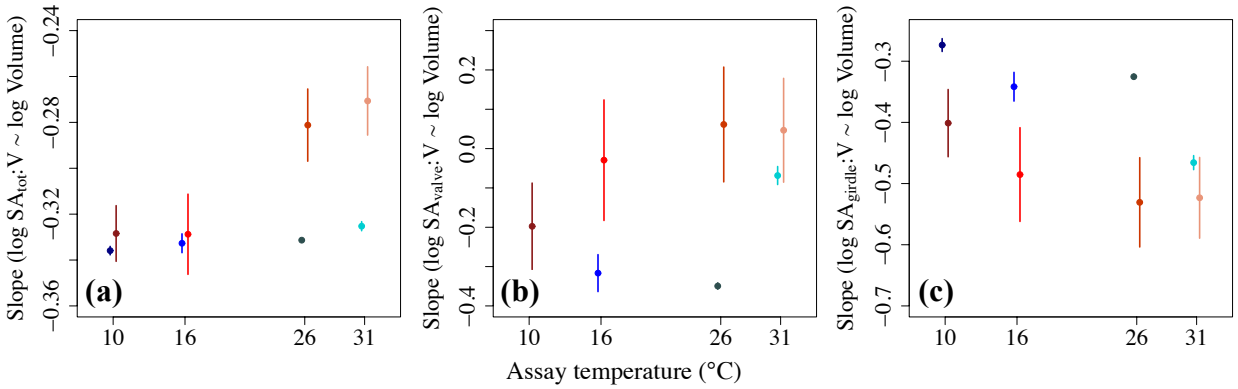

Figure 19: Slopes of (a) total surface area-to-volume ratio (SA_{tot}:V) of the frustule; (b) SA_{valve}:V; and (c) SA_{girdle}:V as functions of frustule volume at the 10, 16, 26 and 31°C assay temperatures. Blue shades are 16°C-selected populations, red shades are 31°C-selected populations. Points are slopes estimated from the linear mixed-effects model fits. Error bars are 95% confidence intervals, also estimated from the model fits. Non-overlapping confidence intervals indicate significant differences. Areas are in units of μm^2, volumes are in units of μm^3. The units of SA:V are $\mu m^{2/3}$.

Table 7: RM-ANOVA testing effects of selection temperature, assay temperature and frustule volume on ratios of *T. pseudonana* total frustule surface area, valve surface area, girdle surface area to frustule volume, and the ratio of valve surface area to girdle surface area. Linear measurements are in units of μm, areas are μm^2, volumes are μm^3.

Trait	Effect	df	MS	F-statistic	P-value
$SA_{total}:V$	log Volume	1,104	1.43	21529	<0.0001
	Assay temp.	3,104	0.0029	43.87	<0.0001
	Selection temp.	1,104	0.0009	12.97	0.0005
	log V × Assay temp.	3,104	<0.0001	0.175	0.91
	log V × Sel temp.	1,104	0.001	14.85	0.0002
	Assay temp. × Sel. temp.	3,104	0.0003	4.17	0.0079
	Log V × A. temp. × S. temp.	3,104	0.0002	2.88	0.039
	Error	104	0.0001	--	--
$SA_{valve}:V$	log Volume	1,104	0.80	112.129	<0.0001
	Assay temp.	3,104	0.34	47.21	<0.0001
	Selection temp.	1,104	0.11	15.15	0.0002
	log V × Assay temp.	3,104	0.016	2.21	0.091
	log V × Sel temp.	1,104	0.073	10.19	0.0018
	Assay temp. × Sel. temp.	3,104	0.026	3.70	0.014
	Log V × A. temp. × S. temp.	3,104	0.0048	0.68	0.57
	Error	104	0.0071	--	--
$SA_{girdle}:V$*	log Volume	1,104	1.90	1066.01	<0.0001
	Assay temp.	3,104	0.084	47.21	<0.0001
	Selection temp.	1,104	0.027	15.15	0.0002
	log V × Assay temp.	3,104	0.0040	2.21	0.091
	log V × Sel temp.	1,104	0.018	10.19	0.0018
	Assay temp. × Sel. temp.	3,104	0.0066	3.70	0.014
	Log V × A. temp. × S. temp.	3,104	0.0012	0.68	0.57
	Error	104	0.0018	--	--

*F-statistics and P-values are the same because SA_{valve}:V and SA_{girdle}:V have ofsetting effects on SA_{tot}:V.

Discussion

We maintained replicate populations of the marine diatom *Thalassiosira pseudonana* at 16°C and 31°C for 500 generations, which led to major evolutionary divergence in cellular elemental stoichiometry, photosynthetic efficiency and frustule morphology. We showed that, in addition to being smaller in size, 31°C-selected populations were denser in C, N, P and chlorophyll at all assay temperatures, though we were unable to detect differences between selection groups or trends across assay temperatures in C:N:P elemental ratios. Finally, *T. pseudonana* evolved at 31°C exhibited thermal reaction norms for morphological traits distinct from those of populations evolved at 16°C.

Much attention has been given to warming-driven changes in global phytoplankton community assemblages in recent years (Hare *et al.* 2007; Winder *et al.* 2009; Finkel *et al.* 2010; Thomas *et al.* 2012), which may in turn lead to phytoplankton-mediated biogeochemical change on a global scale (Litchman *et al.* 2006; Weber *et al.* 2012; Craig *et al.* 2013; Toseland *et al.* 2013). However, we are only beginning to understand the role rapid thermal adaptation will play in this scenario. Our study adds a number of valuable insights to the growing body of research on evolutionary changes in phytoplankton metabolic, stoichiometric, morphological and other physiological traits (Schlüter *et al.* 2014; Padfield *et al.* 2016; Yvon-Durocher *et al.* 2017). For example, we show that the temperature dependence of cellular C, N and P contents and elemental ratios in phytoplankton may depend to a great extent on their evolutionary history, i.e. what temperature regimes a population has experienced, even, or perhaps especially in very recent evolutionary history. Schlüter *et al.* (2014) found that after ~460 generations of evolution at an elevated temperature (26.3°C), populations of the coccolithophore *Emiliana huxleyi* had lower particulate organic carbon (POC) per cell than those evolved at a lower temperature

(15°C), especially when assayed at the elevated temperature. Likewise, we observed lower particulate C per cell in *T. pseudonana* populations evolved at 31°C than in those evolved at 16°C, with the greatest difference observed at the 31°C assay temperature. However, in both Schlüter *et al.* (2014) and our study, lower C per cell was likely simply a result of smaller cell size. When controlled for cell size, particulate C *per biovolume* was higher in 31°C-selected *T. pseudonana* populations, indicating a higher C density per cell.

Padfield *et al.* (2016) showed strong evidence that evolution of carbon use efficiency (CUE) (respiration/photosynthesis) could explain evolutionary adaptation to temperature in phytoplankton. They found evidence to support the hypothesis that respiration increases with temperature faster than photosynthesis, but that the difference between these two slopes could be reduced through thermal adaptation. While we did not test CUE directly, we showed that C assimilation rates per unit chlorophyll *a* (μg C μg chl a^{-1} d^{-1}) were similar between 16°C- and 31°C-selected populations (pooled across assay temperatures), despite differences in C density. This discrepancy can likely be explained by higher chl *a* per biovolume in 31°C-selected populations, especially at the higher assay temperatures. Warm-adapted *T. pseudonana* may have increased chl *a* production per unit of biovolume produced, boosting photosynthesis relative to respiration and leading to an accumulation of C in the cell. This rapid accumulation of C may have facilitated earlier, more rapid cell division, contributing to selection for smaller cell sizes in the 31°C-selected populations (Jørgensen 1966,1968), which in turn would facilitate C uptake, as well as uptake of N and P (Atkinson *et al.* 2003). Denser N and P in 31°C-selected populations may simply be a result of a total increase in resource requirements driven by higher rates of photosynthesis and reproduction in 31°C-selected populations. High-temperature selection may have resulted in constitutive early cell division, as 31°C-selected cells were smaller at all four

assay temperatures. It is unclear, however, how 31°C-selected cells achieved higher nutrient densities at 10°C and 16°C, rather than at only the two highest assay temperatures (26°C and 31°C).

To date, most research on global patterns in phytoplankton stoichiometry have indicated that both N:P and C:P increase with temperature (Martiny *et al.* 2013; Toseland *et al.* 2013; Yvon-Durocher *et al.* 2015b), and at least one mesocosm experiment has produced similar results (Yvon-Durocher *et al.* 2017). As in some other laboratory-based studies (Thompson *et al.* 1992b; Montagnes & Franklin 2001), we did not detect any influence of selection temperature or assay temperature on N:P molar ratios in our cultures, and large outliers prevented us from detecting any trends in C:P or C:N ratios. Notably, C:N ratio did not vary with temperature in either the global (Yvon-Durocher *et al.* 2015b) or mesocosm (Yvon-Durocher *et al.* 2017) studies that measured it. Given our inability to detect any influence of temperature on N:P ratios, we are unable to offer evidence for or against the mechanistic hypothesis proposed by Toseland *et al.* (2013) (higher translation efficiency leading to N limitation).

T. pseudonana showed not only remarkable plasticity in its ability to respond to ambient temperature by altering the ratio of permeable valve surface area to nonpermeable girdle surface area via phenotypic plasticity, but also a marked divergence in the degree of this plasticity (that is, in the slopes of its thermal reaction norms for morphology) between 16°C- and 31°C-selected populations. Both selection groups allocated more surface area to the valve faces when grown at 26°C and 31°C without appreciably changing overall frustule volume or total surface area-to-volume ratio. This ability is strong evidence that, rather than change its cell size in response to rapid changes in temperature, *T. pseudonana* simply alters its geometry to compensate for the biophysical challenges of existing at high temperature (Harrison *et al.* 1977; Joint *et al.* 1987;

Cortese & Gersonde 2007; see also Atkinson *et al.* 2003). Despite the maintenance of frustule volume across assay temperatures, the effect of volume on SA_{valve}:V was relatively greater, and that on SA_{girdle}:V was relatively smaller in 16°C-selected populations. The difference in the magnitudes of these effects can be attributed to the relative scaling of the area of the circular valve face ($\pi \cdot r_{valve}^2$) versus the rectangular girdle ($[\pi \cdot d_{valve}] \cdot l_{girdle}$). Whether maintenance of frustule volume is hard-coded in the genome or whether it is incidental is not clear.

Support for both hypotheses for the TSR proposed by Atkinson *et al.* (2003) can be found here. First, the smaller overall size of 31°C-selected cells compared to 16°C-selected cells, combined with the higher nutrient density in the former, supports the hypothesis that rapid growth selects for earlier cell division, which decreases the average cell size of the population. This can be viewed as an evolutionary effect. In the short term, *T. pseudonana* is plastic with respect to its allocation of surface area to valves versus girdles, suggesting resource limitation at 26°C and 31°C, most probably by CO_2, given the N- and P-saturated culture medium.

This study is a valuable addition to two areas of knowledge about the ecology, evolution, and physiology of phytoplankton. First, we have shown that elemental stoichiometry, cell size, and thermal reaction norms for a set of critical physiological traits (cell morphological traits) in a marine diatom can evolve rapidly, over a few hundred generations, in response to a sustained temperature environment. Studies of this kind are few, and to our knowledge none to date has been done on a marine diatom (but see Schlüter *et al.* 2014; Padfield *et al.* 2016; Yvon-Durocher *et al.* 2017). Second, we have shown that a diatom can cope with the biophysical challenges of rapid temperature change by plastically altering its geometry without changing its size. To our knowledge, this has not been shown before in this context. Follow-up studies of the genetic

controls of cell size and morphology in *T. pseudonana* would speak volumes to this system, and may be well within reach (Armbrust *et al.* 2004).

APPENDICES

APPENDIX C:

Chapters 2 & 3 description of linear mixed-effects models

To test effects of selection temperature and assay temperature on fatty acid content and composition, we fit weighted linear mixed-effects models to data for total fatty acid content (TFA), percent saturated FA (pSFA), percent monounsaturated FA (pMUFA), percent polyunsaturated FA (pPUFA), mean chain length (MCL), and degree of unsaturation (WUnSat), and for each individual FA class, with *selection temperature* and *assay temperature* as fixed effects, and a random intercept and slope (across assay temperatures) for each replicate population to account for repeated measures across assay temperatures. Unequal variances between *selection temperature* groups and among *assay temperature* groups were common, so we included two identity variance functions in the full model using the "varIdent()" and "varComb()" functions from the R package "nlme" (Pinheiro & Bates 2018). Some models were not improved by the inclusion of these variance functions, and some were equally good with and without a *selection temperature × assay temperature* interaction effect. Thus, we compared log likelihoods of four nested models to determine whether variance functions and/or interaction terms could be dropped in each case. The four nested models used are as follows:

Model C1: full model

$$Y \sim \beta_{0ij} + \beta_{0ij} + \beta_1 A + \beta_2 S + \beta_3 AS + \varepsilon,$$
$$\beta_{0ij} \sim N\left(\beta_{0j}, \sigma^2_{\beta_0}\right), \quad \beta_{1ij} \sim N\left(\beta_{1j}, \sigma^2_{\beta_1}\right), \quad \varepsilon_1 \sim N\left(0, f(A)\right), \quad \varepsilon_2 \sim N\left(0, f(S)\right),$$

$$f(A) = \gamma_{0_1} + \gamma_1 A, \qquad \gamma_1 \neq 0$$

$$f(S) = \gamma_{0_2} + \gamma_2 S, \qquad \gamma_2 \neq 0$$

Model C2: interaction included, weights dropped

$$Y \sim \beta_{0ij} + \beta_{0ij} + \beta_1 A + \beta_2 S + \beta_3 AS + \varepsilon, \quad \beta_{0ij} \sim N\left(\beta_{0j}, \sigma^2_{\beta_0}\right), \quad \beta_{1ij} \sim N\left(\beta_{1j}, \sigma^2_{\beta_1}\right)$$

Model C3: weights included, interaction dropped

$$Y \sim \beta_{0ij} + \beta_{0ij} + \beta_1 A + \beta_2 S + \varepsilon,$$
$$\beta_{0ij} \sim N\left(\beta_{0j}, \sigma^2_{\beta_0}\right), \quad \beta_{1ij} \sim N\left(\beta_{1j}, \sigma^2_{\beta_1}\right), \quad \varepsilon_1 \sim N\left(0, f(A)\right), \quad \varepsilon_2 \sim N\left(0, f(S)\right),$$

$$f(A) = \gamma_{0_1} + \gamma_1 A, \qquad \gamma_1 \neq 0$$

$$f(S) = \gamma_{0_2} + \gamma_2 S, \qquad \gamma_2 \neq 0$$

Model C4: weights dropped, interaction dropped

$$Y \sim \beta_{0ij} + \beta_{0ij} + \beta_1 A + \beta_2 S + \varepsilon, \quad \beta_{0ij} \sim N\left(\beta_{0j}, \sigma^2_{\beta_0}\right), \quad \beta_{1ij} \sim N\left(\beta_{1j}, \sigma^2_{\beta_1}\right)$$

APPENDIX D:

Chapter 3 Tukey HSD contrast tables

Tukey HSD post-hoc tests

The following tables show results of post-hoc, pairwise comparisons (Tukey HSD) of stoichiometric and morphometric traits among all factors/factor levels for *T. pseudonana* in a factorial (*selection temperature* × *assay temperature*) assay first analyzed with RM-ANOVA (see Tables 2 and 3 in main text). Tables correspond, in order, to individual panels in main text Figures 12-15 and 17-19.

Table D1: All post-hoc, pairwise comparisons (Tukey HSD) for RM-ANOVA comparing *T. pseudonana* particulate C per cell (*μ*mol cell^{-1}) between temperature selection groups and among assay temperature groups. Table corresponds to Figure 12a.

Trait compared	Contrast	Estimate	Std. Error	df	t-ratio	P-value
Particulate C	Selection temp.@ Assay temp.					
	16@10 - 31@10	-0.06	0.23	90	-0.28	1.00
	16@10 - 16@16	-0.06	0.21	12	-0.29	1.00
	16@10 - 31@16	0.12	0.24	12	0.49	1.00
	16@10 - 16@26	-0.36	0.20	12	-1.74	0.67
	16@10 - 31@26	-0.11	0.23	12	-0.48	1.00
	16@10 - 16@31	-1.05	0.21	12	-4.93	0.006
	16@10 - 31@31	0.16	0.27	12	0.58	1.00
	31@10 - 16@16	0.00	0.28	12	0.02	1.00
	31@10 - 31@16	0.18	0.31	12	0.59	1.00
	31@10 - 16@26	-0.29	0.28	12	-1.05	0.96
	31@10 - 31@26	-0.05	0.30	12	-0.16	1.00
	31@10 - 16@31	-0.99	0.29	12	-3.47	0.06
	31@10 - 31@31	0.22	0.33	12	0.67	1.00
	16@16 - 31@16	0.18	0.15	90	1.19	0.93
	16@16 - 16@26	-0.30	0.19	12	-1.53	0.78
	16@16 - 31@26	-0.05	0.22	12	-0.23	1.00
	16@16 - 16@31	-1.00	0.20	12	-4.91	0.006
	16@16 - 31@31	0.22	0.27	12	0.82	0.99
	31@16 - 16@26	-0.47	0.23	12	-2.08	0.48
	31@16 - 31@26	-0.23	0.25	12	-0.91	0.98
	31@16 - 16@31	-1.17	0.24	12	-4.96	0.01
	31@16 - 31@31	0.04	0.29	12	0.14	1.00
	16@26 - 31@26	0.24	0.13	90	1.84	0.59
	16@26 - 16@31	-0.70	0.20	12	-3.47	0.063
	16@26 - 31@31	0.51	0.26	12	1.94	0.55
	31@26 - 16@31	-0.94	0.23	12	-4.13	0.022
	31@26 - 31@31	0.27	0.29	12	0.94	0.98
	16@31 - 31@31	1.21	0.21	90	5.82	<0.0001

Table D2: All post-hoc, pairwise comparisons (Tukey HSD) for RM-ANOVA comparing *T. pseudonana* particulate N per cell (μmol cell^{-1}) between temperature selection groups and among assay temperature groups. Table corresponds to Figure 13b.

Trait compared	Contrast	Estimate	Std. Error	df	t-ratio	P-value
Particulate N	Selection temp.@ Assay temp.					
	16@10 - 31@10	-0.068	0.038	90	-1.77	0.64
	16@10 - 16@16	-0.062	0.053	12	-1.16	0.93
	16@10 - 31@16	-0.040	0.053	12	-0.76	0.99
	16@10 - 16@26	-0.047	0.054	12	-0.86	0.98
	16@10 - 31@26	-0.046	0.054	12	-0.84	0.99
	16@10 - 16@31	-0.171	0.053	12	-3.21	0.10
	16@10 - 31@31	0.006	0.054	12	0.12	1.00
	31@10 - 16@16	0.006	0.054	12	0.10	1.00
	31@10 - 31@16	0.027	0.054	12	0.51	1.00
	31@10 - 16@26	0.021	0.055	12	0.38	1.00
	31@10 - 31@26	0.022	0.055	12	0.40	1.00
	31@10 - 16@31	-0.104	0.054	12	-1.92	0.56
	31@10 - 31@31	0.074	0.054	12	1.36	0.86
	16@16 - 31@16	0.022	0.038	90	0.58	1.00
	16@16 - 16@26	0.015	0.054	12	0.28	1.00
	16@16 - 31@26	0.016	0.054	12	0.30	1.00
	16@16 - 16@31	-0.109	0.053	12	-2.05	0.49
	16@16 - 31@31	0.068	0.054	12	1.27	0.89
	31@16 - 16@26	-0.007	0.054	12	-0.12	1.00
	31@16 - 31@26	-0.005	0.054	12	-0.10	1.00
	31@16 - 16@31	-0.131	0.053	12	-2.45	0.30
	31@16 - 31@31	0.047	0.054	12	0.87	0.98
	16@26 - 31@26	0.001	0.040	90	0.03	1.00
	16@26 - 16@31	-0.124	0.054	12	-2.28	0.37
	16@26 - 31@31	0.053	0.055	12	0.97	0.97
	31@26 - 16@31	-0.126	0.054	12	-2.31	0.36
	31@26 - 31@31	0.052	0.055	12	0.95	0.97
	16@31 - 31@31	0.178	0.038	90	4.64	0.0003

Table D3: All post-hoc, pairwise comparisons (Tukey HSD) for RM-ANOVA comparing *T. pseudonana* particulate P per cell (μmol cell^{-1}) between temperature selection groups and among assay temperature groups. Table corresponds to Figure 12c.

Trait compared	Contrast	Estimate	Std. Error	df	t-ratio	P-value
Particulate P	Selection temp.@ Assay temp.					
	16@10 - 31@10	1E-04	0.0006	96	0.16	1.00
	16@10 - 16@16	-5E-04	0.0009	12	-0.53	1.00
	16@10 - 31@16	2E-04	0.0010	12	0.17	1.00
	16@10 - 16@26	-2E-03	0.0011	12	-2.26	0.38
	16@10 - 31@26	-2E-03	0.0012	12	-1.92	0.56
	16@10 - 16@31	-4E-03	0.0011	12	-3.73	0.042
	16@10 - 31@31	5E-04	0.0012	12	0.41	1.00
	31@10 - 16@16	-6E-04	0.0010	12	-0.62	1.00
	31@10 - 31@16	6E-05	0.0010	12	0.06	1.00
	31@10 - 16@26	-3E-03	0.0011	12	-2.28	0.37
	31@10 - 31@26	-2E-03	0.0013	12	-1.96	0.54
	31@10 - 16@31	-4E-03	0.0011	12	-3.70	0.044
	31@10 - 31@31	4E-04	0.0012	12	0.31	1.00
	16@16 - 31@16	7E-04	0.0007	96	0.98	0.98
	16@16 - 16@26	-2E-03	0.0011	12	-1.80	0.63
	16@16 - 31@26	-2E-03	0.0012	12	-1.51	0.79
	16@16 - 16@31	-3E-03	0.0011	12	-3.24	0.09
	16@16 - 31@31	1E-03	0.0012	12	0.83	0.99
	31@16 - 16@26	-3E-03	0.0012	12	-2.31	0.36
	31@16 - 31@26	-3E-03	0.0013	12	-1.98	0.53
	31@16 - 16@31	-4E-03	0.0011	12	-3.70	0.044
	31@16 - 31@31	3E-04	0.0012	12	0.26	1.00
	16@26 - 31@26	1E-04	0.0012	96	0.12	1.00
	16@26 - 16@31	-1E-03	0.0012	12	-1.21	0.92
	16@26 - 31@31	3E-03	0.0013	12	2.25	0.39
	31@26 - 16@31	-2E-03	0.0013	12	-1.22	0.91
	31@26 - 31@31	3E-03	0.0014	12	1.99	0.52
	16@31 - 31@31	4E-03	0.0011	96	4.19	0.0015

Table D4: All post-hoc, pairwise comparisons (Tukey HSD) for RM-ANOVA comparing *T. pseudonana* particulate chlorophyll *a* per cell (μg cell^{-1}) between temperature selection groups and among assay temperature groups. Table corresponds to Figure 12d.

Trait compared	Contrast	Estimate	Std. Error	df	t-ratio	P-value
Chlorophyll a	Selection temp.@ Assay temp.					
	16@10 - 31@10	0.006	0.0019	93	3.30	0.029
	16@10 - 16@16	0.000	0.0027	12	-0.05	1.00
	16@10 - 31@16	0.006	0.0033	12	1.91	0.57
	16@10 - 16@26	-0.041	0.0034	12	-12.11	<0.0001
	16@10 - 31@26	-0.035	0.0039	12	-8.93	<0.0001
	16@10 - 16@31	-0.029	0.0043	12	-6.60	0.0005
	16@10 - 31@31	-0.022	0.0047	12	-4.70	0.009
	31@10 - 16@16	-0.006	0.0033	12	-1.96	0.54
	31@10 - 31@16	0.000	0.0027	12	-0.05	1.00
	31@10 - 16@26	-0.047	0.0039	12	-12.11	<0.0001
	31@10 - 31@26	-0.041	0.0034	12	-12.11	<0.0001
	31@10 - 16@31	-0.035	0.0047	12	-7.38	0.0002
	31@10 - 31@31	-0.029	0.0043	12	-6.60	0.0005
	16@16 - 31@16	0.006	0.0019	93	3.30	0.029
	16@16 - 16@26	-0.041	0.0032	12	-12.94	<0.0001
	16@16 - 31@26	-0.034	0.0037	12	-9.33	<0.0001
	16@16 - 16@31	-0.028	0.0042	12	-6.85	0.0003
	16@16 - 31@31	-0.022	0.0046	12	-4.82	0.0071
	31@16 - 16@26	-0.047	0.0037	12	-12.77	<0.0001
	31@16 - 31@26	-0.041	0.0032	12	-12.94	<0.0001
	31@16 - 16@31	-0.035	0.0046	12	-7.63	0.0001
	31@16 - 31@31	-0.028	0.0042	12	-6.85	0.0003
	16@26 - 31@26	0.006	0.0019	93	3.30	0.029
	16@26 - 16@31	0.012	0.0046	12	2.66	0.22
	16@26 - 31@31	0.019	0.0050	12	3.71	0.043
	31@26 - 16@31	0.006	0.0050	12	1.20	0.92
	31@26 - 31@31	0.012	0.0046	12	2.66	0.22
	16@31 - 31@31	0.006	0.0019	93	3.30	0.029

Table D5: All post-hoc, pairwise comparisons (Tukey HSD) for RM-ANOVA comparing *T. pseudonana* particulate C per biovolume (μmol μm^{-3}) between temperature selection groups and among assay temperature groups. Table corresponds to Figure 13a.

Trait compared	Contrast	Estimate	Std. Error	df	t-ratio	P-value
Particulate C	Selection temp.@ Assay temp.					
	16@10 - 31@10	-1.04	0.23	93	-4.51	0.0005
	16@10 - 16@16	-0.18	0.39	12	-0.47	1.00
	16@10 - 31@16	-1.22	0.45	12	-2.70	0.21
	16@10 - 16@26	-0.53	0.39	12	-1.36	0.86
	16@10 - 31@26	-1.57	0.45	12	-3.46	0.065
	16@10 - 16@31	-0.74	0.41	12	-1.83	0.61
	16@10 - 31@31	-1.78	0.47	12	-3.81	0.0365
	31@10 - 16@16	0.85	0.45	12	1.88	0.58
	31@10 - 31@16	-0.18	0.39	12	-0.47	1.00
	31@10 - 16@26	0.50	0.45	12	1.11	0.94
	31@10 - 31@26	-0.53	0.39	12	-1.36	0.86
	31@10 - 16@31	0.29	0.47	12	0.63	1.00
	31@10 - 31@31	-0.74	0.41	12	-1.83	0.61
	16@16 - 31@16	-1.04	0.23	93	-4.51	0.0005
	16@16 - 16@26	-0.35	0.37	12	-0.93	0.98
	16@16 - 31@26	-1.38	0.44	12	-3.16	0.11
	16@16 - 16@31	-0.56	0.39	12	-1.44	0.82
	16@16 - 31@31	-1.60	0.45	12	-3.53	0.058
	31@16 - 16@26	0.69	0.44	12	1.57	0.76
	31@16 - 31@26	-0.35	0.37	12	-0.93	0.98
	31@16 - 16@31	0.48	0.45	12	1.05	0.96
	31@16 - 31@31	-0.56	0.39	12	-1.44	0.82
	16@26 - 31@26	-1.04	0.23	93	-4.51	0.0005
	16@26 - 16@31	-0.21	0.39	12	-0.54	1.00
	16@26 - 31@31	-1.25	0.45	12	-2.75	0.20
	31@26 - 16@31	0.82	0.45	12	1.82	0.62
	31@26 - 31@31	-0.21	0.39	12	-0.54	1.00
	16@31 - 31@31	-1.04	0.23	93	-4.51	0.0005

Table D6: All post-hoc, pairwise comparisons (Tukey HSD) for RM-ANOVA comparing *T. pseudonana* particulate N per biovolume (μmol μm^{-3}) between temperature selection groups and among assay temperature groups. Table corresponds to Figure 13b.

Trait compared	Contrast	Estimate	Std. Error	df	t-ratio	P-value
Particulate N	Selection temp.@ Assay temp.					
	16@10 - 31@10	-0.25	0.041	93	-6.17	<0.0001
	16@10 - 16@16	-0.10	0.077	12	-1.32	0.88
	16@10 - 31@16	-0.35	0.087	12	-4.07	0.024
	16@10 - 16@26	-0.09	0.076	12	-1.12	0.94
	16@10 - 31@26	-0.34	0.086	12	-3.92	0.031
	16@10 - 16@31	-0.13	0.079	12	-1.67	0.70
	16@10 - 31@31	-0.38	0.089	12	-4.34	0.015
	31@10 - 16@16	0.15	0.087	12	1.74	0.67
	31@10 - 31@16	-0.10	0.077	12	-1.32	0.88
	31@10 - 16@26	0.17	0.087	12	1.94	0.55
	31@10 - 31@26	-0.09	0.076	12	-1.12	0.94
	31@10 - 16@31	0.12	0.089	12	1.37	0.85
	31@10 - 31@31	-0.13	0.079	12	-1.67	0.70
	16@16 - 31@16	-0.25	0.041	93	-6.17	<0.0001
	16@16 - 16@26	0.02	0.078	12	0.20	1.00
	16@16 - 31@26	-0.24	0.088	12	-2.68	0.22
	16@16 - 16@31	-0.03	0.081	12	-0.37	1.00
	16@16 - 31@31	-0.28	0.091	12	-3.12	0.11
	31@16 - 16@26	0.27	0.089	12	3.04	0.13
	31@16 - 31@26	0.02	0.078	12	0.20	1.00
	31@16 - 16@31	0.22	0.091	12	2.46	0.30
	31@16 - 31@31	-0.03	0.081	12	-0.37	1.00
	16@26 - 31@26	-0.25	0.041	93	-6.17	<0.0001
	16@26 - 16@31	-0.05	0.080	12	-0.58	1.00
	16@26 - 31@31	-0.30	0.090	12	-3.32	0.08
	31@26 - 16@31	0.21	0.090	12	2.31	0.36
	31@26 - 31@31	-0.05	0.080	12	-0.58	1.00
	16@31 - 31@31	-0.25	0.041	93	-6.17	<0.0001

Table D7: All post-hoc, pairwise comparisons (Tukey HSD) for RM-ANOVA comparing *T. pseudonana* particulate P per biovolume (μmol μm^{-3}) between temperature selection groups and among assay temperature groups. Table corresponds to Figure 13c.

Trait compared	Contrast	Estimate	Std. Error	df	t-ratio	P-value
Particulate P	Selection temp.@ Assay temp.					
	16@10 - 31@10	-0.0055	0.0008	93	-7.05	<0.0001
	16@10 - 16@16	-0.0012	0.0018	12	-0.65	1.00
	16@10 - 31@16	-0.0067	0.0020	12	-3.34	0.08
	16@10 - 16@26	-0.0040	0.0020	12	-2.02	0.51
	16@10 - 31@26	-0.0095	0.0021	12	-4.47	0.012
	16@10 - 16@31	-0.0025	0.0019	12	-1.27	0.90
	16@10 - 31@31	-0.0079	0.0021	12	-3.79	0.038
	31@10 - 16@16	0.0043	0.0020	12	2.13	0.45
	31@10 - 31@16	-0.0012	0.0018	12	-0.65	1.00
	31@10 - 16@26	0.0015	0.0021	12	0.70	1.00
	31@10 - 31@26	-0.0040	0.0020	12	-2.02	0.51
	31@10 - 16@31	0.0030	0.0021	12	1.44	0.82
	31@10 - 31@31	-0.0025	0.0019	12	-1.27	0.90
	16@16 - 31@16	-0.0055	0.0008	93	-7.05	<0.0001
	16@16 - 16@26	-0.0028	0.0020	12	-1.42	0.83
	16@16 - 31@26	-0.0083	0.0021	12	-3.90	0.031
	16@16 - 16@31	-0.0013	0.0019	12	-0.65	1.00
	16@16 - 31@31	-0.0067	0.0021	12	-3.22	0.10
	31@16 - 16@26	0.0027	0.0021	12	1.27	0.89
	31@16 - 31@26	-0.0028	0.0020	12	-1.42	0.83
	31@16 - 16@31	0.0042	0.0021	12	2.01	0.51
	31@16 - 31@31	-0.0013	0.0019	12	-0.65	1.00
	16@26 - 31@26	-0.0055	0.0008	93	-7.05	<0.0001
	16@26 - 16@31	0.0015	0.0021	12	0.74	0.99
	16@26 - 31@31	-0.0040	0.0022	12	-1.79	0.64
	31@26 - 16@31	0.0070	0.0022	12	3.18	0.10
	31@26 - 31@31	0.0015	0.0021	12	0.74	0.99
	16@31 - 31@31	-0.0055	0.0008	93	-7.05	<0.0001

Table D8: All post-hoc, pairwise comparisons (Tukey HSD) for RM-ANOVA comparing *T. pseudonana* particulate chlorophyll *a* per biovolume ($\mu g\ \mu m^{-3}$) between temperature selection groups and among assay temperature groups. Table corresponds to Figure 13d.

Trait compared	Contrast	Estimate	Std. Error	df	t-ratio	P-value
Chlorophyll a	Selection temp.@ Assay temp.					
	16@10 - 31@10	-0.010	0.0047	90	-2.18	0.37
	16@10 - 16@16	-0.001	0.0036	12	-0.26	1.00
	16@10 - 31@16	-0.017	0.0042	12	-4.01	0.026
	16@10 - 16@26	-0.043	0.0042	12	-10.27	<0.0001
	16@10 - 31@26	-0.085	0.0052	12	-16.26	<0.0001
	16@10 - 16@31	-0.027	0.0043	12	-6.33	0.0007
	16@10 - 31@31	-0.061	0.0056	12	-10.86	<0.0001
	31@10 - 16@16	0.009	0.0046	12	1.99	0.52
	31@10 - 31@16	-0.007	0.0051	12	-1.29	0.89
	31@10 - 16@26	-0.033	0.0051	12	-6.39	0.0006
	31@10 - 31@26	-0.075	0.0060	12	-12.49	<0.0001
	31@10 - 16@31	-0.017	0.0052	12	-3.27	0.09
	31@10 - 31@31	-0.051	0.0064	12	-8.02	0.0001
	16@16 - 31@16	-0.016	0.0036	90	-4.40	0.0008
	16@16 - 16@26	-0.042	0.0039	12	-10.84	<0.0001
	16@16 - 31@26	-0.084	0.0050	12	-16.84	<0.0001
	16@16 - 16@31	-0.026	0.0040	12	-6.56	0.0005
	16@16 - 31@31	-0.060	0.0054	12	-11.13	<0.0001
	31@16 - 16@26	-0.026	0.0044	12	-5.86	0.0014
	31@16 - 31@26	-0.069	0.0055	12	-12.54	<0.0001
	31@16 - 16@31	-0.010	0.0046	12	-2.28	0.37
	31@16 - 31@31	-0.044	0.0058	12	-7.60	0.0001
	16@26 - 31@26	-0.043	0.0053	90	-8.10	<0.0001
	16@26 - 16@31	0.016	0.0045	12	3.43	0.07
	16@26 - 31@31	-0.018	0.0058	12	-3.15	0.11
	31@26 - 16@31	0.058	0.0056	12	10.46	<0.0001
	31@26 - 31@31	0.024	0.0066	12	3.66	0.047
	16@31 - 31@31	-0.034	0.0057	90	-5.91	<0.0001

Table D9: All post-hoc, pairwise comparisons (Tukey HSD) for RM-ANOVA comparing *T. pseudonana* carbon assimilation number (μg C μg Chl a^{-1}). Table corresponds to Figure 15a.

Trait compared	Contrast	Estimate	Std. Error	df	t-ratio	P-value
C/Chl a	Selection temp.@ Assay temp.					
	16@10 - 31@10	-256.6	125.0	96	-2.05	0.45
	16@10 - 16@16	-30.9	101.6	12	-0.30	1.00
	16@10 - 31@16	-157.8	136.5	12	-1.16	0.93
	16@10 - 16@26	248.4	83.9	12	2.96	0.14
	16@10 - 31@26	277.3	89.9	12	3.09	0.12
	16@10 - 16@31	119.9	84.4	12	1.42	0.83
	16@10 - 31@31	243.0	91.2	12	2.67	0.22
	31@10 - 16@16	225.7	136.2	12	1.66	0.71
	31@10 - 31@16	98.8	163.8	12	0.60	1.00
	31@10 - 16@26	505.0	123.5	12	4.09	0.023
	31@10 - 31@26	533.9	127.6	12	4.18	0.020
	31@10 - 16@31	376.5	123.8	12	3.04	0.13
	31@10 - 31@31	499.6	128.6	12	3.89	0.032
	16@16 - 31@16	-126.9	125.7	96	-1.01	0.97
	16@16 - 16@26	279.3	84.2	12	3.32	0.081
	16@16 - 31@26	308.3	90.1	12	3.42	0.069
	16@16 - 16@31	150.8	84.6	12	1.78	0.64
	16@16 - 31@31	273.9	91.4	12	3.00	0.14
	31@16 - 16@26	406.2	124.0	12	3.28	0.087
	31@16 - 31@26	435.1	128.1	12	3.40	0.072
	31@16 - 16@31	277.7	124.3	12	2.23	0.40
	31@16 - 31@31	400.8	129.1	12	3.11	0.11
	16@26 - 31@26	28.9	44.3	96	0.65	1.00
	16@26 - 16@31	-128.5	62.2	12	-2.07	0.48
	16@26 - 31@31	-5.4	71.2	12	-0.08	1.00
	31@26 - 16@31	-157.5	70.0	12	-2.25	0.39
	31@26 - 31@31	-34.3	78.1	12	-0.44	1.00
	16@31 - 31@31	123.1	47.8	96	2.58	0.18

Table D10: All post-hoc, pairwise comparisons (Tukey HSD) for RM-ANOVA comparing *T. pseudonana* carbon assimilation rate (μg C μg Chl a^{-1} d^{-1}). Table corresponds to Figure 15c.

Trait compared	Contrast	Estimate	Std. Error	df	t-ratio	P-value
$\Delta C/Chl\ a$	Selection temp.@ Assay temp.					
	16@10 - 31@10	4.2	18.13	96	0.23	1.00
	16@10 - 16@16	-150.2	44.18	12	-3.40	0.072
	16@10 - 31@16	-191.1	83.29	12	-2.30	0.37
	16@10 - 16@26	-96.1	36.78	12	-2.61	0.24
	16@10 - 31@26	-216.8	55.13	12	-3.93	0.030
	16@10 - 16@31	-115.1	34.01	12	-3.38	0.073
	16@10 - 31@31	-49.2	41.99	12	-1.17	0.93
	31@10 - 16@16	-154.4	46.83	12	-3.30	0.084
	31@10 - 31@16	-195.3	84.72	12	-2.31	0.36
	31@10 - 16@26	-100.3	39.92	12	-2.51	0.28
	31@10 - 31@26	-221.0	57.28	12	-3.86	0.034
	31@10 - 16@31	-119.3	37.38	12	-3.19	0.10
	31@10 - 31@31	-53.4	44.77	12	-1.19	0.92
	16@16 - 31@16	-40.9	82.44	96	-0.50	1.00
	16@16 - 16@26	54.1	47.06	12	1.15	0.93
	16@16 - 31@26	-66.6	62.47	12	-1.07	0.95
	16@16 - 16@31	35.1	44.93	12	0.78	0.99
	16@16 - 31@31	101.0	51.24	12	1.97	0.53
	31@16 - 16@26	95.1	84.85	12	1.12	0.94
	31@16 - 31@26	-25.7	94.27	12	-0.27	1.00
	31@16 - 16@31	76.1	83.68	12	0.91	0.98
	31@16 - 31@31	142.0	87.23	12	1.63	0.73
	16@26 - 31@26	-120.7	47.96	96	-2.52	0.20
	16@26 - 16@31	-19.0	37.68	12	-0.50	1.00
	16@26 - 31@31	46.9	45.01	12	1.04	0.96
	31@26 - 16@31	101.7	55.73	12	1.83	0.62
	31@26 - 31@31	167.6	60.93	12	2.75	0.20
	16@31 - 31@31	65.9	28.76	96	2.29	0.31

Table D11: All post-hoc, pairwise comparisons (Tukey HSD) for RM-ANOVA comparing *T. pseudonana* frustule diameter (μm) between temperature selection groups and among assay temperature groups. Table corresponds to Figure 17a.

Trait compared	Contrast	Estimate	Std. Error	df	t-ratio	P-value
Frustule diameter	Selection temp.@ Assay temp.					
	16@10 - 31@10	0.77	0.07	99	11.64	<.0001
	16@10 - 16@16	0.21	0.10	12	2.17	0.43
	16@10 - 31@16	0.97	0.12	12	8.37	<.0001
	16@10 - 16@26	-0.39	0.10	12	-4.07	0.024
	16@10 - 31@26	0.38	0.12	12	3.26	0.090
	16@10 - 16@31	-0.46	0.12	12	-3.80	0.037
	16@10 - 31@31	0.31	0.14	12	2.26	0.38
	31@10 - 16@16	-0.56	0.12	12	-4.80	0.007
	31@10 - 31@16	0.21	0.10	12	2.17	0.43
	31@10 - 16@26	-1.15	0.12	12	-9.97	<.0001
	31@10 - 31@26	-0.39	0.10	12	-4.07	0.024
	31@10 - 16@31	-1.22	0.14	12	-8.93	<.0001
	31@10 - 31@31	-0.46	0.12	12	-3.80	0.037
	16@16 - 31@16	0.77	0.07	99	11.64	<.0001
	16@16 - 16@26	-0.60	0.09	12	-6.27	0.0008
	16@16 - 31@26	0.17	0.12	12	1.47	0.81
	16@16 - 16@31	-0.66	0.12	12	-5.55	0.002
	16@16 - 31@31	0.10	0.14	12	0.74	0.99
	31@16 - 16@26	-1.36	0.12	12	-11.79	<.0001
	31@16 - 31@26	-0.60	0.09	12	-6.27	0.0008
	31@16 - 16@31	-1.43	0.14	12	-10.46	<.0001
	31@16 - 31@31	-0.66	0.12	12	-5.55	0.002
	16@26 - 31@26	0.77	0.07	99	11.64	<.0001
	16@26 - 16@31	-0.07	0.12	12	-0.57	1.00
	16@26 - 31@31	0.70	0.14	12	5.12	0.004
	31@26 - 16@31	-0.83	0.14	12	-6.12	0.0009
	31@26 - 31@31	-0.07	0.12	12	-0.57	1.00
	16@31 - 31@31	0.77	0.07	99	11.64	<.0001

Table D12: All post-hoc, pairwise comparisons (Tukey HSD) for RM-ANOVA comparing *T. pseudonana* frustule length (μm) between temperature selection groups and among assay temperature groups. Table corresponds to Figure 17b.

Trait compared	Contrast	Estimate	Std. Error	df	t-ratio	P-value
Frustule length	Selection temp.@ Assay temp.					
	16@10 - 31@10	0.77	0.13	96	6.03	<.0001
	16@10 - 16@16	0.16	0.15	12	1.04	0.96
	16@10 - 31@16	0.58	0.13	12	4.52	0.012
	16@10 - 16@26	0.64	0.17	12	3.74	0.041
	16@10 - 31@26	1.28	0.13	12	9.55	<.0001
	16@10 - 16@31	0.55	0.18	12	3.10	0.11
	16@10 - 31@31	1.48	0.14	12	10.86	<.0001
	31@10 - 16@16	-0.61	0.12	12	-5.09	0.005
	31@10 - 31@16	-0.20	0.09	12	-2.30	0.36
	31@10 - 16@26	-0.14	0.14	12	-0.99	0.97
	31@10 - 31@26	0.50	0.09	12	5.38	0.003
	31@10 - 16@31	-0.22	0.15	12	-1.50	0.79
	31@10 - 31@31	0.71	0.10	12	7.27	0.0002
	16@16 - 31@16	0.42	0.11	96	3.64	0.010
	16@16 - 16@26	0.47	0.16	12	2.93	0.15
	16@16 - 31@26	1.12	0.12	12	9.03	<.0001
	16@16 - 16@31	0.39	0.17	12	2.29	0.37
	16@16 - 31@31	1.32	0.13	12	10.43	<.0001
	31@16 - 16@26	0.06	0.14	12	0.42	1.00
	31@16 - 31@26	0.70	0.09	12	7.82	0.0001
	31@16 - 16@31	-0.03	0.15	12	-0.19	1.00
	31@16 - 31@31	0.90	0.09	12	9.67	<.0001
	16@26 - 31@26	0.64	0.14	96	4.55	0.0004
	16@26 - 16@31	-0.09	0.18	12	-0.46	1.00
	16@26 - 31@31	0.84	0.15	12	5.80	0.002
	31@26 - 16@31	-0.73	0.15	12	-4.79	0.007
	31@26 - 31@31	0.20	0.10	12	2.02	0.51
	16@31 - 31@31	0.93	0.15	96	6.12	<0.0001

Table D13: All post-hoc, pairwise comparisons (Tukey HSD) for RM-ANOVA comparing *T. pseudonana* frustule volume (μm^3) between temperature selection groups and among assay temperature groups. Table corresponds to Figure 17c.

Trait compared	Contrast	Estimate	Std. Error	df	t-ratio	P-value
Frustule volume	Selection temp.@ Assay temp.					
	16@10 - 31@10	35.24	2.57	99	13.72	<.0001
	16@10 - 16@16	4.25	2.82	12	1.51	0.79
	16@10 - 31@16	39.49	3.82	12	10.35	<.0001
	16@10 - 16@26	-0.88	2.79	12	-0.32	1.00
	16@10 - 31@26	34.36	3.79	12	9.06	<.0001
	16@10 - 16@31	1.26	3.15	12	0.40	1.00
	16@10 - 31@31	36.50	4.06	12	8.98	<.0001
	31@10 - 16@16	-30.99	3.82	12	-8.12	0.0001
	31@10 - 31@16	4.25	2.82	12	1.51	0.79
	31@10 - 16@26	-36.13	3.79	12	-9.53	<.0001
	31@10 - 31@26	-0.88	2.79	12	-0.32	1.00
	31@10 - 16@31	-33.99	4.06	12	-8.36	<.0001
	31@10 - 31@31	1.26	3.15	12	0.40	1.00
	16@16 - 31@16	35.24	2.57	99	13.72	<.0001
	16@16 - 16@26	-5.13	2.68	12	-1.91	0.57
	16@16 - 31@26	30.11	3.71	12	8.11	0.0001
	16@16 - 16@31	-2.99	3.06	12	-0.98	0.97
	16@16 - 31@31	32.25	3.99	12	8.08	0.0001
	31@16 - 16@26	-40.37	3.71	12	-10.87	<.0001
	31@16 - 31@26	-5.13	2.68	12	-1.91	0.57
	31@16 - 16@31	-38.24	3.99	12	-9.58	<.0001
	31@16 - 31@31	-2.99	3.06	12	-0.98	0.97
	16@26 - 31@26	35.24	2.57	99	13.72	<.0001
	16@26 - 16@31	2.14	3.02	12	0.71	1.00
	16@26 - 31@31	37.38	3.97	12	9.42	<.0001
	31@26 - 16@31	-33.11	3.97	12	-8.34	<.0001
	31@26 - 31@31	2.14	3.02	12	0.71	1.00
	16@31 - 31@31	35.24	2.57	99	13.72	<.0001

Table D14: All post-hoc, pairwise comparisons (Tukey HSD) for RM-ANOVA comparing *T. pseudonana* frustule <u>total</u> surface area (μm^2) to volume (μm^3) ratio between temperature selection groups and among assay temperature groups. Table corresponds to Figure 18a.

Trait compared	Contrast	Estimate	Std. Error	df	t-ratio	P-value
Fr. SA_{total} : V ratio	Selection temp.@ Assay temp.					
	16@10 - 31@10	-0.23	0.014	99	-16.99	<.0001
	16@10 - 16@16	-0.029	0.025	12	-1.14	0.94
	16@10 - 31@16	-0.26	0.029	12	-8.99	<.0001
	16@10 - 16@26	-0.009	0.024	12	-0.39	1.00
	16@10 - 31@26	-0.24	0.028	12	-8.55	<.0001
	16@10 - 16@31	-0.026	0.027	12	-0.97	0.97
	16@10 - 31@31	-0.26	0.030	12	-8.41	<.0001
	31@10 - 16@16	0.20	0.029	12	6.99	0.0003
	31@10 - 31@16	-0.029	0.025	12	-1.14	0.94
	31@10 - 16@26	0.22	0.028	12	7.88	0.0001
	31@10 - 31@26	-0.009	0.024	12	-0.39	1.00
	31@10 - 16@31	0.20	0.030	12	6.67	0.0004
	31@10 - 31@31	-0.026	0.027	12	-0.97	0.97
	16@16 - 31@16	-0.23	0.014	99	-16.99	<.0001
	16@16 - 16@26	0.019	0.023	12	0.85	0.99
	16@16 - 31@26	-0.21	0.027	12	-7.93	0.0001
	16@16 - 16@31	0.002	0.026	12	0.09	1.00
	16@16 - 31@31	-0.23	0.029	12	-7.79	0.0001
	31@16 - 16@26	0.25	0.027	12	9.38	<.0001
	31@16 - 31@26	0.019	0.023	12	0.85	0.99
	31@16 - 16@31	0.23	0.029	12	7.96	0.0001
	31@16 - 31@31	0.002	0.026	12	0.09	1.00
	16@26 - 31@26	-0.23	0.014	99	-16.99	<.0001
	16@26 - 16@31	-0.017	0.025	12	-0.68	1.00
	16@26 - 31@31	-0.25	0.028	12	-8.68	<.0001
	31@26 - 16@31	0.21	0.028	12	7.49	0.0001
	31@26 - 31@31	-0.017	0.025	12	-0.68	1.00

Table D15: All post-hoc, pairwise comparisons (Tukey HSD) for RM-ANOVA comparing *T. pseudonana* valve only surface area (μm^2) to total frustule volume (μm^3) ratio between temperature selection groups and among assay temperature groups. Table corresponds to Figure 18b.

Trait compared	Contrast	Estimate	Std. Error	df	t-ratio	P-value
$SA_{valve} : V$ ratio	Selection temp.@ Assay temp.					
	16@10 - 31@10	-0.09	0.014	96	-6.30	<.0001
	16@10 - 16@16	-0.01	0.014	12	-0.98	0.97
	16@10 - 31@16	-0.06	0.013	12	-4.71	0.008
	16@10 - 16@26	-0.08	0.019	12	-4.11	0.0222
	16@10 - 31@26	-0.17	0.016	12	-10.38	<.0001
	16@10 - 16@31	-0.07	0.021	12	-3.09	0.12
	16@10 - 31@31	-0.21	0.018	12	-11.86	<.0001
	31@10 - 16@16	0.07	0.013	12	5.85	0.001
	31@10 - 31@16	0.03	0.011	12	2.30	0.36
	31@10 - 16@26	0.01	0.018	12	0.62	1.00
	31@10 - 31@26	-0.08	0.015	12	-5.45	0.003
	31@10 - 16@31	0.02	0.020	12	1.17	0.93
	31@10 - 31@31	-0.13	0.017	12	-7.49	0.0001
	16@16 - 31@16	-0.05	0.012	96	-4.08	0.002
	16@16 - 16@26	-0.06	0.018	12	-3.55	0.056
	16@16 - 31@26	-0.16	0.015	12	-10.22	<.0001
	16@16 - 16@31	-0.05	0.020	12	-2.52	0.27
	16@16 - 31@31	-0.20	0.017	12	-11.74	<.0001
	31@16 - 16@26	-0.02	0.017	12	-0.90	0.98
	31@16 - 31@26	-0.11	0.014	12	-7.60	0.0001
	31@16 - 16@31	0.00	0.020	12	-0.14	1.00
	31@16 - 31@31	-0.15	0.016	12	-9.45	<.0001
	16@26 - 31@26	-0.09	0.020	96	-4.72	0.0002
	16@26 - 16@31	0.01	0.024	12	0.53	1.00
	16@26 - 31@31	-0.14	0.021	12	-6.50	0.0005
	31@26 - 16@31	0.11	0.022	12	4.83	0.007
	31@26 - 31@31	-0.04	0.019	12	-2.34	0.35
	16@31 - 31@31	-0.15	0.023	96	-6.47	<.0001

Table D16: All post-hoc, pairwise comparisons (Tukey HSD) for RM-ANOVA comparing *T. pseudonana* girdle only surface area (μm^2) to total frustule volume (μm^3) ratio between temperature selection groups and among assay temperature groups. Table corresponds to Figure 18c.

Trait compared	Contrast	Estimate	Std. Error	df	t-ratio	P-value
Frustule SA:V$_{girdle}$	Selection temp.@ Assay temp.					
	16@10 - 31@10	-0.14	0.012	99	-11.54	<.0001
	16@10 - 16@16	-0.04	0.019	12	-2.10	0.46
	16@10 - 31@16	-0.18	0.023	12	-7.83	0.0001
	16@10 - 16@26	0.07	0.017	12	4.15	0.021
	16@10 - 31@26	-0.07	0.021	12	-3.15	0.11
	16@10 - 16@31	0.08	0.021	12	3.85	0.035
	16@10 - 31@31	-0.05	0.024	12	-2.25	0.39
	31@10 - 16@16	0.10	0.023	12	4.24	0.018
	31@10 - 31@16	-0.04	0.019	12	-2.10	0.46
	31@10 - 16@26	0.21	0.021	12	9.98	<.0001
	31@10 - 31@26	0.07	0.017	12	4.15	0.021
	31@10 - 16@31	0.22	0.024	12	8.97	<.0001
	31@10 - 31@31	0.08	0.021	12	3.85	0.035
	16@16 - 31@16	-0.14	0.012	99	-11.54	<.0001
	16@16 - 16@26	0.11	0.018	12	6.14	0.0009
	16@16 - 31@26	-0.02	0.022	12	-1.15	0.93
	16@16 - 16@31	0.12	0.022	12	5.53	0.002
	16@16 - 31@31	-0.01	0.025	12	-0.56	1.00
	31@16 - 16@26	0.25	0.022	12	11.45	<.0001
	31@16 - 31@26	0.11	0.018	12	6.14	0.0009
	31@16 - 16@31	0.26	0.025	12	10.32	<.0001
	31@16 - 31@31	0.12	0.022	12	5.53	0.002
	16@26 - 31@26	-0.14	0.012	99	-11.54	<.0001
	16@26 - 16@31	0.01	0.020	12	0.53	1.00
	16@26 - 31@31	-0.13	0.023	12	-5.36	0.003
	31@26 - 16@31	0.15	0.023	12	6.27	0.0008
	31@26 - 31@31	0.01	0.020	12	0.53	1.00
	16@31 - 31@31	-0.14	0.012	99	-11.54	<.0001

Table D17: All post-hoc, pairwise comparisons (Tukey HSD) for RM-ANOVA comparing *T. pseudonana* girdle surface area (μm^2) to valve surface area ratio between temperature selection groups and among assay temperature groups. Table corresponds to Figure 18d.

Trait compared	Contrast	Estimate	Std. Error	df	t-ratio	P-value
Fr. SA_{valve}:SA_{girdle}	Selection temp.@ Assay temp.					
	16@10 - 31@10	-0.03	0.017	96	-1.51	0.80
	16@10 - 16@16	-0.01	0.019	12	-0.66	1.00
	16@10 - 31@16	0.03	0.018	12	1.88	0.59
	16@10 - 16@26	-0.16	0.028	12	-5.54	0.002
	16@10 - 31@26	-0.17	0.026	12	-6.65	0.0004
	16@10 - 16@31	-0.18	0.038	12	-4.82	0.007
	16@10 - 31@31	-0.22	0.035	12	-6.46	0.0006
	31@10 - 16@16	0.01	0.018	12	0.72	0.99
	31@10 - 31@16	0.06	0.017	12	3.47	0.064
	31@10 - 16@26	-0.13	0.028	12	-4.74	0.008
	31@10 - 31@26	-0.15	0.025	12	-5.80	0.0015
	31@10 - 16@31	-0.16	0.038	12	-4.21	0.019
	31@10 - 31@31	-0.20	0.034	12	-5.81	0.002
	16@16 - 31@16	0.05	0.019	96	2.42	0.24
	16@16 - 16@26	-0.14	0.029	12	-4.98	0.005
	16@16 - 31@26	-0.16	0.027	12	-6.00	0.001
	16@16 - 16@31	-0.17	0.039	12	-4.44	0.013
	16@16 - 31@31	-0.21	0.035	12	-6.01	0.001
	31@16 - 16@26	-0.19	0.028	12	-6.71	0.0004
	31@16 - 31@26	-0.21	0.026	12	-7.91	0.0001
	31@16 - 16@31	-0.22	0.038	12	-5.68	0.002
	31@16 - 31@31	-0.26	0.035	12	-7.41	0.0002
	16@26 - 31@26	-0.02	0.034	96	-0.48	1.00
	16@26 - 16@31	-0.03	0.044	12	-0.64	1.00
	16@26 - 31@31	-0.07	0.041	12	-1.68	0.70
	31@26 - 16@31	-0.01	0.043	12	-0.28	1.00
	31@26 - 31@31	-0.05	0.040	12	-1.33	0.87

REFERENCES

REFERENCES

Aksnes DL, Egge JK. 1991. A theoretical model for nutrient uptake in phytoplankton. *Marine Ecology Progress Series* **70**:65-72.

Armbrust EV, Berges JA, Bowler C, Green BR, Martinez D, *et al.* 2004. The genome of the diatom *Thalassiosira pseudonana*: ecology, evolution, and metabolism. *Science* **306**:79–86.

Atkinson D. 1994. Temperature and organism size-a biological law for ectotherms? *Advances in Ecological Research* **25**:1-58.

Atkinson D. 1995. Effects of temperature on the size of aquatic ectotherms: exceptions to the general rule. *Journal of Thermal Biology* **20**:61-74.

Atkinson D, Ciotti BJ, Montagnes DJS. 2003. Protists decrease in size linearly with temperature: ca. 2.5% $°C^{-1}$. *Proceedings of the Royal Society B-Biological Sciences* **270**:2605-2611.

Corkrey R, McMeekin TA, Bowman JP, Ratkowsky DA, Olley J, Ross T. 2014. Protein thermodynamics can be predicted directly from biological growth rates. *PLoS One* **9**:e96100.

Cortese G, Gersonde R. 2007. Morphometric variability in the diatom *Fragilariopsis kerguelensis*: implications for Southern Ocean paleoceanography. *Earth and Planetary Science Letters* **257**:526-544.

Craig SE, Thomas H, Jones CT, Li WKW, Greenan BJW, *et al.* 2013. Temperature and phytoplankton cell size regulate carbon uptake and carbon overconsumption in the ocean. *Biogeosciences* **10**:11255-11282.

Edwards KF, Klausmeier CA, Litchman E. 2011. Evidence for a three-way trade-off between nitrogen and phosphorus competitive abilities and cell size in phytoplankton. *Ecology* **92**:2085-2095.

Eppley RW. 1972. Temperature and phytoplankton growth in the sea. *Fishery Bulletin* **70**:1063-1085.

Eppley RW, Sloan PR. 1966. Growth rates of marine phytoplankton: correlation with light absorption by cell chlorophyll-*a*. *Physiologia Plantarum* **19**:47-59.

Fawley MW. 1984. The Effects of light intensity and temperature interactions on the growth characteristics of *Phaeodactylum tricornutum* (Bacillariophyceae). *Journal of Phycology* **20**:67-72.

Field CB, Behrenfeld MJ, Randerson JT, Falkowski PG. 1998. Primary production of the biosphere: integrating terrestrial and oceanic components. *Science* **281**:237-240.

Finkel ZV, Beardall J, Flynn KJ, Quigg A, Rees TAV, *et al.* 2010. Phytoplankton in a changing world: cell size and elemental stoichiometry. *Journal of Plankton Research* **32**:119-137.

Gillooly JF, Brown JH, West GB, Savage VM, Charnov EL. Effects of size and temperature on metabolic rate. *Science* **293**:2248-2251.

Guillard RRL, Hargraves PE. 1993. *Stichochrysis immobilis* is a diatom, not a chrysophyte. *Phycologia* **32**:234-236.

Hare CE, Leblanc K, DiTullio GR, Kudela RM, Zhang Y, *et al.* 2007. Consequences of increased temperature and CO_2 for phytoplankton community structure in the Bering Sea. *Marine Ecology Progress Series* **352**:9-16.

Harrison PJ, Conway HL, Holmes RW, Davis CO. 1977. Marine diatoms grown in chemostats under silicate or ammonium limitation. III. Cellular chemical composition and morphology of *Chaetoceros debilis*, *Skeletonema costatum*, and *Thalassiosira gravida*. *Marine Biology* **43**:19-31.

Joint IR, Pomroy AJ, Robinson GA, Morris RJ, McCartney MJ. 1987. Morphological changes in *Skeletonema costatum* (Bacillariophyceae) during a spring bloom in a marine ecosystem enclosure. *British Phycological Journal* **22**:119-124.

Jørgensen EG. 1966. Photosynthetic activity during the life cycle of synchronous *Skeletonema* cells. *Physiologia Plantarum* **19**:789-799.

Jørgensen EG. 1968. The adaptation of plankton algae. II. Aspects of the temperature adaptation of *Skeletonema costatum*. *Physiologia Plantarum* **21**:423-427.

Lenth RV. 2016. Least-squares means: the R package lsmeans. *Journal of Statistical Software* **69**:1-33.

Litchman E, Klausmeier CA, Miller JR, Schofield OM, Falkowski PG. 2006. Multi-nutrient, multi-group model of present and future oceanic phytoplankton communities. *Biogeosciences* **3**:607-663.

Martiny AC, Pham CTA, Primeau FW, Vrugt JA, Moore JK, *et al.* 2013. Strong latitudinal patterns in the elemental ratios of marine plankton and organic matter. *Nature Geoscience* **6**:279-283.

Menzel DW, Corwin N. 1965. The measurement of total phosphorus in seawater hased on the liberation of organically bound fractions by persulfate oxidation. *Limnology and Oceanography* **10**:280-282.

Montagnes DJS, Franklin DJ. 2001. Effect of temperature on diatom volume, growth rate, and carbon and nitrogen content: reconsidering some paradigms. *Limnology and Oceanography* **46**:2008-2018.

Neori A, Vernet M, Holm-Hansen O, Haxo FT. 1986. Relationship between action spectra for chlorophyll a fluorescence and photosynthetic O2 evolution in algae. *Journal of Plankton Research* **8**, 537-548.

O'Donnell DR, Hamman CR, Johnson EC, Kremer CT, Klausmeier CA, Litchman E. 2018. Rapid thermal adaptation in a marine diatom reveals constraints and tradeoffs. *Global Change Biology* doi: 10.1111/gcb.14360. **[Epub ahead of print]**

Padfield D, Yvon-Durocher G, Buckling A, Jennings S, Yvon-Durocher G. 2016. Rapid evolution of metabolic traits explains thermal adaptation in phytoplankton. *Ecology Letters* **19**:133-142.

Pinheiro J, Bates D, DebRoy S, Sarkar D and R Core Team. 2018. *nlme: Linear and Nonlinear Mixed Effects Models*. R package version 3.1-137, https://CRAN.R-project.org/package=nlme.

Polovina JJ, Howell EA, Abecassis M. Ocean's least productive waters are expanding. *Geophysical Research Letters* **35**:1-5.

Ratkowsky DA, Olley J, Ross T. 2005. Unifying temperature effects on the growth rate of bacteria and the stability of globular proteins. *Journal of Theoretical Biology* **233**:351-362.

Rhee G-Y, Gotham IJ. 1981. The effect of environmental factors on phytoplankton growth: temperature and the interactions of temperature with nutrient limitation. *Limnology and Oceanography* **26**:635-648.

Sarmiento JL, Slater R, Barber R, Bopp L, Doney SC, *et al.* 2004. Response of ocean ecosystems to climate warming. *Global Biogeochemical Cycles* **18**:1-23.

Schlüter L, Lohbeck KT, Gutowska M, Gröger JP, Riebesell U. Adaptation of a globally important coccolithophore to ocean warming and acidification. *Nature Climate Change* **4**:1024-1030.

Thomas MK; Kremer CT; Klausmeier CA; Litchman E. 2012. A global pattern of thermal adaptation in marine phytoplankton. *Science* **338**:1085-1088.

Thompson PA, Guo M, Harrison PJ. 1992a. Effects of variation in temperature. I. On the biochemical composition of eight species of marine phytoplankton. *Journal of Phycology* **28**:481-488.

Toseland A, Daines SJ, Clark JR, Kirkham A, Strauss J, *et al.* 2013. The impact of temperature on marine phytoplankton resource allocation and metabolism. *Nature Climate Change* **3**:1-6.

Weber T, Deutsch C. 2012. Oceanic nitrogen reservoir regulated by plankton diversity and ocean circulation. *Nature* **489**:419-422.

Winder MR, Reuter JE, Schladow SG. 2009. Lake warming favours small-sized planktonic diatom species. *Proceedings of the Royal Society B-Biological Sciences* **276**:427-435.

Yvon-Durocher G, Dossena M, Trimmer M, Woodward G, Allen AP. 2015b. Temperature and the biogeography of algal stoichiometry. *Global Ecology and Biogeography* **24**:662-570.

Yvon-Durocher G, Schaum C-E, Trimmer M. 2017. The temperature dependence of phytoplankton stoichiometry: investigating the roles of species sorting and local adaptation. *Frontiers in Microbiology* **8**:1-14.